Particle diffusion in elastically coupled narrow parallel channels

Mohau Jacob Mateyisi

Dissertation presented for the degree of
DOCTOR OF PHILOSOPHY
in the Faculty of Science at Stellenbosch University.

Supervisor: Professor Kristian K. Müller-Nedebock
Co-Supervisor: Dr Leandro Boonzaaier
December 2014

Stellenbosch University http://scholar.sun.ac.za

DECLARATION

By submitting this thesis electronically, I declare that the entirety of the work contained therein is my own, original work, that I am the sole author thereof (save to the extent explicitly otherwise stated), that reproduction and publication thereof by Stellenbosch University will not infringe any third party rights and that I have not previously in its entirety or in part submitted it for obtaining any qualification.

Copyright © 2014 Stellenbosch University
All rights reserved

Stellenbosch University http://scholar.sun.ac.za

Abstract

We investigate a model system for particle diffusion in elastically coupled one-dimensional narrow channels. The elastic coupling of the channels is such that channels mutually affect the stochastic dynamics of particles. This kind of constrained and coupled stochastic diffusion may occur in supramolecular lattices where pore occupancy by guest particles may induce a reversible mechanical deformation of the lattice hence, affecting particle evolution in neighbouring pores. The model is explored first for out-of-equilibrium conditions, where we look mainly at the kinetic properties of the system, and thereafter under equilibrium conditions, where we try to understand the nature of dynamic correlation within the coupled channel system. For an out-of-equilibrium version of the model the focus is placed on the steady state behaviour of the two elastically coupled finite channels. The channels are kept in contact with particle reservoirs at the boundaries. Three current-density regimes of different distinct behaviour are identified using a simulation experiment. The sensitivity of the system mean occupancy profile and the steady state particle flux to small and large coupling parameter strength are explored. We find that, for small coupling strength, the system steady state profile and flux behaviour can be approximated by a simple mean field theory ignoring density-density correlations. We present the analytic description of the system using a cellular automaton formalism and then we generalize the theory for a multi-coupled channel system using a hopping particle dynamics approach. For small coupling parameter values, the analytic results are confirmed by the stochastic simulation. From the equilibrium perspective, we model the elastically coupled channel system as a system of infinite narrow channels having a uniform guest particle occupancy and we calculate density fluctuation correlation functions. The elastic coupling between channels is modelled as short range interacting potential and the particle evolution is modelled through Langevin dynamics. The dynamics are cast into the functional integral formalism expressed in terms of the collective particle number density, current density and the associated density response fields. The resulting generating functional takes these fields into consideration within the random phase approximation (RPA) up to second order. For a short range interaction potential, we uncover the behaviour of the system by looking at the influence of the inter-channel interaction strength on the dynamic density-density correlation functions. We conclude that the system long time limit effective friction coefficient is reduced with increase in the coupling parameter values while the strength of

Stellenbosch University http://scholar.sun.ac.za

thermal forces for the effective system becomes renormalized. We also find out that the RPA breaks down under certain conditions, signalling a transition to a behaviour that is no longer characterised by a homogeneous density. The work presented here provides the beginnings for microscopic insights into the filling, filtering and storage processes for which certain types of microporous materials can be utilised.

Stellenbosch University http://scholar.sun.ac.za

Opsomming

Ons ondersoek 'n modelstelsel vir die diffusie van deeltjies in elasties gekoppelde, een-dimensionele nou kanale. Die elastiese koppeling is sodanig dat die stogastiese dinamika wedersyds beïnvloed word. Hierdie gekoppelde en aan dwangvoorwaardes onderhewig diffusie kan in supermolekulêre roosters gebeur waar die besetting van holtes deur deeltjies 'n omkeerbare meganiese vervorming van die kristalrooster kan veroorsaak en sodoende die tydontwikkeling in 'n aangrensende porie beïnvloed. Die model word eers vir nie-ewewig toestande ondersoek, waar ons hoofsaaklik die kinetiese eienskappe van die stelsel beskou, en daarna word dit vir ewewig ondersoek, waar ons die aard van die dinamiese korrelasie binne die gekoppelde kanaalstelsel probeer verstaan. Vir die nie-ekwilibrium weergawe van die model word die fokus op die gedrag van twee gekoppelde en eindige kanale se bestendige toestand gerig. Die porieë bly aan hulle eindpunte in kontak met reservoirs van deeltjies. Daar word drie deeltjiestroom-digtheid gebiede geïdentifiseer met behulp van 'n simulasie-eksperiment. Die sensitiewiteit van die stelsel se gemiddelde deeltjiebesettingsprofiel en die deeltjievloed in 'n bestendige toestand is ondersoek vir groot en klein koppelingsparameters. Vir klein koppelingsterkte vind ons dat die stelsel se bestendige toestand deeltjiebesettingspofiel en deeltjievloed deur 'n eenvoudige gemiddelde-veld teorie beskryf kan word, waar digtheid-degtheids korrelasies verontagsaam kan word. Ons bied die analitiese beskrywing aan vir die gekoppelde stelsel deur van 'n sellulêre outomaat-formalisme gebruik te maak, en om dan die teorie te veralgemeen vir 'n stelsel bestaande uit vele aanmekaar gekoppelde porieë ,deur gebruik te maak van 'n formalisme waarin deeltjies tussen holtes hop. Die analtiese resultate word vir kleine waardes van die koppelingsparameter deur 'n rekenaarsimulasie bevestig. Vir die ekwilibrium gesigspunt modelleer ons die gekoppelde stelsel van kanale as oneindig nou, met 'n homogene verdeling van die deeeltjiebesetting en ons bereken digtheids-korrelasiefunksies. Die elastiese vebinding tussen porieë word deur 'n kortrykwydte potensiaal gemodelleer en die deeltjies se dinamika met behulp van Langevin-dinamika. Die dinamika word met behulp van die funksionaal integraalformalisme uitgedruk in terme van die deeltjiegetaldigtheid-, stroomdigtheid- en meegaande antwoordvelde. Die resulterende genererende funksionaal neem hierdie hoeveelhede tot tweede order binne die "random field approximation" (RPA). Vir 'n potensiaal met kort rykwydte, ondersoek ons die stelsel se gedrag deur die dinamiese digtheid-digtheidskorrelasie te ondersoek. Ons lei af dat die stelsel se langtyd effektiewe wrywingskoëffisiënt afneem met die toename in

Stellenbosch University http://scholar.sun.ac.za

die koppelingsparameter se waardes terwyl die sterkte van die termiese kragte vir die effektiewe stelsel renormeer word. Ons vind ook dat die RPA onder sekere omstandighede sy geldigheid verloor, wat 'n oorgang kan beteken wat nie meer deur 'n homogene digtheid beskryf kan word nie. Die werk wat hier aangebied word dui die eerste stappe aan vir hoe mikroskopiese insigte vir vul-, filter- en stoorprosesse vir sekere tipes mikroporeuse materiale gebruik kan word.

Stellenbosch University http://scholar.sun.ac.za

Aknowledgements

I would like to thank my supervisor Professor Kristian K. Müller-Nedebock and co-supervisor Doctor Leandro Boonzaaier for their guidance during my postgraduate studies. Their patience, encouragement and support made it possible for me to complete this project. The sense of humour that accompanied our weekly project meetings and the physics insights shared by fellow members of the soft condensed matter physics group kept me motivated through out me studies.

I am very thankful to Professor Weigel for reliably availing the computational facilities for the simulation part of this project.

I am very grateful to DAAD for the study grant (A/11/07860) awarded to me through AIMS administration. Without the complimentary financial assistance from Stellenbosch physics department, a timely completion of this project could have not been possible.

I would like to thank fellow students and members of the physics department for their friendship and scientific exchanges. It has been a privilege and pleasure to share office space with C.M Rohwer, K. Möller, S.M. Pachong, H.J.R Van Zyl and J. Meylahn. My studies benefited from their knowledge and skill which they so generously shared.

I would like to thank my family and friends for their continued encouragement and prayers. Special thanks goes to my wife Anicia, who has always been by my side during the course of my postgraduate education, and my Son Bukhulubakhe whose arrival brought so much energy in my studies. Most importantly, I would like to thank the almighty God who blessed every effort that led to this dissertation.

Stellenbosch University http://scholar.sun.ac.za

Contents

Stellenbosch University http://scholar.sun.ac.za

Stellenbosch University http://scholar.sun.ac.za

Stellenbosch University http://scholar.sun.ac.za

Stellenbosch University http://scholar.sun.ac.za

List of Tables

Stellenbosch University http://scholar.sun.ac.za

List of Figures

Stellenbosch University http://scholar.sun.ac.za

Stellenbosch University http://scholar.sun.ac.za

Stellenbosch University http://scholar.sun.ac.za

Chapter 1

Introduction and outline

Recently the topic particle transport in porous materials is receiving renewed interest in a number of research fields. Interesting research problems originate from fields outside traditional physics disciplines such as chemistry [Jacobs et al., 2012] and biology [Hille, 2001]. From the references above we learn that porous hosts can be found either in naturally occurring systems or artificially synthesized systems. The advances in the synthesis techniques for porous materials are such that various classes of organic and metallic porous structures that are crystalline, amorphous or ordered in nature can be synthesized at an industrial scale. Porous hosts with pores that are fully interconnected such that a guest molecule diffusing in the material can access the entire domain can be produced. Porous materials with controllable properties and adjustable pore size, that can be made of similar size to a possible molecular inclusions, are also achievable [Li et al., 2009]. The structural properties of the porous materials make them candidate material for application in molecular storage, filtration and catalysis (for more examples see [Ma, 2009]).

1.1 Porosity

According to Barbour [Barbour, 2006] for a material to be classified as porous there must be an evidence of permeability, of the material to certain guest species, within a specific phase. In principle such a material should be left *substantially unaffected* by the uptake or removal of the guest particles. Barbour (2006) further continues to classify porosity in the

Stellenbosch University http://scholar.sun.ac.za

literature under three main categories:*virtual porosity*, *conventional porosity* and *porosity without pores* . Virtual porosity is described as the easiest kind of porosity that can take various forms. It is created by deletion of selected atoms from a file containing asymmetric units of a crystal structure. Traditionally porous materials, that are characterized by the existence of a permeable channel within the structure of the material, exhibit conventional porosity. In experimental studies of micro-porous materials such channels can be mapped through their atomic coordinates. Porosity without pores is a category of micro-porosity which is relatively new and this work is of particular relevance to it. Materials exhibiting porosity without pores only have discrete voids that fleetingly interconnect to permit guest particle transfer between cavities. This means that porosity in the material is dynamic and guest particle diffusion is by virtue of thermal motion or guest-induced motion of the host molecules. This category of materials present a possibility for the design of robust voids that are unaffected by the choice of a guest molecule leading to hosts that are able to accommodate an assortment of guest molecules.

The specific type of porous material that is studied here consist of multiple connected molecular complexes that have guest molecule accessible cavities in a specific phase. The host molecules are inter-connected in such a way that it is possible for a guest particle to diffuse from one host cavity to another following a one dimensional path. Fig. 1.1 shows a very simplified structure of the main features of the porous molecular complex that is connected to some particle reservoirs at the ends. Such porous system inspire a number of important questions for instance, it would be interesting to know how the interaction of the diffusing guests among themselves and with the host molecule affect the diffusion in some collective way. For the case when the porous structure are packed such that the one dimensional pores are dynamically and elastically coupled, the interesting question that arise is how do the elastic coupling between pores affect the filling dynamics of the system.

In general, porous materials throw open a number of interesting questions from theoretical perspective to the applications perspective. There is need for a theoretical framework describing the system's diffusive behaviour, for any given natural or artificial porous material, from universal physics principles through a theory that is independent of the atomic design of the porous material. Although theories of such type are not so handy in making predictions about very detailed molecular systems, they form a reliable basis for our understanding as they are good in producing extreme limit behaviour of otherwise complex

Stellenbosch University http://scholar.sun.ac.za

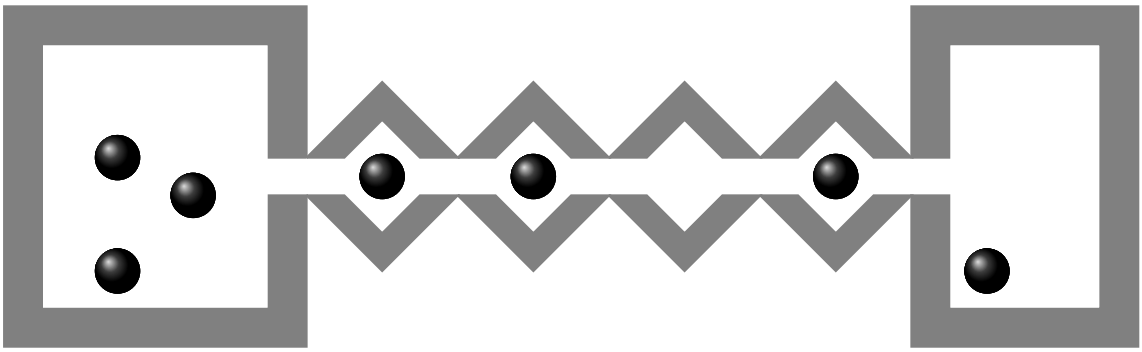

FIG. 1.1. A depiction of a one dimensional micro-porous system constituted by interconnected molecular complexes (v-shaped gray regions). The white region occupied by guest molecules (gray balls) represent the host cavities. The region between cavities is such that guest molecules of a specific size can diffuse from one cavity to another. The pore is connected to particle reservoirs (rectangular) at the ends.

systems. When it comes to practical applications, it is often necessary to have a conceptual overview of probable phenomena in porous channels. Such phenomena may be system specific and may potentially be observed under a certain set of conditions, which could be sensibly formulated.

Stellenbosch University http://scholar.sun.ac.za

In this dissertation we construct a general theory of diffusion in a micro-porous material that is characterized by elastically coupled voids arranged in channels (which shall also be referred to as files). By solving an idealized simple one dimensional microscopic model of the system, some macroscopic properties of the real systems are attained.

Stellenbosch University http://scholar.sun.ac.za

1.2 Studied porous system properties

Among the macroscopic characteristics of the pores that we calculate from the theoretical considerations are: the steady state mean pore occupancy, particle flux, and mean density fluctuation correlations/response functions as well as the effective friction experienced by individual particles in a multi coupled file system. To achieve this, we model the porous system based on basic principles of non-equilibrium statistical physics. We describe the diffusive behaviour of the system under the influence of the boundary reservoir density and the elastic coupling between pores. The model equations for describing the transport properties are set for a discrete lattice version of the system and reduced to a set of simple partial differential equations amenable to a numeric or analytic treatment at a mean field level. We also account for the role played by dynamic correlation between particle occupancy states expressed in terms of collective variables.

The insights gained from our simple model could potentially inform research in other related problems such as research aimed at understanding the movement of molecules in carbon nanotubes [Berezhkovskii and Hummer, 2002] and active diffusion of particle through cell membranes [Hille, 2001]. These are the type of diffusion problems where the movement of particles is confined in every other direction except one. An accurate description of these system can be attained by sensibly reducing the system to an equivalent one dimensional description. In instances where particle movement can effectively explore more than one dimension, interesting insights about the properties of the system can still be attained, to some extend, by abstracting the system as a quasi-one dimensional system.

1.3 Analytic methods for micro-porous systems

Although, for a number of decades, research in porous media has been active and wide-ranging, there is no universally accepted theory describing diffusion in porous systems. However, a number of analytic approaches aimed at describing diffusion in narrow pores have been contributed in the literature. In the family of discrete models, there are so-called *rate theories* [Chou, 1998; Stephan et al., 1983] which are commonly used in the study of ion channel systems. Regardless of the fact that rate theories are capable of making a lot of

Stellenbosch University http://scholar.sun.ac.za

predictions about the properties of real pores, they suffer from several drawbacks. Firstly, the model equations used are often phenomenological. Secondly, when ion occupancy sites are characterized by wide and deep energy walls having several particles, the diffusion of particles cannot be sensibly described. Thirdly, the height of the energy barrier between occupancy sites is usually hard to estimate. In a situation where the transported particles have strong interactions at short range, the kinematic type of interaction used, often does not account for effects such as occupancy state correlations hence, this approach presents an oversimplified description of the real systems.

A continuous classical description of charged particles diffusion in narrow pores can also be constructed though Poisson-Boltzmann equations (PB) or Poisson-Nernst-Planck equation (PNP) that can be expressed in terms of average particle concentrations, see [Eisenberg, 1996, 1999] for a review and references therein. This approach is found to perform badly in predicting properties of very narrow pores. A revised version of this approach which uses the so-called conditional Poisson-Nernst-Planck equation (C-PNP) has been proposed [Nadler et al., 2004]. The approach generalizes equilibrium statistical physics ideas based on PB, used to model simple fluids, to study narrow pore nonequilibrium steady state properties. Despite the generality and robustness of the approach, this theory does not lead to a closed system of equations. It leads to an infinite hierarchy of multiparticle equations, which are similar to the Bogolyubov-Born-Green-Kirkwood-Yvon (BBGKY) hierarchy of equations [Alexeev, 2004], the truncation of which is a highly non-trivial task.

A continuous description of the narrow pore system based on the multidimensional Fokker-Planck equation or Langevin equation [Gardiner, 1985] is achievable. A Fokker-Plank equation can also exist as a continuum limit of the rate theory approach [Stephan et al., 1983] for an extremely large number of binding sites. This is a good candidate for constructing a robust, general and detailed analytic description of diffusion in the narrow pores. The method is versatile enough and can reliably incorporate effects such as complex energy profiles inside the pore and explicit particle-particle interactions. The influence of external fields and pore-pore interactions can be incorporated in a sensible manner. The aspect of our work that is dealing with collective dynamic correlations is based on the Langevin equation description of individual particle dynamics. The resulting system of Langevin equations is solved in the context of functional integral formalism. When using the Langevin approach, dealing with boundary conditions for a finite system usually re-

Stellenbosch University http://scholar.sun.ac.za

quires a lot of thought and caution. We choose a situation where individual files are very long. In this limit, we can assume that the coupled channel system is at equilibrium and we study the nature of the system density fluctuation correlations.

The kinetic properties of the systems are accessed by dealing with a specific case when there is kinetic balance between the pore ends and the respective reservoirs. In this case, we are able to describe the particle entry and exit events without having to introduce unknown kinetic constants. This allows us to describe the system without having to define explicit macroscopic details of reservoir-pore interface. This sets our work apart from the existing formalisms of the prevailing analytical theories.

Looking at the available analytical methods, out-of-equilibrium systems as opposed to equilibrium systems still face deep methodological challenges. The primary reason being that, there is no global out-of-equilibrium state thus, in describing an out-of-equilibrium system one must also characterize the nature of the system. For instance, one must state whether a system is about to relax to an equilibrium state or whether a system is subject to an external field that keeps it permanently in an out-of-equilibrium state or whether system in an out-of-equilibrium steady state. Because of the diversity of non-equilibrium states, there is no single free energy based minimisation principle that works in describing non-equilibrium systems, therefore non-equilibrium system must be modelled case by case. For a historical and conceptual account of the foundations, goals and obstacles in developing non-equilibrium statistical physics, see [Lawrence, 1993].

One of the key factors that predetermine various classes of model abstraction is the relative host-guest size. In a scenario where the pore size is large relative to the particle size, among the simplest transport models that have been successfully developed, is that of bulk diffusion in a narrow two dimensional ($2D$) channel [Kalinay and Percus, 2006, 2005]. Here the essential task is to perform a reasonable reduction on the transverse degrees of freedom in a simple diffusion motion. The target is to obtain the corrections to the diffusion coefficient. Often the correction is expressible in terms of a parameter that describe the curvature of the boundary at various positions along the longitudinal coordinate x such as channel cross-sectional area $\mathcal{A}(x)$. The curvature of the boundary, in this case, may be attributed to effects such as pore clogging by neighbouring particles [Bowles et al., 2004] or some geometric features of the pore leading to entropic effects on particle diffusion

Stellenbosch University http://scholar.sun.ac.za

[Zwanzig, 1992].

In a scenario where individual pores are so narrow that they prohibit particle overtaking (single-file effects [Levitt, 1973; Percus, 1974]), a generalized projection leads to an effective hardcore interaction between particles, typical of $1D$ transport, with individual particles interacting through self exclusion. In our system of interest particle host channels are so narrow that single-file effects must be incorporated in the model. The porous host channels are soft to an extent that guest particles geometrically deform the host channels locally. Particle diffusion is not only constrained by the walls of the host but by the ability of the guest particles to elastically deform the host pore hence, presenting the particles in the neighbouring pores with obstacles. These obstacles may potentially induce particle co-operatively leading to a modified diffusive behaviour for individual particles.

In the study of particle diffusion in narrow infinite channels, particularly in studies looking at particle diffusion in the presence of obstacles or in situations where there are several species at high concentrations, anomalous behaviour has been observed experimentally and reported in the literature [Guigas and Weiss, 2008]. The theory which closely account for this observed behaviour suggests that the mean square displacement grows with time as t^{θ}, where $\theta < 1$. This indicates that obstacles or increased concentration hinder diffusion in some way, resulting in a violation of Fick's law. This phenomenon is called by a number of names such as *molecular crowding* [Banks and Fradin, 2005; Uversky et al., 2008; Weiss et al., 2004] and *single-file diffusion* [Brzank and Schütz, 2007; Chatterjee and Schütz, 2010; Wei et al., 2000]. Single-file diffusion can be modelled from various approaches. First principle based approaches include hydrodynamic models, which are often formulated in terms of non-linear constitutive equations [Popkov and Salerno, 2004] and symmetric simple exclusion process (SSEP) in one dimension. The bulk of this work comprises an application of SSEP ideas for modelling out-of-equilibrium particle dynamics in a multiple coupled channel system. This formalism allows us to include pore-pore interaction in the model equation through a tunable interaction parameter.

The SSEP can be classified as the easiest and perhaps best studied technique for modelling stochastic interacting particle systems [Liggett, 1985]. In a SSEP, particles propagate diffusively in all directions of a d-dimensional lattice. The diffusion of particles is under the hardcore constraint that two particles cannot occupy the same lattice site. Systems

Stellenbosch University http://scholar.sun.ac.za

obeying equilibrium conditions can be handled in this approach by defining the lattice on a ring and enforcing conservation of particles [Lecomte et al., 2012]. Non-equilibrium steady states can be modelled through the driven SSEP which is a simple exclusion process in which particles can enter or leave the bulk at the boundaries. Using this framework, time-dependent correlation functions [Santos and Schütz, 2001], current and density large deviations as well as fluctuations [Akkermans et al., 2013; Derrida and Gerschenfeld, 2009; Derrida and Retaux, 2013; Derrida et al., 2002] have lately been calculated. We use the SSEP ideas to develop a generalized mean field theory for multi-coupled files. The relevance of this approach in modelling diffusion of colloidal particles in narrow channels has been demonstrated [Chou, 1998; Chou and Lohse, 1999]. What distinguishes our model from many one-dimensional narrow pore diffusion models solved using SSEP method, is the level of complexity presented by the elastic pore coupling. We maintain a symmetric exchange of particles between the respective pores ends and the reservoir. The particle diffusion is driven only by the density gradient between the reservoirs at the respective ends of the files. We are not aware of any other work that keeps the SSEP particle hopping rules symmetric throughout all the coupled files.

Another useful approach, that is utilized in this dissertation to make a description of diffusion in porous hosts in terms of states density variables, is the cellular automata modelling which demands that space, time and particle velocity be taken as discrete variables. The mesoscopic cellular automata approach is able to reproduce macroscopic phenomena by modelling local microscopic dynamics through a simplified description. The microscopic description includes the necessary basic requirements of fundamental physics such as the conservation laws and symmetry properties. Through this approach the system model equations, that are easily reducible to continuous coupled partial differential equations, are expressible in terms of the average collective density of the automaton states in the respective channels. We will not attempt to take the reader through every aspects of the cellular automata theory here rather, it is safe to direct the reader to interesting detailed and mathematical account of cellular automata modelling of physical systems that is presented in the literature by Bastien Chopard and Michel Droz [Bastien and Michel, 1998].

Stellenbosch University http://scholar.sun.ac.za

1.4 Simulation methods for micro-porous systems

The most direct simulation approaches for investigating diffusion in narrow pores is Molecular Dynamics (MD) simulation [Demontis and Suffritti, 1997; Hahn and Kärger, 1996] and Brownian Dynamics (BD) simulation [Nelissen et al., 2007]. The central idea here is to solve the equations of motion for individual particles in the channel and obtain physical properties of the system by taking time averages over simulated trajectories. Through these methods, the information about the function of biological ion channels, for instance, can be effectively obtained. For systems with a large particle number these methods suffer limitations imposed by computer power and methodological complications. However, there is no doubt that the limitations could be ultimately overcome through advances in the available computer hardware and simulation algorithms.

In this work we adopt cellular automata simulation ideas to explore the dynamical properties of the coupled file system at steady state. The cellular simulation is not used only within its computational capacity but also in the spirit of a computer laboratory experiment for testing ideas about the real diffusion phenomena in the coupled pores. The strength of this approach lies in the fact that particle update rules for the system can afford simultaneity in the evolution of particles in all the files hence permitting the calculation of equal time correlation averages. The random sequential updating (RSU) Monte Carlo method [Richards, 1977] is also implemented as an alternative approach to obtain the average steady state particle flux and particle density profiles for the system. RSU is a fairly easy algorithm to implement and it has been commonly used in the study of asymmetric simple exclusion processes (ASEP) in the literature [Rajewsky et al., 1998]. For stationary properties of a system, the RSU method is exact. It is, unable to reproduce dynamic behaviour such as equal time occupancy states correlations and it is susceptible to computational inefficiencies.

1.5 This dissertation

The dissertation is organized as follows: In chapter 2 we present a description of the system under consideration and we propose a simple toy model for the dynamics of the

Stellenbosch University http://scholar.sun.ac.za

particles in the porous system that is detailed enough to help in the understanding of the system diffusive behaviour subject to the system dominating constraints. Using a Monte Carlo simulation and a cellular automaton simulation we explore the steady state behaviour of the system by measuring the macroscopic quantities such as the steady state particle flux, steady state density and the associated density-density correlations. Within a cellular automaton context, analytic expressions for the steady state particle occupancy profile and the steady state particle flux for a weakly coupled and uncorrelated version of the system are derived in chapter 3. The analytic theory is then generalized in the frame-work of SSEP. In chapter 4 the dynamic density correlation functions for a related system at equilibrium are calculated using the functional integral approach. The effect of the interfile coupling on the effective friction coefficient and the strength of the random forces is highlighted. The chapter concludes with a rational of how the single file effects and the density-density corrections can be sensibly incorporated in the kinetic part of the theory. In chapter 5, we also present an outlook of how the ideas and insights from this work could be further extended to other related systems with particles undergoing some form of constraint diffusion process.

Stellenbosch University http://scholar.sun.ac.za

Chapter 2

System description and dynamic simulations

In this chapter we describe the model system with which the bulk of this dissertation is concerned. We start by introducing the structural aspects of the system along with some chemical details for the real system under consideration. A special focus will be placed only on the properties that are important in understanding the basis of our model assumptions. The second half of the chapter discusses two simulation methods for simulating the steady state behaviour of the system. The insights gained from the simulations give way to the analytical treatment of the system.

2.1 Diffusion in organic and metal organic porous materials

As mentioned earlier this work is motivated largely by an experimental study of micro-porous materials. Micro-porous materials may be organic and metal-organic in nature. A Porous host can be constituted by single molecule or multiple molecules that assemble to form a guest accessible cavity. Single molecule hosts are called *cavitands* while multiple molecule hosts are called *clathrands* Fig. 2.1.

Host molecules may be covalently bonded to form a crystalline lattice having guest accessible cavities as part of a repeating motif. For a schematic diagram showing a projection

Stellenbosch University http://scholar.sun.ac.za

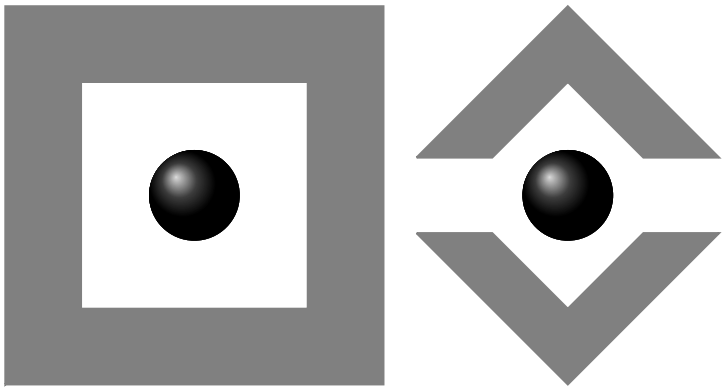

(a) (b)

FIG. 2.1. A depiction of single molecule host, (a) *cavitand*, and a two molecule host, (b) *clathrand*.

of a porous crystal lattice that is made up of clathrands molecules Fig. 2.2. These materials are characterised by a selective binding due to mutual affinity between part of the complex that act as a host and any molecule or ion that is a guest within the lattice. A host molecule can be distinguished from the guest molecule by the fact that its binding sites diverge within the complex while those of the guest converge within the complex.

The uptake of guest molecules by the host is generally referred to as a *sorption* process. The sorption process may be chemical or physical in nature. Chemical sorption involves formation of significant chemical bonds between the host and the guest molecule while the physical sorption involves weaker forces that entail long range electrostatic forces and Van der Waals' interactions. Such weak forces are typical of a gas molecule in contact with a surface of a solid.

In our system of interest the host-guest dynamics involve physical sorption. The diffusion through the material is generally non-activated but it is a spontaneous process. In fact, an experimentally supported established notion about the particle diffusion mechanism is that guest molecules diffuse through the host on account of rigid and spontaneous *shivering* by the host molecules. This allow neighbouring voids to become briefly interconnected hence presenting the guest molecule with an opportunity to *hop* to the next host cavity [Jacobs, 2009]. The host molecule deformation, upon the uptake of the guest, leads to a temporary distortion of the voids in the neighbourhood. We will refer to this type of deformation

Stellenbosch University http://scholar.sun.ac.za

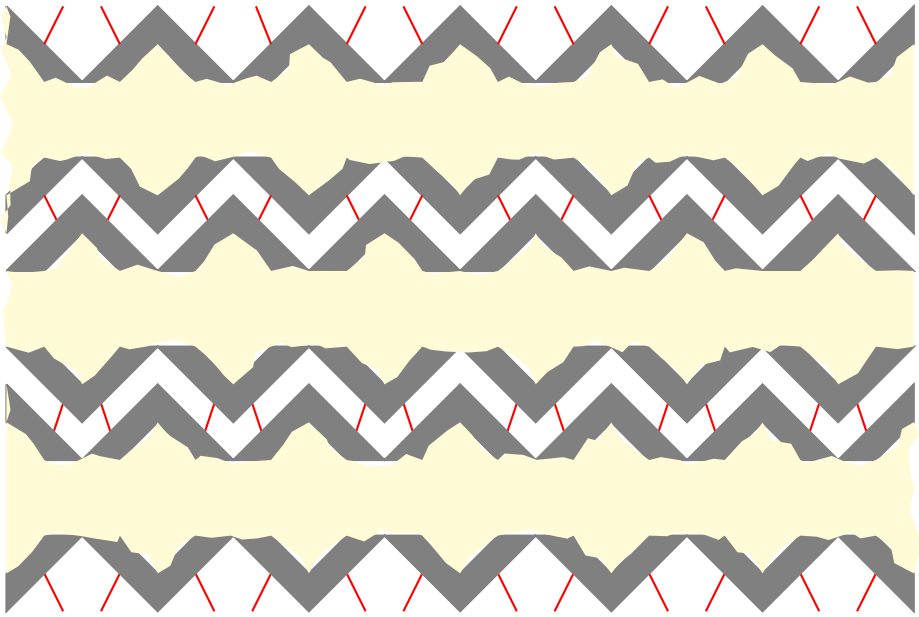

FIG. 2.2. A depiction a molecular lattice. Gray walls bound columns of host molecules (yellow region) that can be related by a simple guest particle translation. The guest molecules are jointed together by bonds (red sticks) such as hydrogen bonds to form a lattice.

as an *elastic coupling*. Despite the mechanical deformation of the neighbouring pores, upon occupancy by a guest particle, the core structure of the host remains intact. In this chapter we study the diffusion process in a scenario where they system is kept out of equilibrium by a density gradient between the particle source reservoir and the particle collecting reservoir.

2.2 The porous system toy model

We consider the porous system from a slightly simpler perspective. The intricate host molecule complex is modelled through finite one dimensional coupled channels that make it possible for the guest particle to diffuse in the one dimensional pores without exchanging the host channel. This crude mapping of the pores is equally suitable for cavitands as well as for clathrands as long as the elastic coupling between pores is reasonably accounted for. The channels are kept elastically coupled in the sense that the inclusion of a guest particle leads to a structural deformation of the host channel locally hence, constricting

Stellenbosch University http://scholar.sun.ac.za

the movement of particles in the neighbouring positions from the adjacent channels. All channels are modelled as identical cylindrical objects while the guest particles are modelled as indistinguishable spherical objects interacting only through self-exclusion.

Despite ignoring the complexities that are presented by the molecular topology of the host molecules, this model turns out to be a feasible simplification of the real system as experimental specifications of a porous material are usually achieved by stating the maximum radius of a spherical guest molecule that will pass through the narrowest region of a continuous pore. The practicality of the approach is judged on the basis that many channels are almost circular in cross section and some guests molecules can generally be approximated by spherical entities. As demonstrated in Fig. 2.2, for ease of analysis we think of a projection of the toy model to a single plane.

The guest particle motion is modelled through a discrete unbiased one dimensional stochastic motion that is constrained by the occupancy of the neighbouring sites from the adjacent channels. This is achieved by introducing probabilistic particle hopping rules which reproduce analogous particle diffusion instigated by molecule thermal agitation or shivering within a porous host. The rules are kept symmetric about the respective channels with the extreme ends of the channels in contact with the particle reservoirs. Each reservoir is assumed to have a uniform particle density and the particles exchange between host channels and the reservoirs is assumed to be kinetically balanced. A reservoir at the left is kept at a different density from the one at the right. The density gradient keeps the system consistently out of equilibrium. For a visualisation of a two channel version of the toy model see Fig. 2.3. In this system the particle dynamics are locally not externally biased but symmetrically constrained by the occupancy of particles from the adjacent channels, therefore the type of model presented above falls under a family of constrained SSEP.

In experimental investigations geared towards the development of porous materials for industrial applications, statistical analysis of occupancy factors under various physical conditions is necessary however, there are technical challenges that limit progress in getting reliable and accurate data. Sample purity is reported as one of the factors which is often a big challenges when producing the desired amount of sample necessary for quantitative analysis that involves taking averages of several trials of measurements [Jacobs, 2009]. Another route to gaining insight about the transport and equilibrium properties of the

Stellenbosch University http://scholar.sun.ac.za

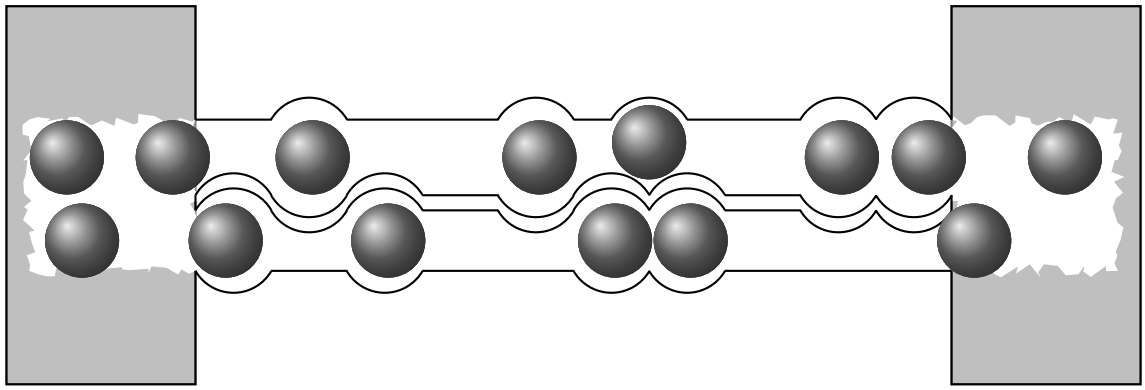

FIG. 2.3. A toy model for a system of two coupled channels showing a projection of the coupled channel in the $xy-$plane. The molecular channels that are accessible to the guest molecules are shown under deformation by the guest particles (grey spheres). The channels are connected to the reservoirs (designated by rectangular regions shaded in grey).

porous system is through stochastic simulations.

In the subsequent sections, we detail two simulation approaches that could be used to explore the system at steady state. The first method is the Monte Carlo Random Sequential Updating (RSU) [Rajewsky et al., 1998] which is exact for stationary properties but computationally inefficient for time dependent behaviour. The second method is the cellular automaton method (CU). It overcomes the inefficiency inherent in RSU method and guarantees macroscopic properties that can also be accessible by various analytic methods.

2.3 Discrete-time Monte Carlo: random sequential updating

In order to perform a Monte Carlo type simulation, the model is mapped to a discrete lattice version of length N. The particles in each file occupy discrete positions on a one dimensional lattice with each of the reservoirs featuring through sites that are immediate to the lattice extreme ends. The occupancy variable of a site may take values zero or one signifying the absence or presence of a particle. We use the notation τ_i and $\bar{\tau}_i$ to denote the occupancy variables at an ith site of the respective coupled channels lattices. At time

Stellenbosch University http://scholar.sun.ac.za

step, the discrete-time Monte Carlo algorithm is carried out as follows:

For each one dimensional lattice, representing a channel, an integer $i \in \{1, 2, \cdots, N\}$ is randomly select to choose a site.

- If i is such that $1 \leq i \leq N$, we implement the bulk particle dynamics which means that at any occupied site in the bulk, a particle probabilistically hops to either site $i-1$ or site $i+1$, if the site is unoccupied. The probability of each hop depends on the occupancy of a site adjacent to the site i and the site adjacent to the destination site from the neighbouring channel. In case of an unsuccessful hop a particle remain stationary.

- For site $i = 0$, we implement left boundary particle dynamics. A particle enters the system from a reservoir on condition that the destination site is vacant. If the site $i = 0$ is occupied by a particle, the particle can randomly decide to hop out of the file or to proceed into site $i = 1$.

- At site $i = N$, we implement the right boundary dynamics which are similar to the left boundary dynamics but at a different reservoir density.

At the boundary the hopping probabilities do not depend on the neighbouring lattice occupancy. In this way the particle injection and extraction rates depend largely on the reservoir densities and the reservoirs are kept at kinetic balance with the bulk of the system. The reservoir dynamics reflects correlations inside the reservoirs. The internal probabilistic hopping rules on any site i in the bulk can be summarised by the following stochastic Monte Carlo hopping equation

$$\begin{aligned} \delta\tau_i \;\; = \;\; & -\eta(i, i+1)\tau_i(1-\tau_{i+1})\tau_{i-1} \\ & -\eta(i, i-1)\tau_i(1-\tau_{i-1})\tau_{i+1} \\ & -\eta'(i, i+1)\tau_i(1-\tau_{i+1})(1-\tau_{i-1}) \\ . \quad & -\eta'(i, i-1)\tau_i(1-\tau_{i+1})(1-\tau_{i-1}). \end{aligned} \tag{2.1}$$

Here τ_i assume value a 1 if a site i is occupied and it assumes a value 0 if the site is unoccupied by a particle. The quantities η and η' are random variables which also take the values 0 or 1 according to a random variable r. The variable r has a uniform distribution on

Stellenbosch University http://scholar.sun.ac.za

the interval $[0, 1]$. We introduce the probability $p_{i,j}$ such that $\eta(i, j) = 1$ if $0 \leq r(i, j) \leq p_{i,j}$ and $\eta(i, j) = 0$ if $r(i, j) > p_{i,j}$. The random variable $\eta'(i, j) = 1$ if $0 \leq r(i, j) \leq 2p_{i,j}$ and $\eta'(i, j) = 0$ if $r(i, j) > 2p_{i,j}$. It is easy to see that

$$\langle \eta(i, j) \rangle = p_{i,j} \quad \text{and} \quad \langle \eta'(i, j) \rangle = 2p_{i,j}, \tag{2.2}$$

where the angle brackets $\langle \cdots \rangle$ denote an average over many randomly selected values of r. Each transition $i \to j$ involves an independent call to the random number generator, hence each choice of $r(i, j)$ is probabilistically independent. In every Monte Carlo sweep step, if the evolution of a randomly selected particle at position i is restricted by the occupancy of the adjacent channel sites, the rate of the next possible transition, say w_0, is reduced by a constant non-zero factor ϵ such that the new rate

$$w = w_0(1 - \epsilon). \tag{2.3}$$

We think of the parameter ϵ as indicative of the strength of the elastic coupling between files. The probability of each particle transition to the left or to the right depends on the occupancy of the adjacent channel states from the neighbouring files. Let us consider an instance when sites $\bar{\tau}_{i-1} = 1$ and $\bar{\tau}_i = 0$ with sites $\tau_{i-1} = 0, \tau_i = 1$ and $\tau_{i+1} = 0$. The probability that a particle in the first channel at site τ_i hops left is $p_{i,i-1} = \frac{w_0(1-\epsilon)}{2w_0 - \epsilon w_0} = \frac{1-\epsilon}{2-\epsilon}$ while the probability that the particle hops right is $p_{i,i+1} = \frac{w_0}{2w_0 - \epsilon w_0} = \frac{1}{2-\epsilon}$. Table 2.1 shows the probability of the left and right particle hop for a given neighbourhood within a two coupled channel system.

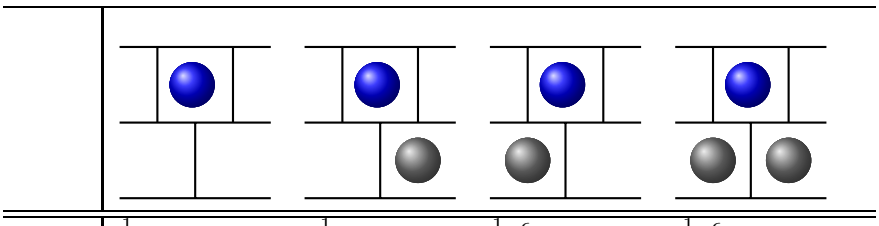

$p_{i,i-1}$	$\frac{1}{2}$	$\frac{1}{2-\epsilon}$	$\frac{1-\epsilon}{2-\epsilon}$	$\frac{1-\epsilon}{2-2\epsilon}$
$p_{i,i+1}$	$\frac{1}{2}$	$\frac{1-\epsilon}{2-\epsilon}$	$\frac{1}{2-\epsilon}$	$\frac{1-\epsilon}{2-2\epsilon}$

TABLE. 2.1. Hopping probabilities look-up table for a particle (shown in blue) for a given neighbourhood particle configuration (shown in grey). The empty squares designate unoccupied lattice sites.

At each Monte Carlo step, the lattice is randomly sampled a number of times that correspond to the total number of sites on the lattice. In each sampling a site on the lattice is

Stellenbosch University http://scholar.sun.ac.za

selected and the hopping equation (2.1) is applied applied to the site. At each application of the hopping equation, if $\delta\tau_i = 0$ the site is skipped without any changes. This correspond to a situation when there is no particle at a site or a situation where there is no vacant state in both the left and the right neighbourhood of the site. If $\delta\tau_i = -1$, a jump occurs occurs to the left with a probability $p_{(i,i-1)}$ or to the right with a probability $p_{i,i+1}$.

We denote a left and right moving current at a site by $J_L(i)$ and $J_R(L)(i)$. If the particle hop to the left is successful, we implement changes $\tau_i \to \tau_i - 1$, $\tau_{i-1} \to \tau_{i-1} + 1$ and we set the corresponding left moving current $J_L(i) = 1$. In a similar way if the particle hop to the right is successful we effect changes $\tau_i \to \tau_i - 1$, $\tau_{i+1} \to \tau_{i+1} + 1$ and the corresponding site right moving particle current $J_R(i) = 1$. For a system consisting of two coupled files each having N lattice sites, these steps are repeated $2(N + 1)$ times. This constitutes the evolution corresponding to a unit Monte Carlo Sweep (MCS) - unit simulation time. This approach ensures the fact that the number of attempted moves per unit time is proportional to the size of the system. As opposed to continuous Monte Carlo methods operating in continuously varying time, RSU schemes measure algorithmic time in fixed intervals.

The system is open in the sense that the particle hopping rules allow a symmetric exchange of particle between the files and the reservoirs. We denote the left boundary density connected to the first and second file by n_L and $\bar{n}_L$. The corresponding right reservoir densities for the files are denoted by n_R and $\bar{n}_R$ respectively. We choose equal boundary densities $n_L = \bar{n}_L$ and $n_R = \bar{n}_R$ for the left and the right reservoir respectively to maintain the system symmetric about the two channels. For details about possible ways in which the system can be initialised see appendix A.1.

2.3.1 The open system steady state global density temporal behaviour

The system steady state is reached through the discussed stochastic dynamic particle hopping rules. The system is allowed to reach steady state after 10^7 MCS, each having 2×N particle hopping sampling steps, where $N = 201$ is the lattice size for each channel. Looking at a system of decoupled parallel channels ($\epsilon = 0$), we learn that at any given MCS, for any choice of boundary reservoir density other than $n_L = n_R = \bar{n}_L = \bar{n}_R = 1$,

Stellenbosch University http://scholar.sun.ac.za

the total site occupancy of each channel fluctuates like a random walk over a large range of values. The fluctuations happen about a unique mean total site occupancy. This behaviour is typical of open systems of channels that allow for an exchange of particle with reservoirs. At steady state the mean densities fluctuate about their respective mean occupancy given by

$$n_G = \frac{1}{N}\sum_{i=1}^{N}\langle \tau_i(t)\rangle_{\rm ss} \quad \text{and} \quad \bar{n}_G = \frac{1}{N}\sum_{i=1}^{N}\langle \bar{\tau}_i(t)\rangle_{\rm ss}\,. \tag{2.4}$$

The steady state mean channel occupancy is the key observable. In this case the notation $\langle\cdot\rangle$ denote a coarse-grained time average while τ_i and $\bar{\tau}_i$ designate the respective occupancy of an ith site on the channel lattice. The subscript ss reminds us that the measurements are taken from a system has that reached the steady state. In Fig. 2.4 we show the random walk behaviour of the mean channel density per MCS which is symmetric about the mean value. An important point to note is that these large density deviations about the mean in this case decrease with an increase in the system size. The choice of boundary reservoir density values directly determine the value of the mean bulk density for a channel and steady state particle flux.

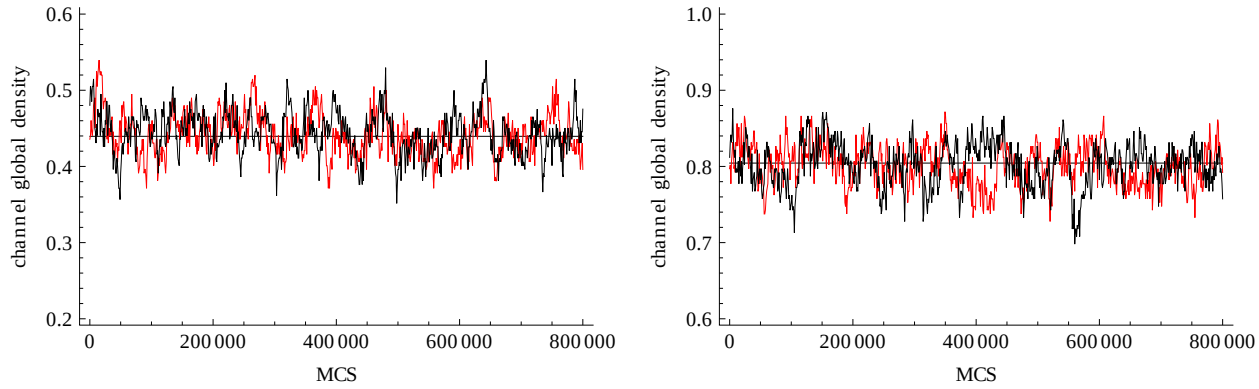

FIG. 2.4. Global density temporal behaviour for channel one (red coloured graph) and two (black coloured graph) in the case when the two channels are decoupled ($\epsilon = 0$) the reservoir densities n_L,n_R are set to: (a) 0.8 and 0.16; (b) 0.8 and 0.8 respectively.

Stellenbosch University http://scholar.sun.ac.za

2.3.2 Decoupled system steady state density current relation

Although the global density does not tell much about the individual particle behaviour, it is a particularly interesting quantity as it can be used analogously to the order parameter in classifying the emerging current density regimes for a decoupled system. At any given time the evolution of the mean bulk density of the system is determined by the reservoir density gradient along with the interfile interaction. In Fig. 2.5 the average global density results and the steady state current results for a fixed left reservoir density $n_L = 0.8$ are shown. When $n_L = n_R$, the system naturally equilibrates in which case, the average net flux $J_{\rm ss} = \bar{J}_{\rm ss} = 0$ while the average bulk density is the same as the reservoir densities.

Upon increasing the difference between the reservoir densities $\Delta n_r = \Delta\bar{n} = n_L - n_R$, the system is driven out of equilibrium and the steady state flux departs from its equilibrium value. When the right reservoir densities n_R are varied in such a way that $n_L \geq n_R$, we learn that the global mean density declines linearly with an increase in the gradient between the reservoirs Fig. 2.5(a) while the corresponding steady state current increases linearly Fig. 2.5(b). This behaviour is typical of driven systems having symmetric particle hopping rules.

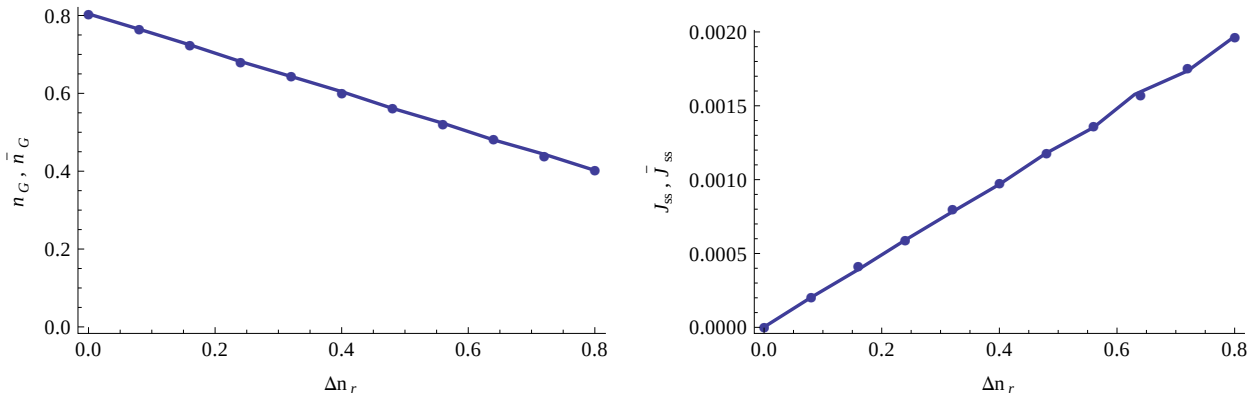

(a) (b)

FIG. 2.5. The global density n_G,$\bar{n}_G$ (a) and steady state current $J_{\rm ss}, \bar{J}_{\rm ss}$ (b) response to changes in the density gradient between reservoirs for channel one (line) and channel two(filled circles). The respective left reservoirs are kept at density $n_L = 0.8$ and the reservoir gradient Δn_r is varied in equally spaced steps. For each value of n_R the system started from different initial conditions and it was allowed to reach steady state over 10^7 Monte Carlo sweeps (MCS). The averages are taken over 10^7 MCS steps.

Stellenbosch University http://scholar.sun.ac.za

To characterise the current density relation more exactly, we used the Monte Carlo simulation to obtain the steady state current and the mean global density for different values of the right and left reservoir density Fig. 2.6. For a decoupled version of the system, we see a linear relationship between the difference of the reservoirs' density and the steady state flux. A summary of the global density-current relationship for various values of the difference between the right and left reservoir is given by the contour plots shown in Fig.2.7. In this case steady state flux appears to be independent of the global density.

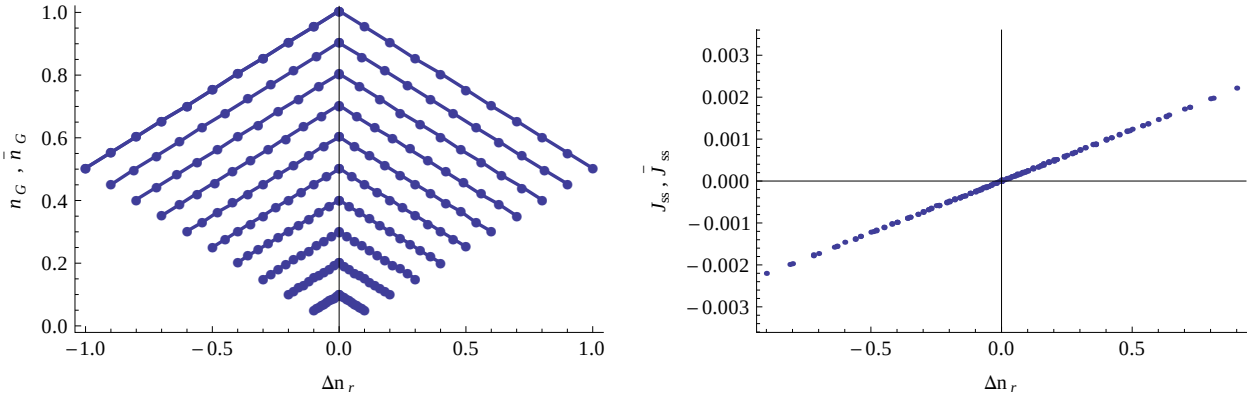

(a) (b)

FIG. 2.6. A summary of the RSU simulation results showing the steady state average global density $(n_G, \bar{n}_G)$ and steady state flux J_{ss} response to changes in the reservoir density. In (a) the steady state results for channel one (line) and channel two(filled circles) for varied values of the left reservoir densities n_L is shown while in (b) the corresponding steady state current flux is shown. The reservoir gradient Δn_r is varied in equally spaced steps. For each value of n_R the system started from independent initial conditions and the system was allowed to reach steady state over 10^7 Monte Carlo sweeps (MCS). The averages are taken over 10^7 MCS steps.

The fact that we can have the same current for different densities is an indication that the system manifests interesting steady-state current-density regimes. The regimes are analogous to the current-density phases that have been reported for a two coupled channel system with particles obeying asymmetric exclusion rules on a ring [Popkov and Peschel, 2001]. By comparing the two systems, we learn that in our system the steady state current-density can be classified into three main regimes of qualitative similar behaviour namely: Low density [LD], High density [HD] and Maximal current [MC] regime Fig. 2.8.

Stellenbosch University http://scholar.sun.ac.za

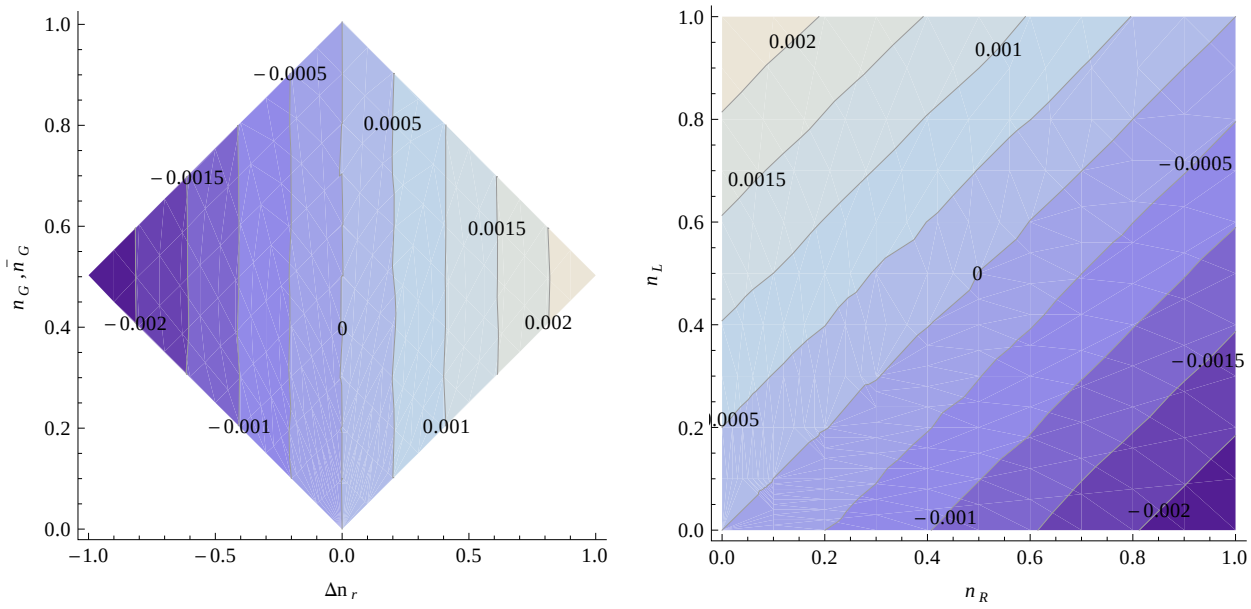

FIG. 2.7. A contour plot showing the relationship between the steady state current J_{ss}, the global mean density and the difference of the reservoir densities Δn_r (a) and a contour plot (b) showing the dependence of steady state current on the reservoir density n_L, n_R; The respective left reservoirs are kept at fixed density and the reservoir gradient Δn_r is varied in equally spaced steps. For each combination of n_L, n_R the system started from different initial conditions and it was allowed to reach steady state over 10^7 Monte Carlo sweeps (MCS). The averages are taken over 10^7 MCS steps.

Stellenbosch University http://scholar.sun.ac.za

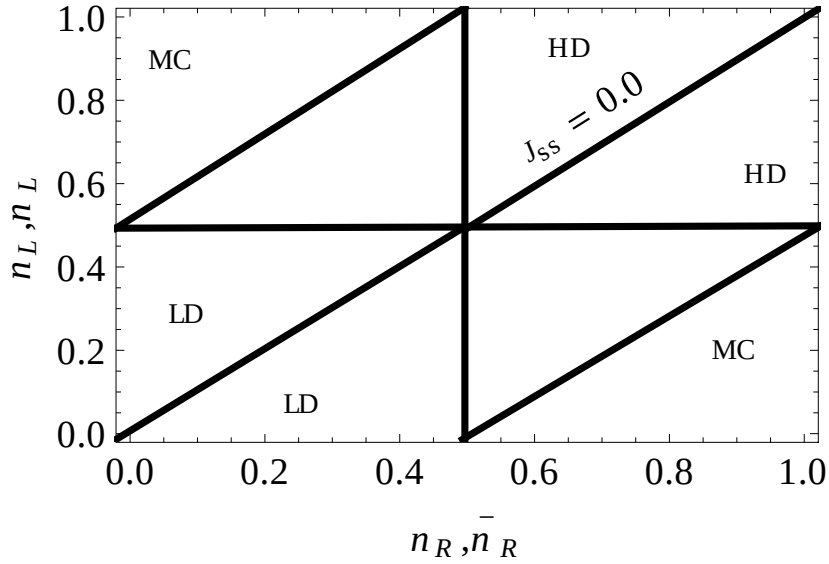

FIG. 2.8. A symmetry based depiction of the identified steady state current-density regimes that can be characterised by a distinctive current or density behaviour. The regions labelled LD, HD and MC correspond to the low density, high density and maximal current regime

For a single file system with asymmetric hopping rules, a steady state density profile can manifest these density regimes separated by a domain wall. The boundary between these current-density phases can easily be estimated analytically under a mean field theoretical treatment or by using extremal current principle. In such asymmetric single file system simulations the density phase transition point is estimated by identifying the location of the domain wall which is always located between the different phases. In our case the symmetry of the particle evolution rules are such that the co-existence of two density phase separated by a domain wall is not possible. This is due to the symmetry of the particle hopping rules. A systematic criterion identifying the boundary between different current-density regimes is not immediately obvious.

2.3.3 System sensitivity to the coupling strength

The interaction between the channels directly influence the transport properties of the system. In Fig. 2.9 we see a rather interesting scenario where the apparently simple chaotic pattern portrays a spatial coexistence of many global density phases between the two files. This happen upon switching on the interfile interaction parameter. This means that an

Stellenbosch University http://scholar.sun.ac.za

excursion of the global density of one file beyond the mean bulk density is accompanied by an excursion of the global density of the other file but in an opposite direction. The sum of the two densities is nearly constant. This could be a signal of the formation of dynamic particle clusters that could be related to possible traffic jam type behaviour within a file. For a driven asymmetric exclusion processes [Popkov and Peschel, 2001], similar patterns have also been reported under the name *seesaw phases* and *mixed phases*.

For our system seesaw phases are predominantly observed when the system is about to reach equilibrium. When the reservoir density drive the system out of equilibrium, the channels mean global density n_G evolution manifests mixed phases. In Fig. 2.9 typical mixed phases and seesaw phases for the bulk density are shown. The boundaries between the mixed phase and seesaw phase is not easy to draw as the system makes a continuous transition between the respective phases.

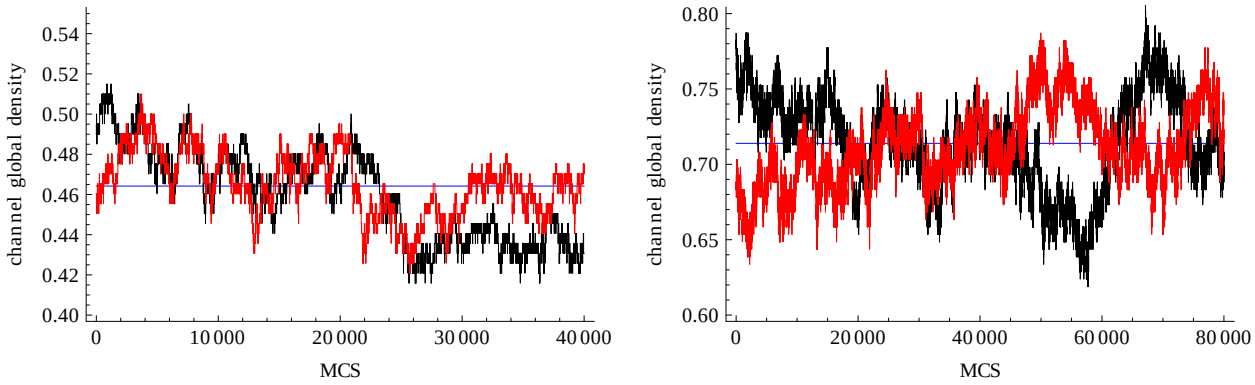

(a) MIXED PHASE (b) SEE-SAW PHASE 2

FIG. 2.9. The temporal behaviour of the global density for channel one (coloured red) and channel two (coloured black) obtained from the Monte Carlo simulation. The measurement of the channel global density are taken at every Monte Carlo seep (MCS). The two graphs are obtained from the reservoir densities and interaction parameter values: n_L,n_R,ϵ: (a) 0.90,0.00,0.4; (b) 0.90,0.81,0.4.

The existence of the global density phases suggests a possibility of interesting dynamic local structures such as equal time dynamic correlations. The RSU method is not a good alternative for accessing such dynamic quantities owing to the fact that measurements are performed after each MCS, which is not proportional to the real time. In the next section we present the cellular automaton simulation method which is very useful in accessing local dynamic observables such as the equal time particle density correlations.

Stellenbosch University http://scholar.sun.ac.za

2.4 Cellular automaton simulation

A cellular automaton is assembled by placing a sequential machine at each lattice point of a d-dimensional array and then connecting such machines uniformly. In our case a sequential machines is analogous to a node which consists of three cells with each cell having a different sense of velocity direction. The system is then evolved in discrete time steps. This discrete time system is evolved through a parallel update of the states of the sequential machines and a simultaneous state transition. One of the main advantages of a cellular automaton is its clear correspondence to a physical system it simulates. This means that a cellular automaton may not only be used within its computational capacity but also in the spirit of a computer laboratory experiment for testing ideas about a real physical phenomena. General features of a cellular automaton are listed below:

1. A discrete d-dimensional lattice of cells indexed by integers.
2. A set of cells grouped to constitute a node with all cells and therefore all nodes having equivalent properties.
3. Each cell and therefore each node can assume one state in a finite set of its respective possible states.
4. Each node interact with nodes that are in its neighbourhood.
5. A local transition rule which state how a state of a node evolves into a new configuration after a single discrete time step, taking into account possible interactions with its neighbourhood.

The original cellular automata were designed with deterministic transition rules. However, probabilistic local transition rules that bear the anticipated macroscopic system behaviour can also be constructed. In particular the influence of microscopic system interaction can easily be included in the scheme in a form of local phenomenological transition rules.

Stellenbosch University http://scholar.sun.ac.za

2.4.1 The one-dimensional two coupled files automaton

In this section, we explain how our model is mapped to a cellular automaton using the presented standard cellular automaton scheme. The continuous coupled file system is mapped to a discrete lattice version shown in Fig. 2.10. Each of the two files is represented by a lattice of size $2 \times N$ (coloured) and the reservoirs at the respective ends are represented by the non coloured regions of the lattice. Each of the reservoir lattice is of size 2×3.

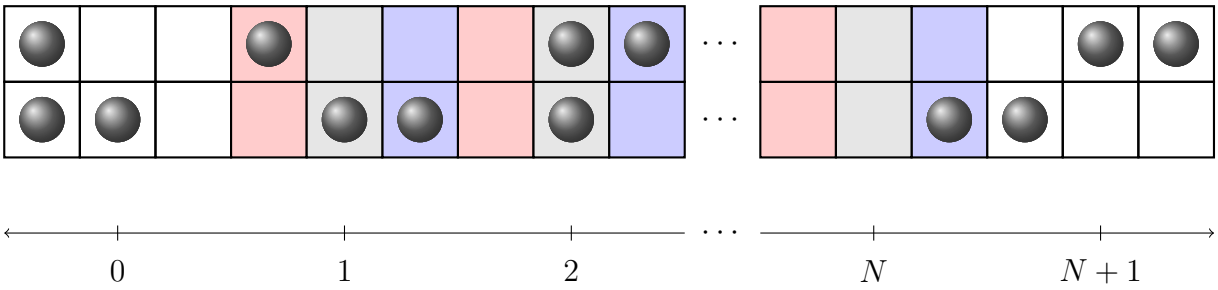

FIG. 2.10. A lattice for the two channel cellular automaton simulation. The non coloured part of the lattice represents the left and right reservoirs respectively. The coloured part of the lattice represents the channels. Particles occupying lattice cells having the same colour code have the same velocity direction after the collision step.

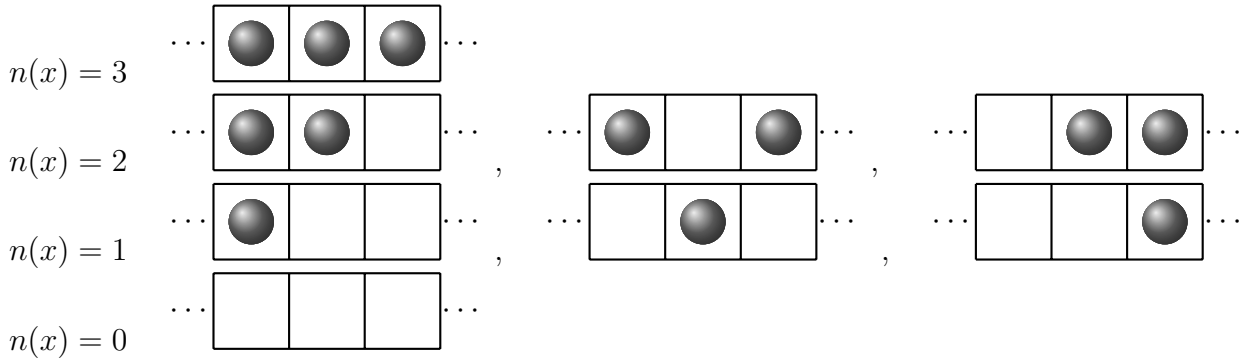

TABLE. 2.2. Figures in this table show all possible particle configurations at a node x in a one dimensional lattice; $n(x)$ denotes the total particle occupancy of the node x.

The cells in each row of the lattice are grouped into nodes. Each node consists of an array of three cells and each of these cells may be empty or occupied by at most one particle. All possible occupancy states of a node are shown in Table 2.2. For the case of two elastically coupled file system, the neighbourhood of a node in the bulk, for instance node x, consists of the next neighbouring nodes $x - \lambda$ and $x + \lambda$ from the same file and

Stellenbosch University http://scholar.sun.ac.za

the interacting neighbourhood $\bar{x}$ from the other file. Particles in each node obey uniform interaction rules. The microscopic dynamics entails a repetition of simultaneous particle collision and propagation in discrete time steps.

The particle collision event is a strictly local phenomenon in the sense that it involves a probabilistic shuffling of particles within a node. The probability of a post collision state for a given node, is also determined by the occupancy state of the interacting neighbourhood. It is defined in such a way that the collision rules mimic the influence of the local elastic deformation due to the presence of particles in the adjacent node of a neighbouring file. For example, if a node x in the first file is occupied by a single particle and the interacting neighbourhood is vacant, all post shuffling occupancy states of the first file node are equally probable meaning that the probability that there will be a particle at cell i of the node is $p_i(x) = \frac{1}{3}$, where the index $i \in \{1, 2, 3\}$ enumerates the cells in a node.

Let us consider the case when both node x and the interacting neighbourhood $\bar{x}$ are simultaneously occupied by only one particle each. The probability that, after the shuffling step, a particle in node x occupies a cell that is adjacent to an occupied cell in the interacting neighbourhood is lower and it may be defined as $p_i(x) = \frac{1-\epsilon}{3-\epsilon}$, while the probability that the particle resides in a cell that is adjacent to an unoccupied cell from the interacting neighbourhood is $p_i(x) = \frac{1}{3-\epsilon}$. Table 2.3 is dedicated to showing the probability of various post shuffling end states given the occupancy of a corresponding interacting neighbourhood. Note that particle collision at a node conserves the number of particles per given node but not the particle momentum because of thermalisation.

After collision the particles are simultaneously translated to the next neighbouring nodes of the same file. The translation rule is as follows: particles occupying the left cell of a node propagate to the left cell of a left neighbouring node and particles occupying the right cell of a node propagate to the right cell of a right neighbouring node while particles in the middle cells remain stationary. Particles can only evolve one-dimensionally along the lattice, with the particle moving as independent random walkers occupying equally spaced lattice sites with occupancy states updated in discrete time steps. For details about how the algorithm is implemented using multi-dimensional arrays see appendix A.2.

The cellular automaton algorithm confirms the boundary driven behaviour established through the RSU algorithm for a decoupled version of the system, We obtain qualitatively

Stellenbosch University http://scholar.sun.ac.za

p_1	$\frac{1}{3}$	$\frac{1}{3-\epsilon}$	$\frac{1-\epsilon}{3-\epsilon}$	$\frac{1-\epsilon}{3-\epsilon}$	$\frac{1}{3-2\epsilon}$	$\frac{1}{3-2\epsilon}$	$\frac{1-\epsilon}{3-2\epsilon}$	$\frac{1}{3}$	
p_2	$\frac{1}{3}$	$\frac{1}{3-\epsilon}$	$\frac{1-\epsilon}{3-\epsilon}$	$\frac{1}{3-\epsilon}$	$\frac{1-\epsilon}{3-2\epsilon}$	$\frac{1-\epsilon}{3-2\epsilon}$	$\frac{1}{3-2\epsilon}$	$\frac{1}{3}$	
p_3	$\frac{1}{3}$	$\frac{1-\epsilon}{3-\epsilon}$	$\frac{1}{3-\epsilon}$	$\frac{1}{3-\epsilon}$	$\frac{1-\epsilon}{3-2\epsilon}$	$\frac{1-\epsilon}{3-2\epsilon}$	$\frac{1-\epsilon}{3-2\epsilon}$	$\frac{1}{3}$	
q_1	$\frac{1}{3}$	$\frac{1}{3-2\epsilon}$	$\frac{1-\epsilon}{3-2\epsilon}$	$\frac{1-\epsilon}{3-2\epsilon}$	$\frac{1-\epsilon}{3-4\epsilon}$	$\frac{1-2\epsilon}{3-4\epsilon}$	$\frac{1-\epsilon}{3-4\epsilon}$	$\frac{1}{3}$	
q_2	$\frac{1}{3}$	$\frac{1-\epsilon}{3-2\epsilon}$	$\frac{1}{3-2\epsilon}$	$\frac{1-\epsilon}{3-2\epsilon}$	$\frac{1-\epsilon}{3-4\epsilon}$	$\frac{1-\epsilon}{3-4\epsilon}$	$\frac{1-2\epsilon}{3-4\epsilon}$	$\frac{1}{3}$	
q_3	$\frac{1}{3}$	$\frac{1-\epsilon}{3-2\epsilon}$	$\frac{1-\epsilon}{3-2\epsilon}$	$\frac{1}{3-2\epsilon}$	$\frac{1-2\epsilon}{3-4\epsilon}$	$\frac{1-\epsilon}{3-4\epsilon}$	$\frac{1-\epsilon}{3-4\epsilon}$	$\frac{1}{3}$	

TABLE. 2.3. A look up table for the post shuffling states probabilities given a neighbourhood configuration. In this table the first row provides possible states for any interacting neighbourhood to node x while the last column depicts probable states for the node x. On the table p_i and q_i denote the shuffling probability when there is only one particle and two particles in the reference node respectively. Each of the probabilities is expressible in terms of the coupling parameter ϵ.

comparable flux and density changes with adjustments in the boundary reservoir densities. See Fig. 2.11[1]. As the coupling parameter is increased, the cellular automaton algorithm proves to be more superior to the RSU as it effectively captures effects such as equal time density-density correlations, this will be more evident in the next section.

[1]The magnitude of the flux is not necessarily identical owing to the fact that channels of different lengths were used for each simulation.

Stellenbosch University http://scholar.sun.ac.za

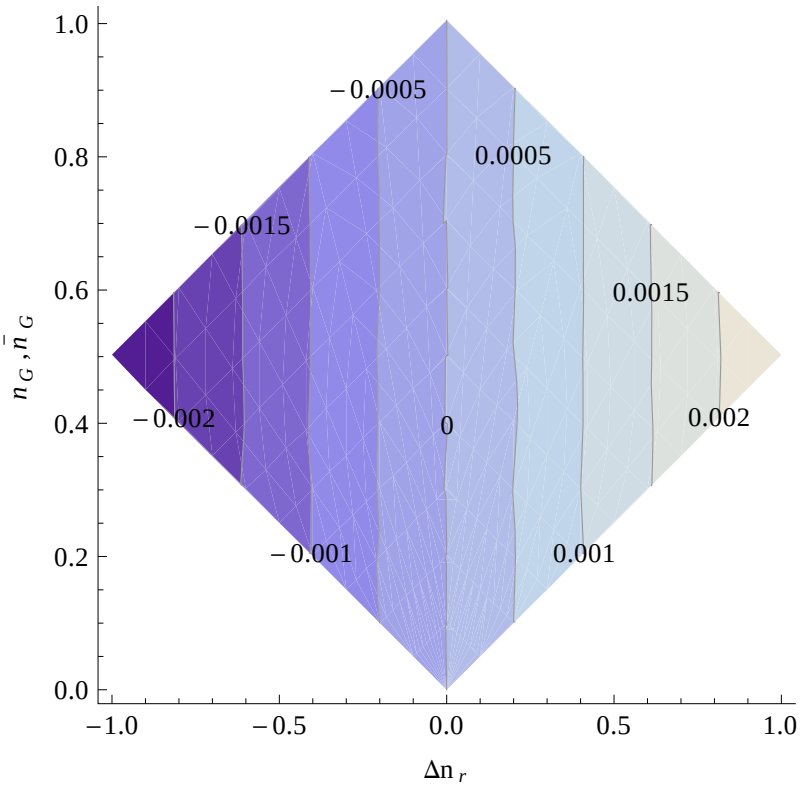

(a)

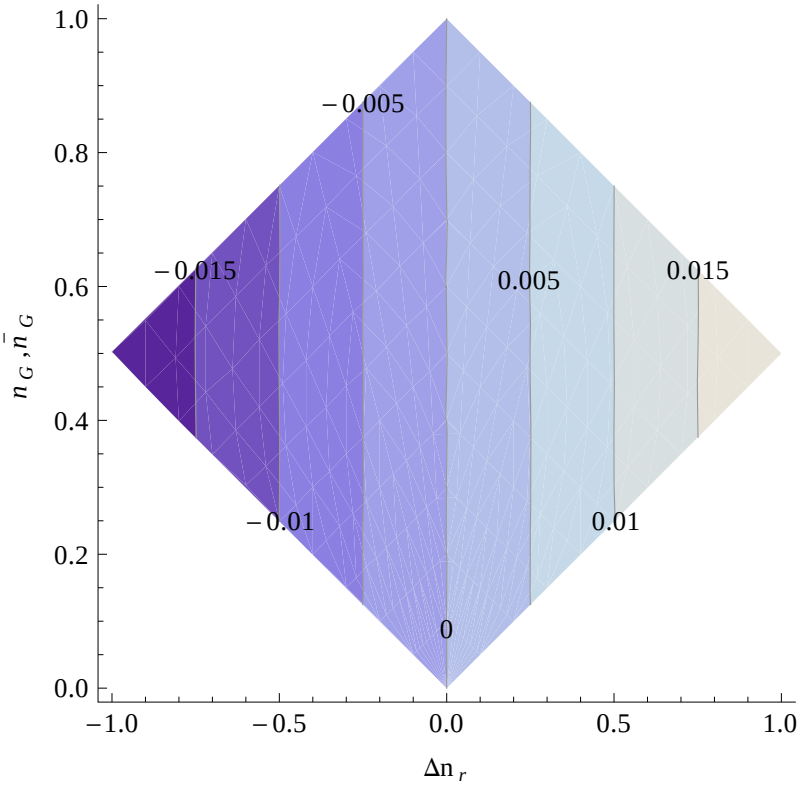

(b)

FIG. 2.11. A contour plot showing the relationship between the steady state current J_{ss}, the system mean global density and the difference between the reservoir densities Δn_r. The contour plot in (a) obtained from RSU simulation for channels of ($N = 201$) sites while that in (b) is obtained from CU simulation for a channels of 51 nodes. Under each method, for any combination of n_L, n_R the system started from different initial conditions and it was allowed to reach steady state over 10^7 time steps. The averages are taken over

Stellenbosch University http://scholar.sun.ac.za

2.4.2 The system sensitivity on the channel coupling strength

Looking at the mean global density for various values of the channel coupling parameter ϵ, the system portrays two interaction regions that are characterised by different qualitative behaviour. This can be seen in Fig. 2.12. In order to interpret the behaviour of the system at the level of global mean density, we have to study the nature of the density profile for each of the regimes.

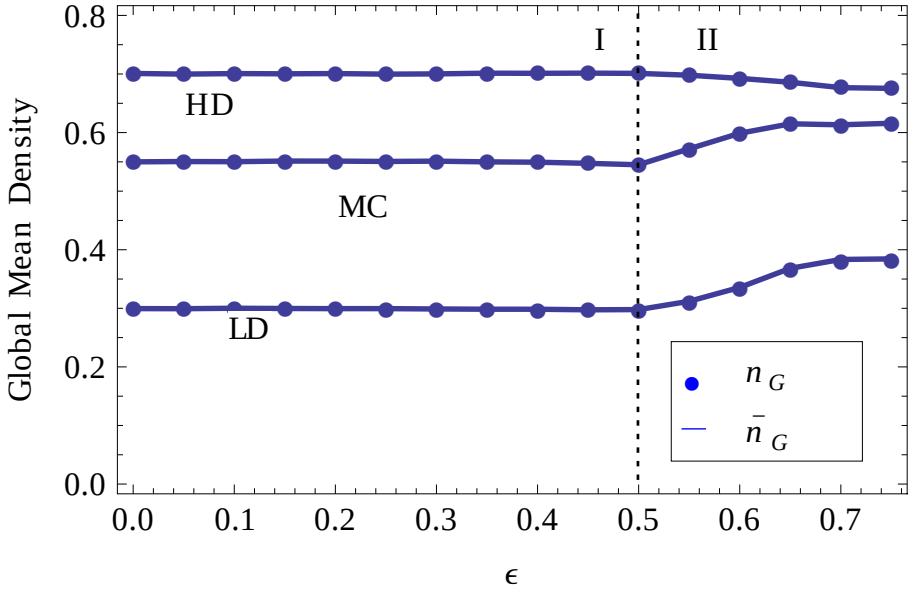

FIG. 2.12. A graph showing how the global density vary with increments in the coupling parameter. The plots show typical global density behaviour in the low density regime (LD): $n_L = 0.4, n_R = 0.2$, high density regime (HD);$n_L = 0.8, n_R = 0.6$ and maximal current regime (MC): $n_L = 0.9, n_R = 0.2$.

For all interaction parameter values, the respective steady state channel density profiles $\rho(x)$ are continuous in the interior of the channels i.e

$$\lim_{x->N} \rho(x) = \lim_{x->N} \bar{\rho}(x) = \rho_R(N) \tag{2.5}$$

and

$$\lim_{x->0} \rho(x) = \lim_{x->0} \bar{\rho}(x) = \rho_L(0). \tag{2.6}$$

For the interaction parameter range $0 \leq \epsilon \leq 0.5$, region(I), the density profile belonging to the LD, HD and MC current density regimes looks almost like a linear interpolation of

Stellenbosch University http://scholar.sun.ac.za

the density between the respective reservoirs Fig. 2.13. This is a behaviour expected when the files are decoupled. However, the plot of the deviation of the density profiles from a simple linear density interpolation between the boundaries,

$$n(x) = n_L - \frac{x}{L}(n_L - n_R), \tag{2.7}$$

is indicative of the fact that the coupling between channels has a little influence on the system steady-state density profile. The magnitude of the percentage deviation for all regimes in this coupling parameter range, suggests that the steady density profile is amenable to some form of mean field treatment which ignores correlations to some extent. Such mean field calculations will be the subject of chapter 3.

Upon comparing the density profile deviations, also shown in Fig 2.13 for different density-current regimes, we conclude that density-density correlations can possibly induce different behaviour depending on the channel local occupancy. An increase in the coupling strength presents the particle flow with obstacles. This leads to a temporary channel blocking which may result in an increase in the channel density for the less densely occupied regions. The flattening of the occupancy profile with an increase in the channel coupling parameter points us to this possibility.

In region (II), $\epsilon > 0.5$, an increase in the channel coupling parameter has a strong impact on the system Fig. 2.14. Looking at the steady state density profiles for the LD and MC we can see that there is an increase in particle density in the regions of the channel having lower density while there is a decrease in density in the regions of the channels having high density.

To rationalise the emerging behaviour for these regimes, for the high coupling parameter range, one can imagine that a time dependent particle site blocking in the channel regions having lower occupancy encourages particle accumulation behind blocked sites leading to a traffic jam like behaviour. This can lead to an increasing in the channel occupancy locally resulting in an overall increase in the global channel mean density. In the HD regime we see a decline in the mean global density. This is simply due to a discouraged simultaneous occupancy of the adjacent sites between channels. Looking at the occupancy profile corresponding to the interaction region II, $(\epsilon > 0.5)$, we also realise that the system node

Stellenbosch University http://scholar.sun.ac.za

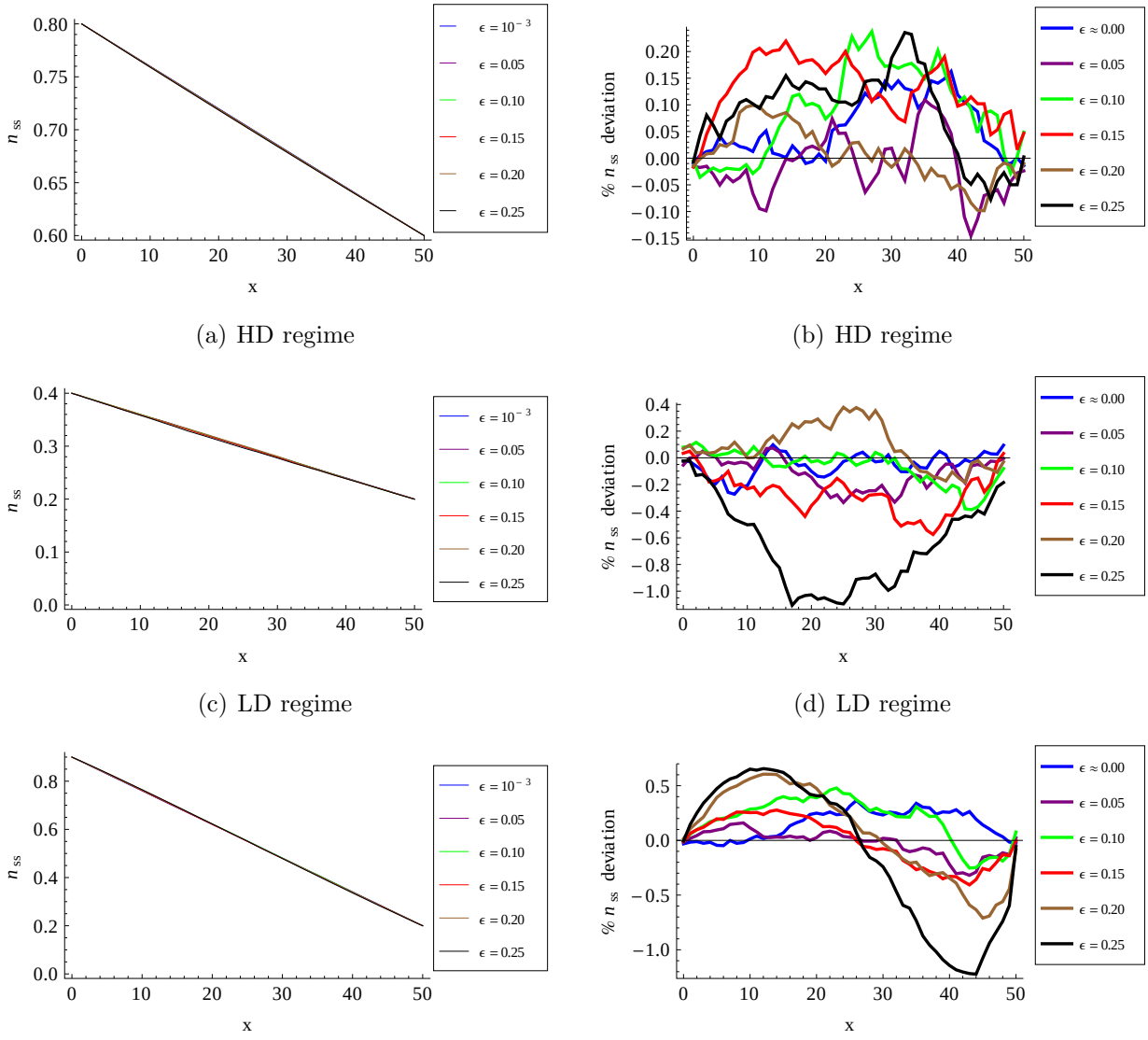

(a) HD regime (b) HD regime

(c) LD regime (d) LD regime

(e) MC regime (f) MC regime

FIG. 2.13. Plot of the weakly coupled two channel system cellular automaton simulation density profile for (a) high density regime (HD): $n_L = 0.8, n_R = 0.6$, (c) the low density regime (LD) $n_L = 0.4, n_R = 0.6$ and (e) Maximal current regime (MC) $n_L = 0.9.n_R = 0.2$. Graphs (b),(d) and (e) present the cellular automaton density profile percentage deviation from the linear interpolation (2.7) for the HD,LD and MC regimes respectively. For each choice of reservoir densities, the simulation was allowed to reach steady state over 10^7 times steps and then the steady state averages were taken over 10^7 time steps.

Stellenbosch University http://scholar.sun.ac.za

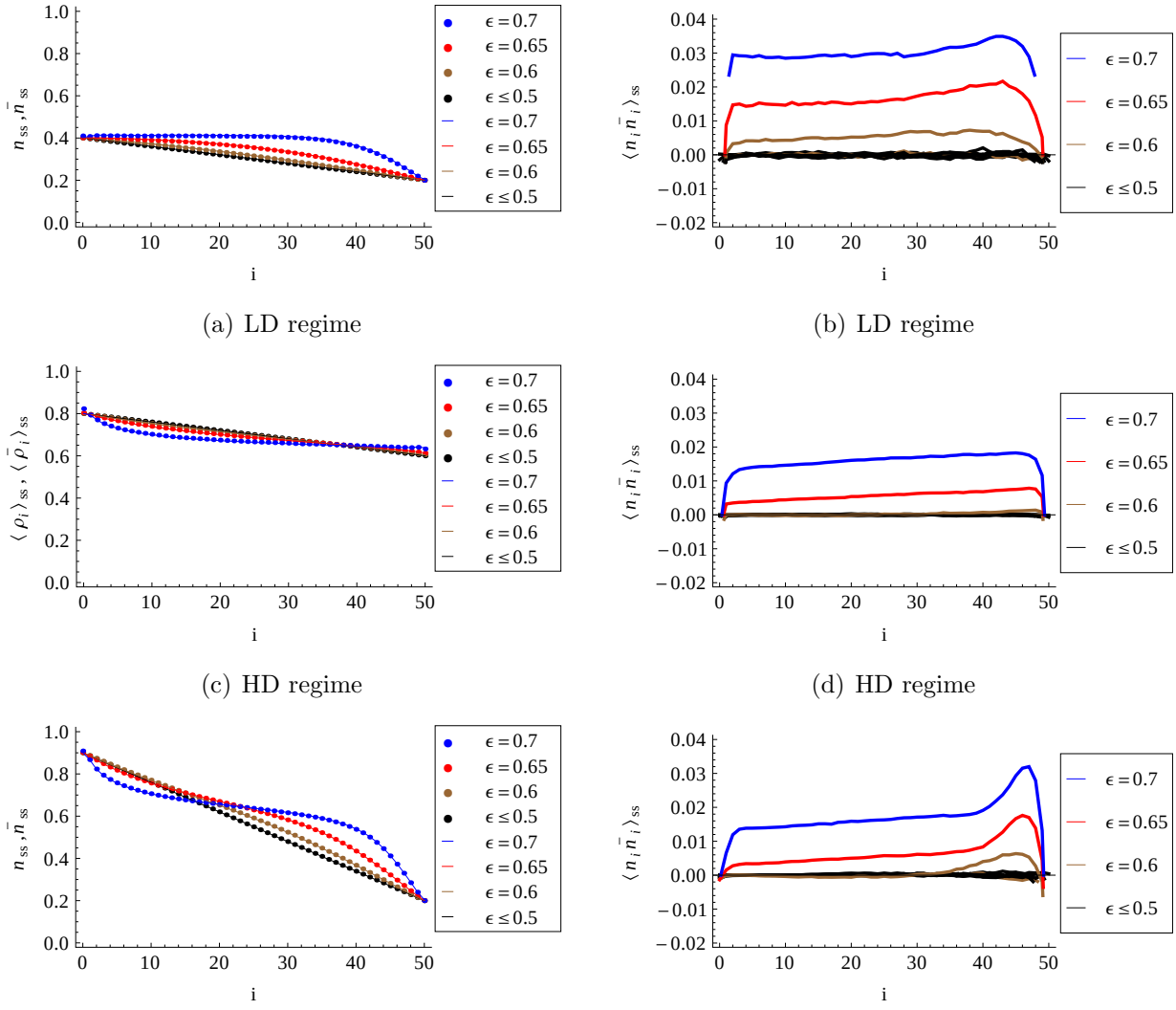

(a) LD regime

(b) LD regime

(c) HD regime

(d) HD regime

(e) MC regime

(f) MC regime

FIG. 2.14. Channel one (line graph) and channel two (dotted graph) steady state density profile obtained from the cellular automaton simulation for the coupled case. The respective graphs show the density profile for:(a) low density regime (LD): $n_L = 0.4, n_R = 0.2$, (c) high density regime (HD): $n_L = 0.8, n_R = 0.6$ and (e) maximal regime regime (MC): $n_L = 0.9, n_R = 0.2$ for different coupling parameters values. The graphs of the interfile site density-density for the (b) LD, (d) HD and (f) MC regimes are obtained from the same boundary reservoir densities as the corresponding density profiles. The graphs shown are for different values of the coupling parameter ϵ.

Stellenbosch University http://scholar.sun.ac.za

occupancy becomes highly correlated. This confirms that channel blocking is accompanied by particle clustering.

The average steady state particle flux in the interaction region I insensitivity to the coupling strength. The evidence of the steady state flux sensitivity to the interaction can be seen Fig. 2.15. Notably there is linear decline in the steady state current with an increase in interaction for all interaction parameters in the range $0.0 \leq \epsilon \leq 0.5$ this is not surprising as the coupling strength presents the particle flow with obstacles which lead to a decline in the particle flux.

We also see a dramatic increase in particle flux for an otherwise correlated system in this strongly coupled case. Clearly the system remodulates the particle flux in such a way that it maximises the efficiency of the diffusion processes in response to the increase in particle occupancy on the less denser regions of the channels. The nature of the dynamical particle behaviour can be identified by studying the structures that form at steady state within a channel for varied values of the interaction parameter.

Stellenbosch University http://scholar.sun.ac.za

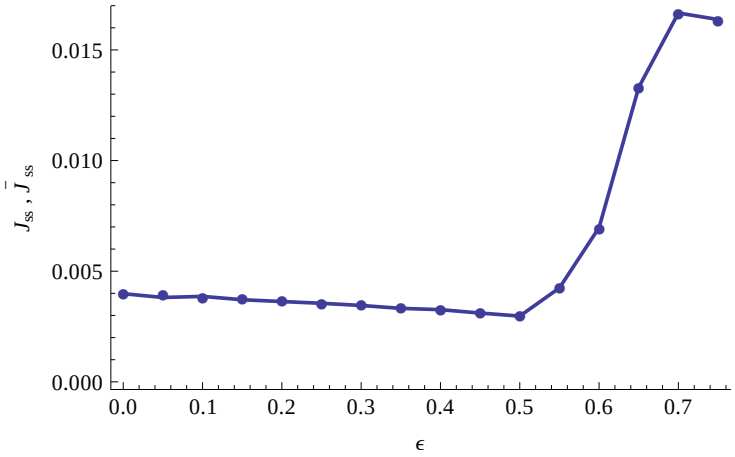

(a)

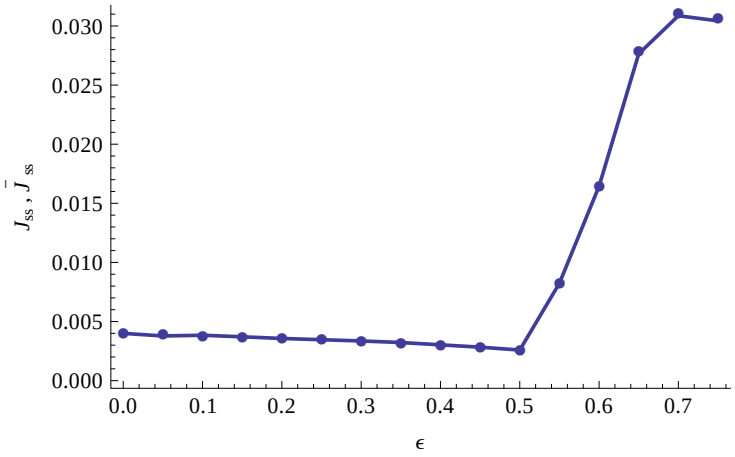

(b)

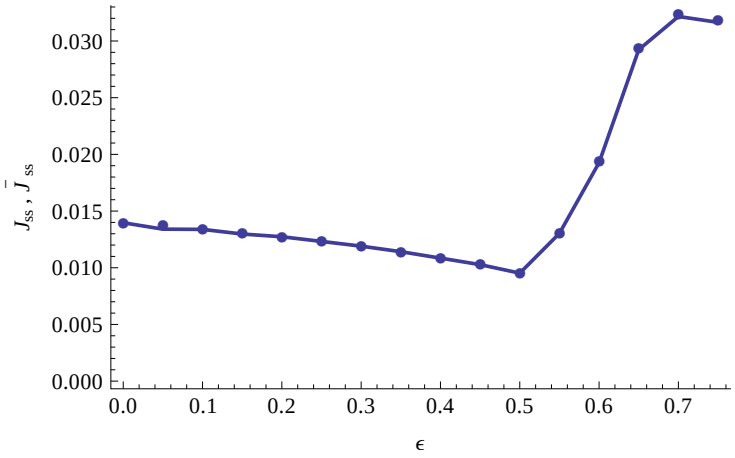

(c)

FIG. 2.15. A plot showing how the steady state particle fluxes (J_{ss} and $\bar{J}_{ss}$) respond to changes in the interaction parameter ϵ for the channel one (line graph) and channel two (dotted graph) respectively. The graphs show typical steady state flux for (a) low density regime (LD): $n_L = 0.4, n_R = 0.2$, (b) high density regime (HD): $n_L = 0.8, n_R = 0.6$ and (c) maximal current regime (MC): $n_L = 0.9, n_R = 0.2$ respectively.

Stellenbosch University http://scholar.sun.ac.za

2.5 Summary of the simulation experiment

In this chapter we have identified some interesting mean global density temporal phases such as see-saw phases and mixed phases. We have also characterised the system in terms of current-density regimes. The system sensitivity to changes in the channel coupling parameter has been explored. We have discovered that for the interaction parameter $\epsilon > 0.5$, the system occupancy profile deviates strongly from a simple linear density interpolation between boundaries. This steady state density profile behaviour is accompanied by a dramatic increase in the steady state flux in contrast to the flux obtained for $\epsilon < 0.5$. We realize that an increase in the coupling parameter discourage occupancy of adjacent sites on the dense regions of the files. This leads to an increase in the occupancy of the file near the reservoir that is kept at a lower density. As that happen the steady state flux remodulates itself to maximize the efficiency of the diffusion process.

Interestingly, for the coupling parameter range $\epsilon \leq 0.5$ correlation do not play a significant role. We anticipate that the system steady state density profile and the particle flux can be predicted by some simple analytic mean field theory without correlations. The next chapter is dedicated to the development of such a mean field theory.

The cellular automata approach is found to be relatively fast as compared to RSU. It successfully produces the dynamic behaviour of the systems as well as the ensemble properties describable by some form of continuous-time master equation or diffusion equation. In the next chapter we shall focus in deriving such equations. By simulating an otherwise continuous system dynamics with a fundamentally discrete simulation scheme, we traded away some physical details of the system, such as individual particle identity. The main drawback of the lost particle identity is that it becomes impossible to track individual particles.

Nevertheless, the beauty of the approach is that it remains faithful to the underlying microscopic physical properties of the system such as particle motion simultaneity, particle interaction locality and perhaps time reversibility. It is also well known that one is able to generate emerging system behaviour such as long range global patterns and correlations without introducing any fundamental length scales other than the size of the neighbourhood about each cell.

Stellenbosch University http://scholar.sun.ac.za

Chapter 3

Analytic treatment of the System cellular automaton

As we have seen in chapter 2 a cellular automaton simulation is based on the notion that stochastic particle dynamics could be achieved through a combination of probabilistic particle collision rules and deterministic particle propagation rules. The same ideas can be extended to formulate a simple analytic theory describing the system at a mean field level under the assumption that the inter-channel density-density correlation could be ignored to some extent. In this chapter we show how the steady state current and the steady state density profile can be calculated from the cellular automaton framework. We start by introducing the notation used in translating the two coupled channel lattice model into an analytic cellular automaton calculation.

3.1 Analytic treatment of two coupled channels cellular automaton

Each channel can be quantified by a one dimensional open boundary lattice domain $X \subset R$, of length L, having lattice nodes labelled by the position variable x. Each node is connected to the next nearest neighbours through a lattice space unit λ. For each node we associate three occupancy states labelled $\tau_1(x,t), \tau_2(x,t)$ and $\tau_3(x,t)$. One particle is allowed to reside per occupancy state at a given time step. This allows us to express the dynamics of each occupancy state $\tau_i(x,t)$ in terms of boolean occupancy variables $\eta_i(x,t)$ through a

Stellenbosch University http://scholar.sun.ac.za

relation $\tau_i(x,t) = \eta_i(x,t) \in \{0,1\}^3$, where the index $i \in \{1,2,3\}$. For each state $\eta_i(x,t) = 0$ denotes the absence of a particle while $\eta_i(x,t) = 1$ indicates the presence of a particle. Each occupancy state in a node is associated with a particle velocity direction c. In particular,

- $\tau_1(x,t)$ is associated with a left moving particle velocity direction $c = -1$,
- $\tau_2(x,t)$ is associated with a stationary particle velocity direction $c = 0$ while,
- $\tau_3(x,t)$ is associated with a right moving particle velocity direction $c = 1$.

3.1.1 Particle Collision

We have seen in chapter 2 that a probabilistic particle collision results in particles exchanging occupancy states, hence leading to particles assuming new velocity directions. Particle collision per node simply means that particles can be created or destroyed per given node in such a way that the number of particles per node is conserved but the particle momentum per node, on the other hand, is not conserved. In that case, for particle number conservation to hold, the inter-channel particle exchange is simply not allowed.

To achieve a random motion of particles at each node we introduce the lattice gas automaton interaction rules ($\mathcal{R}^I$) which probabilistically changes the distribution of each node per time step taking into account the effective collisions that the particles may undergo. In this system a collision step takes care of the effects of deformation due to the presence of particles in adjacent position from neighbouring channels. For a given neighbourhood $\mathcal{N}_3^I(x) = \{x\}$ the before interaction occupancy variables $\eta_i(x,t)$ is replaced by the after interaction state $\eta_i^I(x,t)$ according to a set of probabilistic interaction rules. Formally this can be stated as

$$\mathcal{R}_i^I(\tau_{\mathcal{N}(x)}(t)) = \eta_i^I(x,t), \quad \text{where} \quad \mathcal{R}^I = \{\mathcal{R}_i^I\}_{i=1}^3 \tag{3.1}$$

These interaction rules outline all post collision states according to a probability which is determined by the occupancy of the neighbouring channels. The occupancy states per node, in a one dimensional lattice can be uniquely permuted in six different ways (Table. 3.1). A convenient way of shuffling each node occupancy is by introducing a shuffling Bernoulli-type boolean variable say $\varepsilon_j(x,t) = \{0,1\}$, $j = \{0,\cdots,6\}$, which is independent of the history of the automaton evolution and it is defined such that the probability of

Stellenbosch University http://scholar.sun.ac.za

choosing a post collision state p_j or the probability of choosing the outcome of a post shuffling state is simply the probability of picking each $\varepsilon_j(x,t)$,

$$p_j := P_{\mathcal{N}^I}(\varepsilon_j(x,t)=1) \quad \text{for} \quad j=1,\cdots,6. \tag{3.2}$$

This is achieved by demanding that, for each time step t, for each node of each channel, only one shuffling variable is equal to one. Thus,

$$\sum_{j=1}^{6}\varepsilon_j(x,t)=\sum_{j=1}^{6}p_j=1 \quad \forall x\in N. \tag{3.3}$$

For an isolated channel, the state of the three occupancy states of a node (x,t) can be defined in terms of the occupancy variables and shuffling variables as

$$\tau_1(x,t) = (\varepsilon_1+\varepsilon_2)\eta_1(x,t)+(\varepsilon_3+\varepsilon_4)\eta_2(x,t)+(\varepsilon_5+\varepsilon_6)\eta_3(x,t), \tag{3.4a}$$
$$\tau_2(x,t) = (\varepsilon_3+\varepsilon_2)\eta_1(x,t)+(\varepsilon_1+\varepsilon_6)\eta_2(x,t)+(\varepsilon_2+\varepsilon_4)\eta_3(x,t), \tag{3.4b}$$
$$\tau_3(x,t) = (\varepsilon_5+\varepsilon_6)\eta_1(x,t)+(\varepsilon_2+\varepsilon_5)\eta_2(x,t)+(\varepsilon_1+\varepsilon_3)\eta_3(x,t). \tag{3.4c}$$

In this case, the probability of each post collision configuration is uniform

$$p_j=\langle\varepsilon_j(x,t)\rangle=\frac{1}{3!} \quad \text{and} \quad \sum_{j=1}^{3!}p_j=\sum_{j=1}^{3!}\langle\varepsilon_j(x,t)\rangle=1. \tag{3.5}$$

Since only one of the ε_i's can be non-zero per given time step, the occupancy of each of the three states $\tau_i(x,t)\in\{0,1\}$. The fact that the lattice has a fixed number of occupancy

	τ_1	τ_2	τ_3
ε_1	η_1	η_2	η_3
ε_2	η_1	η_3	η_2
ε_3	η_2	η_1	η_3
ε_4	η_2	η_3	η_1
ε_5	η_3	η_1	η_2
ε_6	η_3	η_2	η_1

TABLE. 3.1. Probable post-shuffling node configurations matched with their selection boolean variable.

states for all nodes allows all the occupancy states to have equal permutations, therefore we can define a permutation group $\mathcal{A}$ isomorphic to a group of permuting m objects $\Pi(m)$ for

Stellenbosch University http://scholar.sun.ac.za

our model. The permutation group turns out to be isomorphic to the multiplicative group $\mathcal{M}(m)$ of $m \times m$ Boolean orthogonal matrices $M = [M_{ij}]$, $i = 1, \cdots, m$ and $j = 1, \cdots, m$ in that each row and column of matrices in $\mathcal{M}$ has only one entry which is equal to unity. We can therefore conclude that the collision operator $\mathcal{R}^I$ is fully characterised by a probability distribution $\mathcal{P}_{\mathcal{M}(m)}$ on $\mathcal{M}(m)$ induced by the isomorphism I on the probability $\mathcal{P}_{\mathcal{A}(m)}$ i.e

$$\mathcal{P}_{\mathcal{M}(3)}(\cdot) = \mathcal{P}_{\mathcal{A}(3)} I^{-1}(\cdot). \tag{3.6}$$

The permutation group for the occupancy state of each node can be expressed as

$$\mathcal{A} = \left\{ \begin{pmatrix} 1 & 0 & 0 \\ 0 & 1 & 0 \\ 0 & 0 & 1 \end{pmatrix}, \begin{pmatrix} 1 & 0 & 0 \\ 0 & 0 & 1 \\ 0 & 1 & 0 \end{pmatrix}, \begin{pmatrix} 0 & 1 & 0 \\ 1 & 0 & 0 \\ 0 & 0 & 1 \end{pmatrix}, \begin{pmatrix} 0 & 0 & 1 \\ 1 & 0 & 0 \\ 0 & 0 & 1 \end{pmatrix}, \begin{pmatrix} 0 & 0 & 1 \\ 0 & 1 & 0 \\ 1 & 0 & 0 \end{pmatrix}, \begin{pmatrix} 0 & 1 & 0 \\ 0 & 0 & 1 \\ 1 & 0 & 0 \end{pmatrix} \right\}.$$

Every matrix element of the group $\mathcal{A}$ corresponds to a unique shuffling variable $\varepsilon_j(x,t)$. The matrices are such that their respective column entries are related to the particle occupancy states states τ_i and the row entries are related to the occupancy variables $\eta_i(x,t)$'s. This allows us to rewrite equations (3.4a), (3.4b) and (3.4c) compactly in the following expressions

$$\tau_i(x,t) = \mathcal{R}(\eta(x,t)) = \sum_{l=1}^{6} \varepsilon_l(x,t) \sum_{k=1}^{3} \eta_k(x,t) a_{ki}^l, \quad i \in \{1,2,3\}, \tag{3.7}$$

where a_{li}^j is a matrix element of $\mathcal{A}_j \in \mathcal{A}$. Now let us consider the case where we have a system of two elastically coupled channels. The above discussed local cellular automaton dynamic rules can be appropriately redefined to incorporate interaction with particles in other channels. For each of the three occupancy states of a node, the post shuffling state occupancy expressed in terms of the shuffling variables ε_l and occupancy variables η_k can be defined as

$$\begin{aligned} \tau_i(x,t) = \mathcal{R}_{\mathcal{N}^I}(\eta(x,t)) \quad &= \quad \sum_{k=1,l=1}^{3,6} \varepsilon_l(x,t)\eta_k(x,t)a_{ki}^l \left(1 - \sum_{k'=1,l'=1}^{3,6} \bar{\varepsilon}_{l'}(x,t)\bar{\eta}_{k'}(x,t)a_{k'i}^{l'}\right) \\ &+ \quad \left(\sum_{l=1,l'=1}^{6,6} \varepsilon_l{}'(x,t)\bar{\varepsilon}_{l'}(x,t) \sum_{k=1,k'=1}^{3,3} \eta_k(x,t)\bar{\eta}_{k'}(x,t)a_{ki}^l a_{k'i}^{l'}\right). \end{aligned} \tag{3.8}$$

The first term on the right in equation (3.8) tells us that: if there is no particle on an adjacent occupancy state i of the neighbouring node from the adjacent channels, the node

Stellenbosch University http://scholar.sun.ac.za

occupancy is exactly that of an uncoupled channel. On the other hand, if there is a particle on the corresponding neighbouring location on the adjacent channel, the ith state is occupied at lower probability

$$\langle \varepsilon_j{}'(x,t)\rangle = (1-\epsilon)\,\langle \varepsilon_j(x,t)\rangle \quad \text{where} \quad \langle \varepsilon_j(x,t)\rangle = p_j. \tag{3.9}$$

3.1.2 Particle propagation

The collision (interaction) step is followed by a deterministic propagation (P) step in which particles are moved simultaneously to the associated neighbouring nodes on the same channels. As mentioned earlier, particle migration happens in the direction of a particle velocity arrow. This means that a particle in occupancy state (x, c_i) at a specific time is moved to another occupancy state $(x + \lambda c_i, c_i)$ in the next time step.

3.2 System steady state macroscopic properties

3.2.1 The channel particle flux

Having defined the microscopic occupancy of each occupancy state, the cellular automaton particle flux can be defined as the difference of the average left moving particle occupancy at node x and the average right moving particle occupancy at a node $x - \lambda$,

$$J(x - 0.5\lambda, t) = \langle \tau_1(x,t)\rangle - \langle \tau_3(x-\lambda,t)\rangle\,. \tag{3.10}$$

The notation $\langle\cdot\rangle$ in this case denotes a coarse grained time average. Using the state occupancy definition in equation (3.8), the steady state current can be expressed as function of the shuffling and occupancy state occupancy variables of the two involved neighbouring

Stellenbosch University http://scholar.sun.ac.za

lattice nodes as follows

$$\begin{aligned} J(x-0.5\lambda,t) &= \left\langle \sum_{k=1,l=1}^{3,6} \varepsilon_l(x,t)\eta_k(x,t)a^l_{k1} - \sum_{s=1,r=1}^{3,6} \varepsilon_r(x-\lambda,t)\eta_s(x-\lambda,t)a^r_{s3} \right\rangle \\ &- \epsilon \left[\left\langle \sum_{l=1,l'=1}^{6,6} \varepsilon_l(x,t)\bar{\varepsilon}_{l'}(x,t) \sum_{k=1,k'=1}^{3,3} \eta_k(x,t)\bar{\eta}_{k'}(x,t)a^l_{k1}a^{l'}_{k'1} \right\rangle \right. \\ &- \left. \left\langle \sum_{r=1,r'=1}^{6,6} \varepsilon_r(x-\lambda,t)\bar{\varepsilon}_{r'}(x-\lambda,t) \sum_{s=1,s'=1}^{3,3} \eta_s(x-\lambda,t)\bar{\eta}_{s'}(x-\lambda,t)a^r_{s3}a^{r'}_{s'3} \right\rangle \right]. \end{aligned} \tag{3.11}$$

The shuffling variables on the two channels ϵ_i and $\bar{\epsilon}_j$ are uncorrelated hence

$$\langle \varepsilon_i(x,t)\bar{\varepsilon}_j(\bar{x},t)\rangle = \langle \varepsilon_i(x,t)\rangle \langle \bar{\varepsilon}_j(\bar{x},t)\rangle = p_i\bar{p}_j. \tag{3.12}$$

Furthermore, the shuffling variables and occupancy variables are statistically independent leading to,

$$\langle \varepsilon_j(x,t)\eta_i(x,t)\rangle = \langle \varepsilon_i(x,t)\rangle \langle \eta_j(x,t)\rangle = p_j(x) \langle \eta_j(x,t)\rangle . \tag{3.13}$$

The fact that the shuffling variables and occupation variables are statistically independent gives us an opportunity to express the current equation in a more compact form

$$\begin{aligned} J(x-0.5\lambda,t) &= -2p \left[\left\langle \sum_{k=1}^{3} \eta_k(x-\lambda,t) - \sum_{k=1}^{3} \eta_k(x,t) \right\rangle \right] \\ &+ 2\epsilon p^2 \left\langle \sum_{k=1}^{3}\sum_{k'=1}^{3} \eta_k(x-\lambda)\bar{\eta}_{k'}(x-\lambda) - \sum_{k=1}^{3}\sum_{k'=1}^{3} \eta_k(x,t)\bar{\eta}_{k'}(x,t) \right\rangle . \end{aligned} \tag{3.14}$$

The steady state current expression can be expressed in terms of the node density variable $n(x)$. At any given time the node density can be be obtained by taking the average of the node states occupancy variables

$$n(x) = \frac{1}{3}(\eta_1(x,t) + \eta_2(x,t) + \eta_3(x,t)). \tag{3.15}$$

In terms of the respective channel node densities, the node occupancy correlation term is given by

$$\left\langle \sum_{k=1,k'=1}^{3,3} \eta_k(x,t)\bar{\eta}_{k'}(x,t) \right\rangle = 9 \langle n(x,t)\bar{n}(x,t)\rangle . \tag{3.16}$$

Stellenbosch University http://scholar.sun.ac.za

Upon using equation (3.16) in equation (3.14) the steady state current can be expressed as

$$\begin{aligned} J(x-0.5\lambda,t) &= -6p\left[\langle n(x-\lambda,t)-n(x,t)\rangle\right] \\ &- 18\epsilon p^2\left\langle n(x-\lambda)\bar{n}(x-\lambda)-n(x,t)\bar{n}(x,t)\right\rangle . \end{aligned} \tag{3.17}$$

To lowest non-trivial order in λ,

$$\begin{aligned} J(x-0.5\lambda,t) &= 6p\frac{\partial}{\partial x}\left(\langle n(x)\rangle - 18\epsilon p\left\langle n(x)\bar{n}(x)\right\rangle\right) \\ &= 3p\frac{\partial}{\partial x}\left(n_{ss}(x) - 6\epsilon p\left(n_{ss}^2(x) + \langle\rho(x)\bar{\rho}(x)\rangle\right)\right) . \end{aligned} \tag{3.18}$$

We have also used the fact that the node density can be expressed as a steady state average node density plus some fluctuations $n(x) = n_{ss} + \rho(x,t)$, where $\langle n(x)\rangle = \langle\bar{n}(x)\rangle = n_{ss}(x)$. Without loss of generality the lattice spacing is set to unity. The steady state average current for the whole system can be found by integrating the equation (3.18) over all nodes

$$\begin{aligned} J &= \frac{1}{L}\int_0^L J(x-0.5\lambda)dx \\ &= -\frac{3p}{L}\left(\left(n_{ss}(0)-n_{ss}(L)\right)\left[1-6\epsilon p\left(n_{ss}(0)+n_{ss}(L)\right)\right]\right) \\ &- 18p^2\frac{\epsilon}{L}\left(\langle\rho_{ss}(0)\bar{\rho}_{ss}(0)\rangle - \langle\rho_{ss}(L)\bar{\rho}_{ss}(L)\rangle\right) . \end{aligned} \tag{3.19}$$

Since the system is assumed to have a symmetric exchange of particles in between the reservoirs and the channel extreme ends, at steady state the mean occupancy of the respective extreme ends is the same as the density of the associated reservoirs, $n_{ss}(0) = \bar{n}_{ss}(0) = n_L$ and $n_{ss}(L) = \bar{n}_{ss}(L) = n_R$. The steady state current expression obtained relates the right and left reservoirs density difference $\Delta n_r = n_L - n_R$ and the average density between the particle reservoirs $n_g = \frac{1}{2}(n_L + n_R)$ and these are coupled to the channel interaction parameter ϵ. This simple analytic steady state current expression tells us that the particle flux throughout the system is contributed by the reservoir settings in conjunction with the emerging density fluctuation correlations between the two coupled channels.

Stellenbosch University http://scholar.sun.ac.za

3.2.2 Current without correlations

In the weak coupling limit, when particle correlations are insignificant, the steady state particle flux can be simply expressed as

$$J_{ss}^{0} = \frac{3p}{L}\left(\Delta n_r - 12p\epsilon\Delta n_r n_g\right). \tag{3.20}$$

The mean field current expression can be trusted to predict the steady state current for the MC regime for very small values of ϵ. In this limit, when the density fluctuations are ignored, the behaviour of the steady state current is summarised in Fig .3.1. As $\epsilon \to 0$, the system flux is purely driven by the reservoir density gradient (Fig .3.1(a)).

As the channel coupling parameter value increases the other terms such as n_g start to contribute. The uncorrelated mean field steady state current is in qualitative agreement with the simulation results for this specific case. The simulation results suggest that an increase in the coupling strength between channels, leads to some interesting dynamics that involve density-density correlations. For a comparison of the mean field steady state particle flux on the MC and HD regime. See Fig .3.2.

3.2.3 The system occupancy profile calculation

An analytic expression for the steady state occupancy profiles of the two coupled channels can be obtained by monitoring the exchange of particles between neighbouring nodes over time. For instance, we can get the instantaneous node occupancy variation of any node x by counting the number of particles going out of the node and those coming into a node per time step. The evolution of the mean node density can then be obtained by computing a long time average of the change in instantaneous node occupancy variation. The change in time of the mean node density $n(x)$ is given by

$$\frac{d}{dt}\langle n(x)\rangle = \langle \tau_3(x-\lambda,t) - \tau_1(x,t) + (\tau_1(x+\lambda,t) - \tau_3(x,t))\rangle\,. \tag{3.21}$$

Since the time average of occupancy difference $\langle\tau_1(x,t)\rangle - \langle\tau_3(x-\lambda,t)\rangle$ is simply the particle flux (3.10) at the respective nodes interface $(x-0.5\lambda)$, the above equation can be

Stellenbosch University http://scholar.sun.ac.za

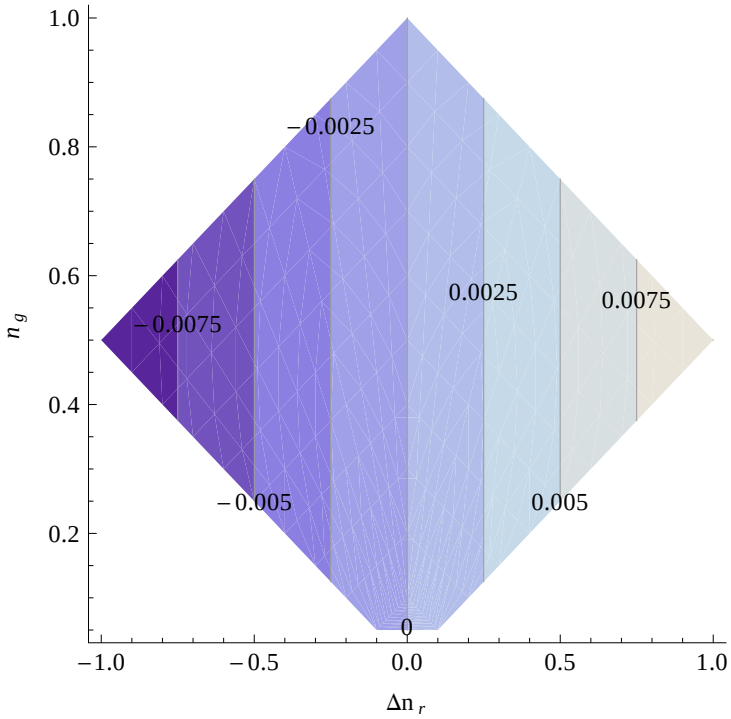

(a)

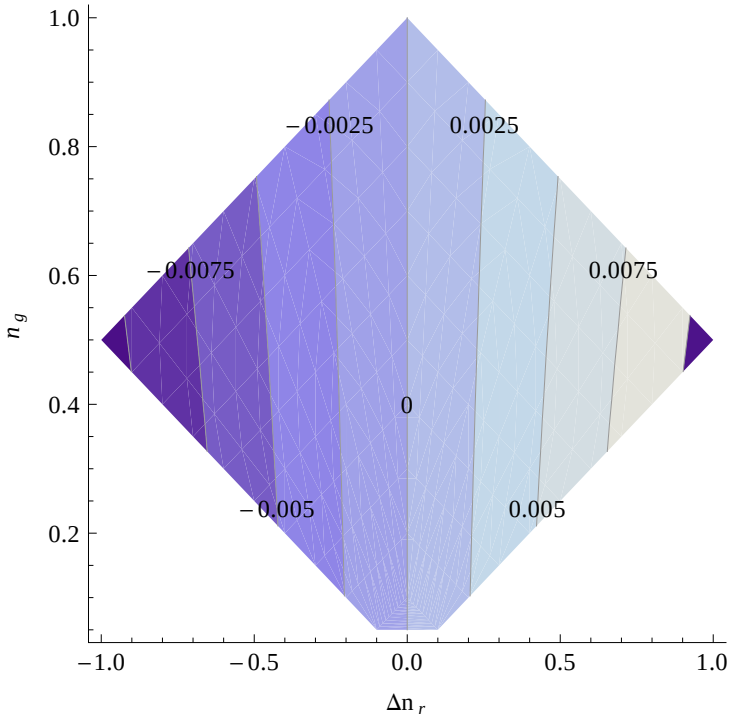

(b)

FIG. 3.1. A contour plot showing the relationship between the steady state current J_{ss} and the difference of the reservoir densities $\Delta n_r = n_L - n_R$ and the average of the reservoir densities $n_g = \frac{1}{2}(n_L + n_R)$ for the weak coupling limit (a) $\epsilon = 0.0001$ and for (b) $\epsilon = 0.4$.

Stellenbosch University http://scholar.sun.ac.za

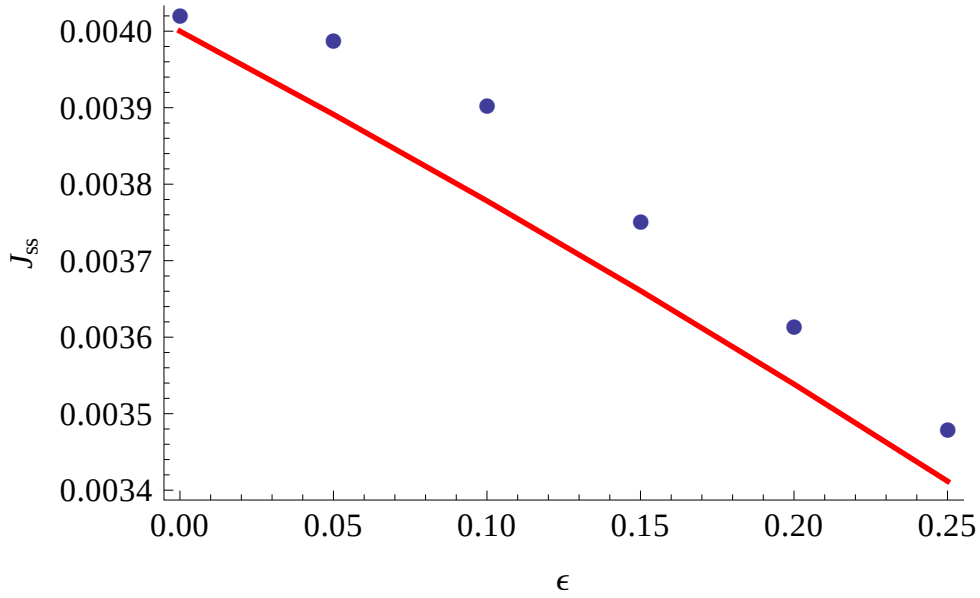

(a) HD

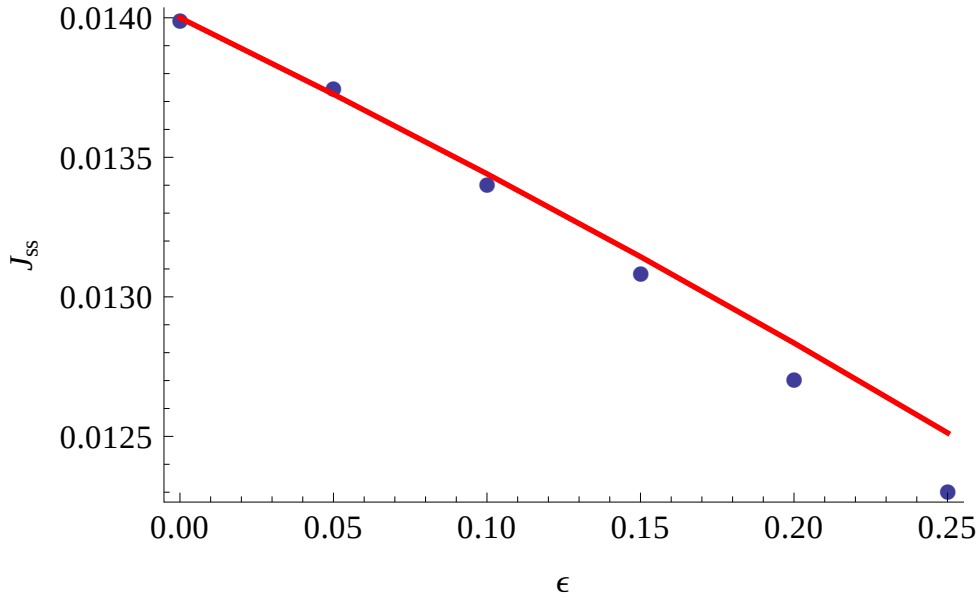

(b) MC

FIG. 3.2. Plot of the steady state current J_{ss} obtained from the cellular automaton simulation (blue dots) and that obtained from the mean field current expression (red line) for varied values of the coupling parameter ϵ. The left and right reservoir densities were set to:(a) $n_L = 0.8, n_R = 0.6$ and (b) $n_L = 0.9, n_R = 0.2$ respectively.

Stellenbosch University http://scholar.sun.ac.za

expressed in terms of node x inter-facial particle flux

$$\frac{d}{dt}\langle n(x)\rangle = J\left(x+0.5\lambda\right) - J\left(x-0.5\lambda\right). \tag{3.22}$$

To lowest order in λ,

$$\begin{aligned}\frac{d}{dt}\langle n(x)\rangle &= -\lambda\frac{\partial}{\partial x}J(x) \\ &= -6p\lambda^2\frac{\partial^2}{\partial x^2}\left\{n_{ss}(x) - 3\epsilon p\left[n_{ss}^2(x) + \langle\rho(x)\bar{\rho}(x)\rangle\right]\right\},\end{aligned} \tag{3.23}$$

At steady state there is no change in the average node density thus $\frac{d}{dt}\langle n(x)\rangle = 0$. Equation (3.23) becomes

$$0 = \frac{\partial^2}{\partial x^2}\left(n_{ss}(x) - 3\epsilon p\left(n_{ss}^2(x) + \langle\rho(x)\bar{\rho}(x)\rangle\right)\right),$$

Upon integrating over the position variable x the expression for the density profile is given by

$$n_{ss}(x) = \frac{1}{6\epsilon p} \pm \sqrt{\frac{1}{36\epsilon^2p^2} - \langle\rho(x)\bar{\rho}(x)\rangle - \frac{1}{3\epsilon p}(c_0x + c_1)} \tag{3.24}$$

where the constants c_0 and c_1 can be easily obtained using the boundary conditions

$$n_{ss}(0) = \bar{n}_{ss}(0) = n_L \quad \text{at} \quad x = 0 \quad \text{and} \tag{3.25}$$

$$n_{ss}(L) = \bar{n}_{ss}(L) = n_R \quad \text{at} \quad x = L. \tag{3.26}$$

Upon using the respective boundary condition at $x = 0$ and $x = L$ we obtain

$$c_1 = n_l - 3\epsilon p\left(n_l^2 + \langle\rho(0)\bar{\rho}(0)\rangle\right) \tag{3.27}$$

and

$$c_0 = \frac{1}{L}\left(n_r - n_l - 3\epsilon p\left(n_r^2 - n_l^2 + \langle\rho(L)\bar{\rho}(L)\rangle - \langle\rho(0)\bar{\rho}(0)\rangle\right)\right). \tag{3.28}$$

The density profile of a node is a positive quantity. The physical solution for $n_{ss}(x)$ is the one which gives a density profile which lies between the reservoir densities. The equation for the channel density in terms of the particle reservoir density becomes

Stellenbosch University http://scholar.sun.ac.za

$$
\begin{aligned}
n_{ss}(x) &= \frac{1}{\epsilon} - \frac{1}{\epsilon}\left\{1 + \frac{\epsilon}{L}\left[2\left(\epsilon n_g - 1\right) x\Delta n_r - L\left(2n_L - \epsilon n_L^2\right)\right.\right. \\
&+ \left.\left. \epsilon L\left(\left\langle \rho_L \bar{\rho}_L \right\rangle - \left\langle \rho(x)\bar{\rho}(x) \right\rangle\right) - \epsilon x\left(\left\langle \rho_L \bar{\rho}_L \right\rangle - \left\langle \rho_R \bar{\rho}_R \right\rangle\right)\right]\right\}^{\frac{1}{2}}, \qquad (3.29)
\end{aligned}
$$

having considered the fact that $p = \frac{1}{6}$.

Upon comparing the steady state density profile obtained from the cellar automaton simulation and that predicted by the mean field theory in the limit of small coupling between channels, looking specifically at the behaviour around $\epsilon \approx 0$, we learn that the simulated density profile and the mean field density profile at steady state are in agreement at least qualitatively. However, the mean field theory with correlations ignored seems to deviate from the simulation steady state profile as the value of the interaction parameter is increased. To see how the density profile predicted by the analytic mean field theory analytic expression deviate from the simple linear interpolation in equation (2.7), see Fig .3.3.

From the nature of the discrepancy between the simulation and the analytic results, it becomes apparent that the dynamic correlations play a non-trivial role in the diffusion process. Looking at the graph of the steady state mean field profile deviation from the simulation steady state density profile provided in Fig .3.4, we see that the percentage deviation for the interaction range $\epsilon \leq 0.25$ is in general very small. We think this deviation can be accounted for by the ignored fluctuation correlations.

Despite the influence of the boundaries it is obvious that kinetic properties of the system depend also on the density-density correlation and the channel coupling parameter in a self consistent manner. The mean field approach that is used to obtain analytic expressions for the steady state current and the steady state channel occupancy profile for the two coupled channel system, within a weak coupling assumption, can be generalised to obtain the corresponding analytic expressions for a multi-coupled channel system.

Stellenbosch University http://scholar.sun.ac.za

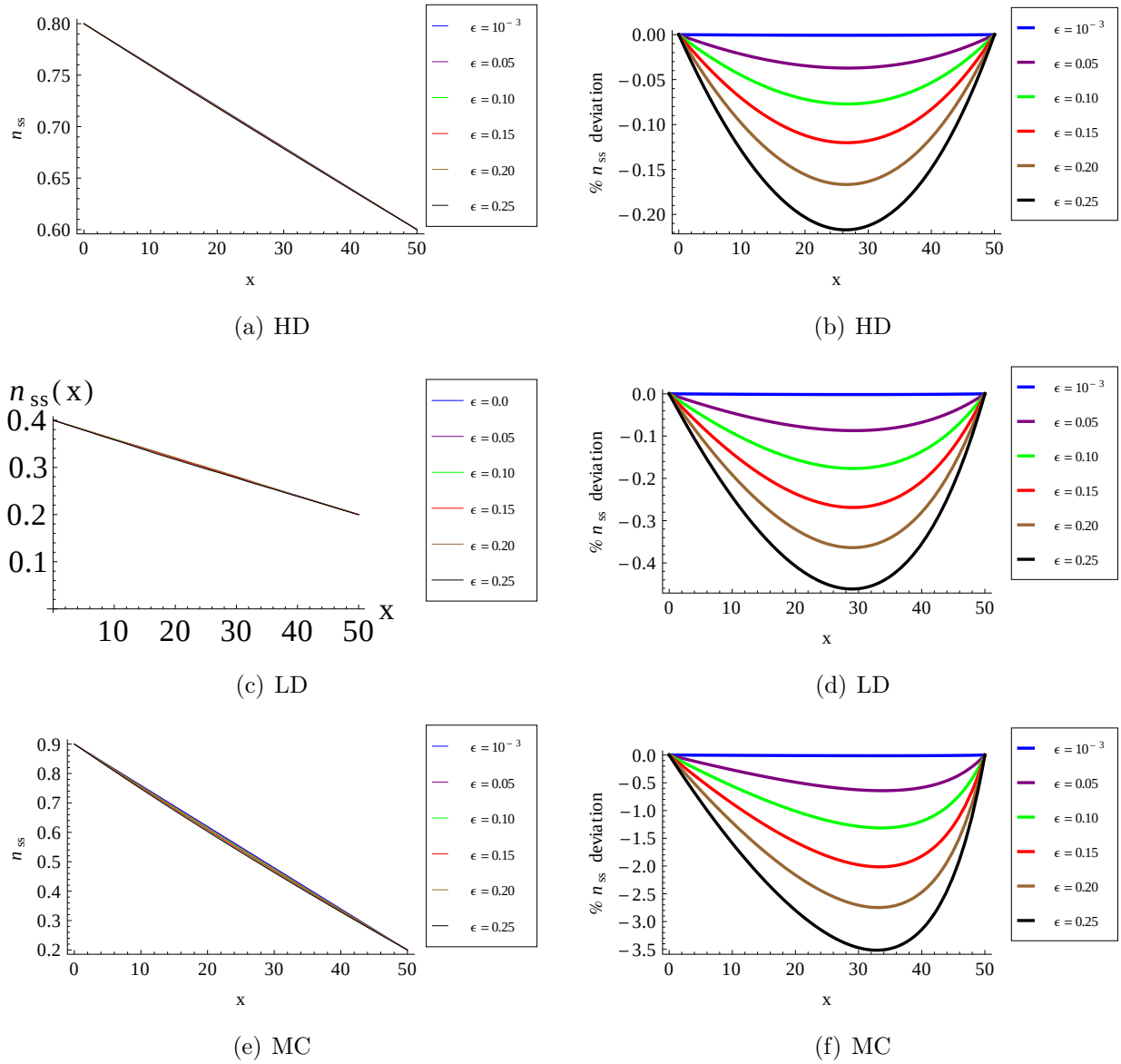

(a) HD (b) HD

(c) LD (d) LD

(e) MC (f) MC

FIG. 3.3. Plot of the weakly coupled two channel system density profile, that is obtained from the mean field analytic method, for (a) the maximal current regime (MC): $n_L = 0.9, n_R = 0.2$,(b) high density regime (HD): $n_L = 0.8, n_R = 0.6$ and (c) low density regime (LD): $n_L = 0.4.n_R = 0.2$. Graphs (b),(d) and (e) present the corresponding percentage deviation of the uncorrelated mean field steady state density profile from a linear density interpolation between the boundaries reservoirs which are kept at the given densities. In this graphs we explore the sensitivity of the density profile for small values of the coupling parameter $\epsilon < 0.5$.

Stellenbosch University http://scholar.sun.ac.za

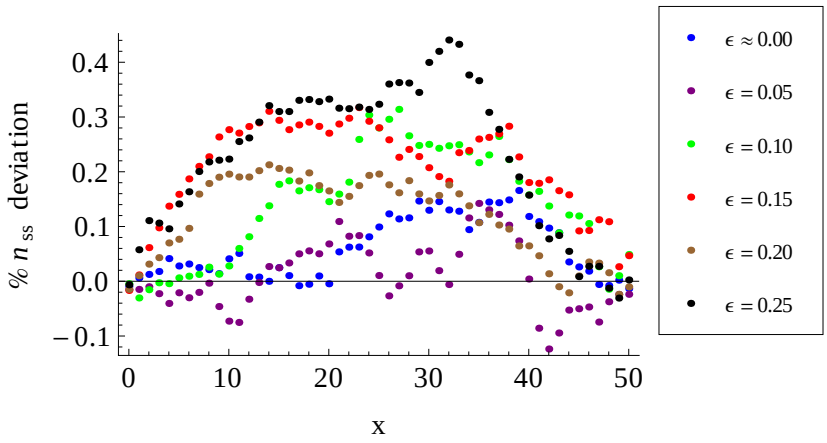

(a) HD regime

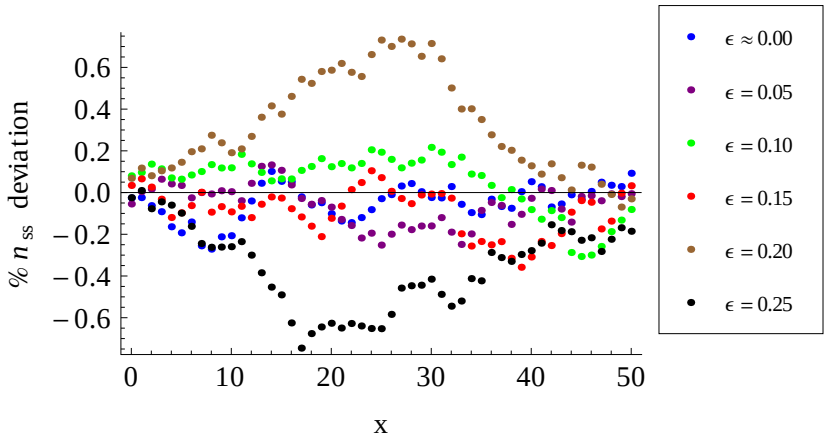

(b) LD regime

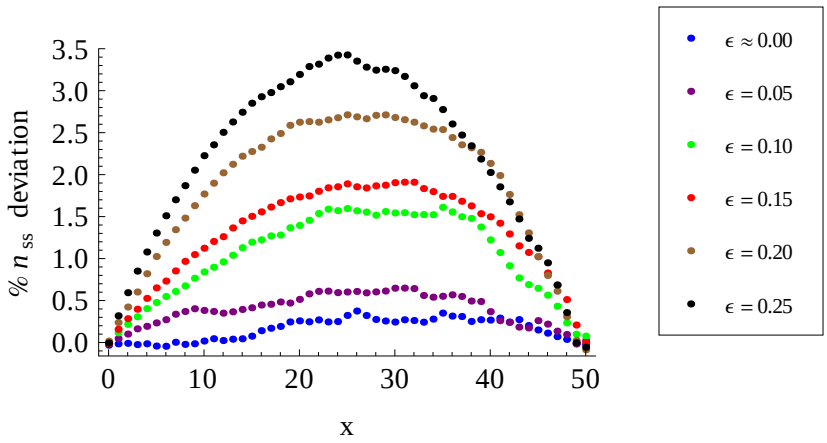

(c) MC regime

FIG. 3.4. Plot of the weakly coupled two channel system percentage deviation of the uncorrelated mean field steady state density profile from the cellular automaton simulation steady state density profile for (a) the high density high density regime (HD): $n_L = 0.8, n_R = 0.6$,(c) the low density regime (LD): $n_L = 0.4, n_R = 0.2$ and (e) maximal current regime (MC): $n_L = 0.9.n_R = 0.2$. The simulation was allowed to reach steady state over 10^7 times steps and then the steady state averages were taken over 10^7 time steps. For each regime the graphs shown are for different values of of the coupling parameter ϵ.

Stellenbosch University http://scholar.sun.ac.za

3.3 Multiple channel system mean field treatment

The generalisation of the coupled channel system for multiple channels will be achieved by thinking of the particle evolution as a form of hopping process on a lattice. This allows us to incorporate the effects of the elastic deformation on the host channel through some site dependent hopping rates. Instead of thinking about the change in the state of occupancy of a node, the dynamic equations will be written out by considering the time evolution of individual states τ_i^j, where the index i runs over the particle occupancy sites and the superscript j enumerates different channels. The particle occupancy variable in this case still assume values zero or unity to denote the absence or presence of a particle respectively.

In a scenario where the channels are decoupled, the change in particle occupancy for an ith site in channel j can be expressed by the following picture equation:

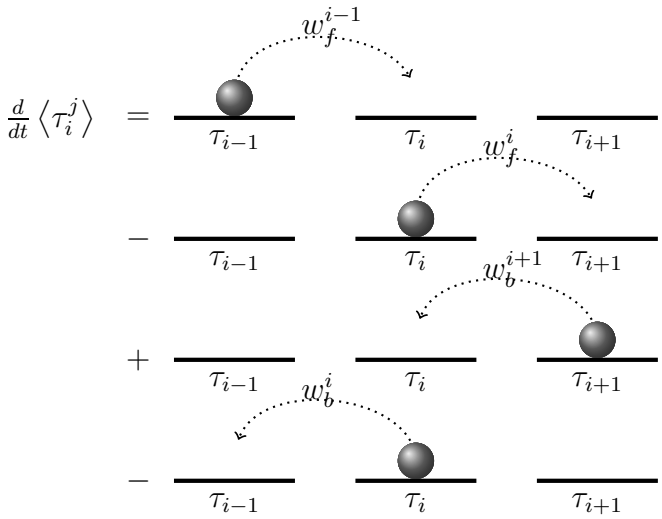

which could be mathematically expressed as

$$\begin{aligned}\frac{d\tau_i}{dt} &= w_f^{i-1}\tau_{i-1}(1-\tau_i) - w_f^i\tau_i(1-\tau_{i+1}) \\ &+ w_b^{i+1}\tau_{i+1}(1-\tau_i) - w_b^i\tau_i(1-\tau_{i-1}),\end{aligned}$$

where the forward and backward hopping rates w_f and w_b determine the time scale in the system. Since the hopping rules are symmetric about the left and right hopping direction

$$\langle w_f^i\rangle = \langle w_b^{i+1}\rangle = w. \tag{3.30}$$

Stellenbosch University http://scholar.sun.ac.za

In a scenario where the channels are weakly coupled, the associated particle transition rates should be modified to incorporate the influence of particles on the neighbouring sites from adjacent channels. We envisage a scenario where each channel has equal number of next neighbouring channels adjacent to it. The lattice sites for the system are arranged in a staggered (wall brick) type of arrangement. In this formation an adjacent site is counted as interacting when it is positioned in such a way that makes the next hop in the forward or backward direction less likely (Fig .3.5).

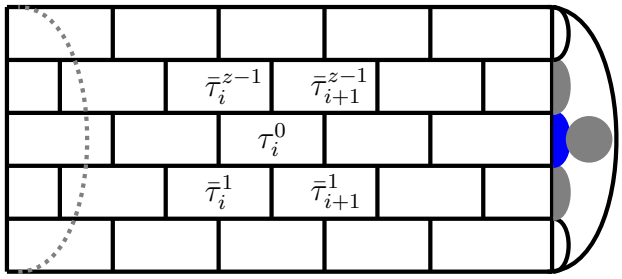

FIG. 3.5. A typical depiction of a sliced view of a 3 dimensional neighbourhood of the reference channel (end filled in blue). The next neighbourhood channels (with ends filled in black) are having sites $\bar{\tau}_i^j$ and $\bar{\tau}_{i+1}^j$ slightly offset from the reference channel sites τ_i. This formation is referred to as staggered arrangement of lattice sites

.

The associated transition rates for the coupled system can be expressed in such a way that they include the influence of the occupancy of the adjacent lattice sites. For instance a forward particle hop from site τ_i to site τ_{i+1} becomes

$$w_{i,i+1} = w_1 \left(1 - \sum_{j=1}^{z-1} \bar{\tau}_i^j\right) + w_2 \sum_{j=1}^{z-1} \bar{\tau}_i^j. \tag{3.31}$$

Here the rate

$$w_2 = w_1(1-\epsilon), \tag{3.32}$$

where the parameter ϵ is the channel coupling parameter. The rate w_1 is equal to the decoupled system average hopping rate w. The forward and backward particle hopping rates get a penalty whenever $\bar{\tau}_i^j = 1$ in any of the $z-1$ couple channels' neighbouring sites. The evolution of the average particle occupancy at any arbitrary site $\bar{\tau}_i^{j'}$ of a reference channel j' is given by

Stellenbosch University http://scholar.sun.ac.za

$$\begin{aligned}\frac{d\tau_i^{j'}}{dt} &= w_f^{i-1}\tau_{i-1}^{j}(1-\tau_i)\left[w_1(1-\sum_{j=1}^{z-1}\bar{\tau}_i^{j})+w_2\sum_{j=1}^{z-1}\bar{\tau}_i^{j}\right]\\ &\quad -w_f^{i}\tau_i(1-\tau_{i+1})\left[w_1(1-\sum_{j=1}^{z-1}\bar{\tau}_{i+1}^{j})+w_2\sum_{j=1}^{z-1}\bar{\tau}_{i+1}^{j}\right]\\ &\quad +w_b^{i+1}\tau_{i+1}(1-\tau_i)\left[w_1(1-\sum_{j=1}^{z-1}\bar{\tau}_{i+1}^{j})+w_2\sum_{j=1}^{z-1}\bar{\tau}_{i+1}^{j}\right]\\ &\quad -w_b^{i}\tau_i(1-\tau_{i-1})\left[w_1(1-\sum_{j=1}^{z-1}\bar{\tau}_i^{j})+w_2\sum_{j=1}^{z-1}\bar{\tau}_i^{j}\right]. \end{aligned} \tag{3.33}$$

A little variation on the theme in this picture compared to the cellular automaton picture is that here the occupancy of the offset adjacent lattice sites from the neighbouring channels lattice reduce the hopping rate for a particle transition to the next site while on the cellular automaton case neighbouring sites from adjacent coupled channels make the probability for a particle to remain stationary after the shuffling state less likely. In principle the two approaches yield a comparable biasing on the overall particle motion.

we assume that the inter-file occupancy for a weakly coupled system are uncorrelated such that $\langle \tau_i\bar{\tau}_i^{j}\rangle = \langle\tau_i\rangle\langle\bar{\tau}_i^{j}\rangle$, the change in site occupancy becomes

$$\begin{aligned}\frac{d\langle\tau_i\rangle}{dt} &= \langle\tau_{i-1}(1-\tau_i)\rangle\left[w_1\langle w_f^{i-1}\rangle+(w_2-w_1)\sum_{j=1}^{z-1}\langle w_f^{i-1}\bar{\tau}_i^{j}\rangle\right]\\ &\quad -\langle\tau_i(1-\tau_{i+1})\rangle\left[w_1\langle w_f^{i}\rangle+(w_2-w_1)\sum_{j=1}^{z-1}\langle w_f^{i}\bar{\tau}_{i+1}^{j}\rangle\right]\\ &\quad +\langle\tau_{i+1}(1-\tau_i)\rangle\left[w_1\langle w_b^{i+1}\rangle+(w_2-w_1)\sum_{j=1}^{z-1}\langle w_b^{i+1}\bar{\tau}_{i+1}^{j}\rangle\right]\\ &\quad -\langle\tau_i(1-\tau_{i-1})\rangle\left[w_1\langle w_b^{i}\rangle+(w_2-w_1)\sum_{j=1}^{z-1}\langle w_b^{i}\bar{\tau}_i^{j}\rangle\right]. \end{aligned} \tag{3.34}$$

Denoting $n_i = \langle\tau_i\rangle$ and assuming that $\langle w_f^m\tau_i^m\rangle = \langle w_b^m\tau_i^m\rangle = wn_i$ for any mth site, we can express the change in site occupancy as

$$\begin{aligned}\frac{dn_i}{dt} &= ww_1((n_{i+1}-n_i)-(n_i-n_{i-1})\\ &+ w(w_2-w_1)(z-1)\left[\bar{n}_in_{i-1}-\bar{n}_{i+1}n_i+\bar{n}_{i+1}n_{i+1}-\bar{n}_in_i\right]. \end{aligned} \tag{3.35}$$

Stellenbosch University http://scholar.sun.ac.za

To obtain the above expression, we have also taken into account the fact that each of the summed-over terms contribute equally, hence the sum can just be replaced by the number of summed-over terms. Because of the symmetry of the model the intra-channel pair correlations terms such as $\langle \tau_i \tau_{i+1} \rangle$ cancel out. For an uncoupled channels with symmetric hopping rules the diffusion of such pairs can in principle be handled separately [Dieterich and Peschel, 1983].

3.3.1 Continuous mean-field limits

Since the lattice points are separated by a constant lattice spacing parameter λ, the neighbouring sites occupancy can be expressed as a function of a continuous spatial variable x by performing the mapping

$$n_{i-1} \rightarrow n(x-\lambda), \tag{3.36a}$$

$$n_i \rightarrow n(x), \tag{3.36b}$$

$$n_{i+1} \rightarrow n(x+\lambda). \tag{3.36c}$$

Having expressed the site occupancy variables in equation (3.35) as functions of x, the site occupancy evolution equation takes the form

$$\frac{dn(x)}{dt} = w\lambda^2 \left[w_1 \frac{\partial^2 n(x)}{\partial x^2} + (w_2 - w_1)(z-1) \frac{\partial}{\partial x} \left(\bar{n(x)} \frac{\partial n(x)}{\partial x} \right) \right]. \tag{3.37}$$

Since the model is symmetric about the respective channels, the particle occupancy evolution in the neighbouring coupled channels is described by similar differential equations that can be expressed as

$$\frac{d\bar{n}(x)}{dt} = w\lambda^2 \left[w_1 \frac{\partial^2 \bar{n}(x)}{\partial x^2} + (w_2 - w_1)(z-1) \frac{\partial}{\partial x} \left(n(x) \frac{\partial \bar{n}(x)}{\partial x} \right) \right]. \tag{3.38}$$

At steady state the occupancy profile does not change in time thus the right hand side of equation (3.37) and (3.38) $\frac{dn}{dt} = \frac{d\bar{n}}{dt} = 0$ leading to

$$0 = \frac{\partial}{\partial x} \left(w_1 \frac{\partial n(x)}{\partial x} + (w_2 - w_1)(z-1)\bar{n}(x) \left(\frac{\partial n(x)}{\partial x} \right) \right) \quad \text{and} \tag{3.39}$$

$$0 = \frac{\partial}{\partial x} \left(w_1 \frac{\partial \bar{n}(x)}{\partial x} + (w_2 - w_1)(z-1)n(x) \left(\frac{\partial \bar{n}(x)}{\partial x} \right) \right). \tag{3.40}$$

Stellenbosch University http://scholar.sun.ac.za

This set of coupled differential equations can easily be solved numerically to obtain the steady state density profiles of the channels for some choice of parameter values for the rate constants and boundary conditions.

3.3.2 Average density profile for the case when channels have identical occupancy

To obtain an analytic expression for the density profile along the reference channel, let us consider the case when the mean density at any positon x along the channels is identical, i.e $n(x) = \bar{n}(x) = n_{ss}(x)$. Then the two steady state mean field equations reduce to a single equation:

$$\frac{d^2}{dx^2}\left(w_1 n_{ss}(x) + (w_2 - w_1)(z-1)\frac{n_{ss}^2(x)}{2}\right) = 0, \tag{3.41}$$

whose general solution is given by

$$n_{ss}^{(0)}(x) = -\frac{w_1}{w_2 - w_1} \pm \sqrt{\frac{w_1}{(w_2 - w_1)(z-1)} + \frac{2J^{(0)}x + c_0}{(w_2 - w_1)(z-1)}}. \tag{3.42}$$

Once again the superscript (0) is used to distinguish this steady state solution in which correlations are ignored from the previous one in which correlations may be taken into account. The constants J and c can easily be determined from the boundary conditions. In fact, we will notice that the constant J is exactly the steady state particle flux $J^{(0)}$ obtained from the cellular automaton approach. All the constants can be obtained from the boundary conditions

$$n_{ss}(x) = n_L \quad \text{at} \quad x = 0 \quad \text{and} \quad n_{ss}(x) = n_R \quad \text{at} \quad x = L. \tag{3.43}$$

At $x = 0$, the general solution (3.42) yields,

$$c_0 = w\left[w_1 n_L + \frac{1}{2}(z-1)(w_2 - w_1)n_L^2\right]. \tag{3.44}$$

and

$$J^{(0)} = -\frac{1}{L}\left[w_1(n_R - n_L) + \frac{1}{2}(z-1)(w_2 - w_1)(n_R^2 - n_L^2)\right]. \tag{3.45}$$

Stellenbosch University http://scholar.sun.ac.za

Substituting equation (3.44) and (3.48) into the equation (3.42) and rearranging we get,

$$\begin{aligned} n_{ss}^{(0)}(x) &= -\frac{w_1}{(w_2-w_1)} \pm \left\{ \frac{w_1^2}{(w_2-w_1)^2(z-1)^2} + \frac{2x(n_L-n_R)}{L(w_2-w_1)(z-1)} \right. \\ &\times \left. \left(w_1 + \frac{1}{2}(z-1)(w_2-w_1)(n_R+n_L) + w_1 n_L + \frac{1}{2}(z-1)(w_2-w_1)n_L^2 \right) \right\}^{\frac{1}{2}}. \end{aligned} \tag{3.46}$$

Upon introducing the weak coupling approximation on the hopping rates $w_2 = (1-\epsilon)w_1$, equation (3.46) reduces to a familiar form of steady density profile obtained from cellular automaton approach with density fluctuation terms left out,

$$\begin{aligned} n_{ss}^{(0)}(x) &= \frac{1}{(z-1)\epsilon} \\ &- \frac{1}{(z-1)\epsilon} \left\{ 1 + \frac{(z-1)\epsilon}{L} \left[2\left((z-1)\epsilon n_g - 1 \right) x\Delta n_r - L\left[2n_L - (z-1)\epsilon n_L^2 \right) \right] \right\}^{\frac{1}{2}}. \end{aligned} \tag{3.47}$$

The terms Δn_r and n_g still denote the difference and the average of the reservoirs densities at the channels ends respectively. The mean field density profile expression incorporates the contribution of the other channels by simply magnifying the coupling parameter ϵ by a factor $z-1$ which corresponds to the number neighbouring channels.

3.4 Summary of the mean field analytic calculation

The subject of this chapter was to develop a simple mean field treatment for the out-of-equilibrium particle dynamics within a weak coupling limit. The objective was achieved from two different approaches. We started with a mean field approach, for a two coupled channel system, that is based on the cellular automaton formalism in which the stochastic particle diffusion is achieved through a combination of probabilistic particle collision and propagation rules. The chapter concludes with a multiple file analytic mean field calculation that is based on the particle hopping dynamics approach. We found that, in the limit when correlation are negligibly small, the channel steady state flux and density profile are described by the respective equations

$$J^{(0)} = -\frac{1}{L}\left[w_1(n_R - n_L) + \frac{1}{2}(z-1)(w_2-w_1)(n_R^2 - n_L^2) \right].$$

Stellenbosch University http://scholar.sun.ac.za

and

$$\begin{aligned} n_{ss}^{(0)}(x) &= \frac{1}{(z-1)\epsilon} \\ &- \frac{1}{(z-1)\epsilon}\left\{1+\frac{(z-1)\epsilon}{L}\left[2\left((z-1)\epsilon n_g-1\right]x\Delta n_r - L\left[2n_L-(z-1)\epsilon n_L^2\right)\right]\right\}^{\frac{1}{2}}, \end{aligned}$$

where n_g and Δn_r are the average and difference of the respective reservoir densities n_R and n_L. Note that the interaction parameter ϵ is amplified by a factor that is related to the number of coupled files.

We learned that the two different approaches yield the some results for the uncorrelated steady state particle occupancy profile and flux. The results are also found to be in a satisfactory qualitative agreement with the simulation results. However, we learned that further consideration of the density-density correlations is needed if the analytic theory is to become truly general and robust. One possibility for improvement is the adaptation of equilibrium density-density correlation function for the out-of-equilibrium scenario, the derivation of which shall be the objective of the next chapter. We hope that our presentation has convinced the reader that the cellular automaton ideas, which worked very well for the simulation study of the system, can also constitute a very powerful technique for an analytic treatment of the kinetic properties of the open coupled channel system.

Stellenbosch University http://scholar.sun.ac.za

Chapter 4

System density-density correlation from collective particle dynamics

In this chapter, our goal is to describe the nature of the dynamic correlations in the coupled channel system. To achieve this, we look at a system of particles, diffusing inside narrow infinite coupled channels close to equilibrium. The dynamics of individual particles are modelled through a set of overdamped Langevin equations. In these equations, describing the evolution of the particles, the effect of deformation on the voids of channels upon occupancy by particles is included through a short range repulsive pair potential. The thermal effects on the particle motion are modelled through a stochastic term.

For a systems of coupled narrow channels, it is quite intuitive that all particles become sufficiently correlated and behave as a single effective particle. This is due to the fact that the displacement of a given particle over a long distance in a specific direction requires that many other particle be shifted into the same direction. In a one dimensional single-file system, the exclusion of mutual passage has been demonstrated to lead to a mean-square displacement $\langle \Delta x^2 \rangle$, which is proportional to the square-root of the observation time, rather than the observation time itself, as it is the case for a system of unrestricted randomly diffusing particles [van Beijeren et al., 1983].

Under single file condition we can assume that the two particles interaction occurs inside a box and that the particle velocities and instants of time for entry and exit from the box are the only determinable quantities. It has also been argued by [Hahn and Kärger, 1995] that

Stellenbosch University http://scholar.sun.ac.za

under these assumptions, if we consider the interaction of adjacent point-like particles in a single file system, there is no way to distinguish whether the particles have freely passed each other without any interaction or whether the particles did interact but maintain their locations relative to each other.

For an illustration of how such a system can evolve leading to a similar particle distribution under both self-excluding and non-interacting condition see Fig. 4.1. For this specific case, it is possible to develop a collective description of the system in terms of particle density and particle density response variables without worrying about the mode of movement of individual particles. This treatment makes it possible to uncover both short time and long time limit behaviour of the system density-density correlation functions without incorporating single file effects which are exclusively determined by the mode of movement of the individual particles.

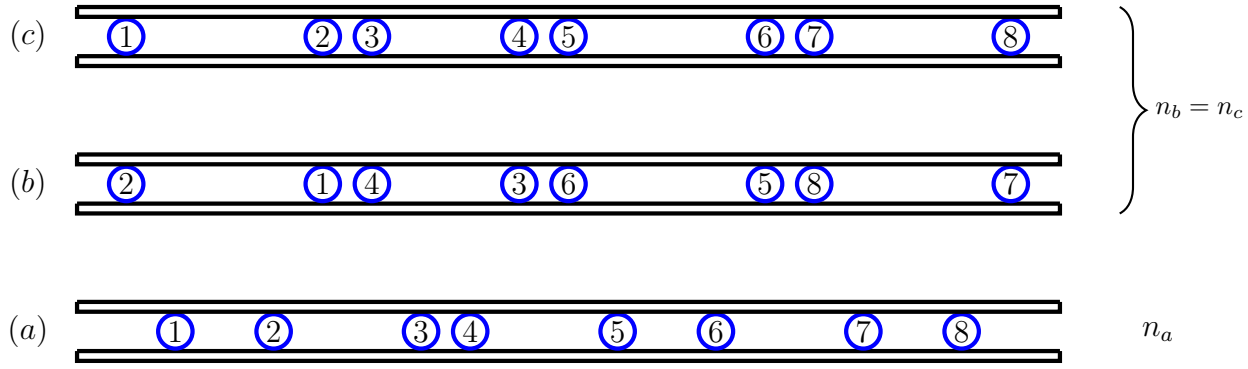

FIG. 4.1. The particle order and spatial distribution for the non-interacting and interacting case. (a) Initial state at $t = 0$ with spatial distribution n_a. (b) End state for non-interacting particles with spatial distribution n_b. In this case, the particle order has changed. (c) End state for interacting particles obeying single-file dynamics with spatial distribution n_c. Note that the order of the particles in (c) is the same as in (a) but the distribution is the same as in (b), $n_c = n_b$.

The collective dynamics of particles diffusing in the two coupled single files can be described using a functional integral representation that is based on a construction developed by Martin, Siggia and Rose (MSR) [De Dominicis and Peliti, 1978; Martin et al., 1973] for describing stochastic dynamics of classical systems. The MSR functional integral formalism is a versatile calculational tool that has been conveniently used in the study of collective dynamics in a number of interesting problems such as the study of Langevin dynamics of

Stellenbosch University http://scholar.sun.ac.za

the glass forming polymer melt [Rostiashvili et al., 1998], the hydrodynamic description of interacting flux line liquid in the presence of quenched disorder [Radzihovsky and Frey, 1993] and the collective dynamics of random polyampholytes [Müller-Nedebock and Vilgis, 1999].

The functional integral approach is suitable for investigating the time dependent properties of collective variables such as particle concentration and particle probability current. In our context, this will be achieved by constructing a generating functional from two coupled stochastic differential equations describing the motion of the guest particles in the host system. This treatment is equally suited for systems that are near and far from thermodynamic equilibrium. In this study the main focus will be on understanding the nature of dynamic correlations near equilibrium.

The particle density homogeneity assumption for the infinitely long channels allows the use of the random phase approximation (RPA) in a dynamical context. We follow the scheme of Fredrickson and Helfand [Fredrickson and Helfand, 1990] for studying the dynamics of collective density fluctuation variables and we obtain correlation functions of such variables by taking functional derivatives of the generating functional $\mathcal{Z}$ with respect to the fields conjugate to the density fluctuation variables.

4.1 The model

The dynamics of any neighbouring jth or τth guest particles diffusing in the system consists of two elastically coupled files, each having a uniform density of guest particles, are describable by a pair of coupled over-damped Langevin equations

$$0 = \mathcal{L}_i(t) = -\zeta \frac{\partial}{\partial t} r_j(t) - \sum_{\tau=1}^{N} \frac{\partial}{\partial r_j} V(r_j(t) - \bar{r}_\tau(t)) + f_j(t), \tag{4.1a}$$

$$0 = \bar{\mathcal{L}}_\tau(t) = -\zeta \frac{\partial}{\partial t} \bar{r}_\tau(t) + \sum_{j=1}^{N} \frac{\partial}{\partial \bar{r}_\tau} V(r_j(t) - \bar{r}_\tau(t)) + \bar{f}_\tau(t). \tag{4.1b}$$

As we have stated in the previous chapters, the guest-host interaction causes a structural deformation of the host channels leading to the channels exerting forces on one another. The respective interaction forces at the jth and τth positions of the first and second chan-

Stellenbosch University http://scholar.sun.ac.za

nels are given by $-\sum_{j=1}^{N}\frac{\partial}{\partial r_\tau}V(r_j(t)-\bar{r}_\tau(t))$ and $\sum_{\tau=1}^{N}\frac{\partial}{\partial r_j}V(r_j(t)-\bar{r}_\tau(t))$. For simplicity, the explicit form of the interaction potential shall be assumed to be Gaussian. The particle evolution is also subject to uncorrelated Gaussian white noise $f_j(t)$ and $\bar{f}\tau(t)$ obeying the fluctuation dissipation theorem of the form

$$\langle f_j(t)f_{j'}(t')\rangle = 2\zeta k_BT\delta_{j,j'}\delta(t-t'), \tag{4.2a}$$

$$\langle \bar{f}_\tau(t)\bar{f}_{\tau'}(t')\rangle = 2\zeta k_BT\delta_{\tau,\tau'}\delta(t-t'). \tag{4.2b}$$

The constant ζ is the bare friction coefficient of the background media and k_BT is the thermal energy. Note that the Langevin equations do not include the non-overtaking nature of particles in narrow channels.

It is possible to solve the Langevin equations for the position variables $r_i(t)$ and $\bar{r}_\tau(t)$ of the particles and then compute correlations by averaging in terms of the weight

$$P(f_i(t)) = \int [df_i]\exp\left(-\frac{1}{2\alpha}\int dt|f_i|^2\right), \tag{4.3}$$

of the respective random forces f_j and $\bar{f}_\tau$. In this description the approach is to make use of the functional integral formalism, of Martin-Siggia-Rose (MSR) [Martin et al., 1973], Dominicis and Peliti [De Dominicis and Peliti, 1978], in which the two Langevin equations are used as delta functional constraints to formulate the solution of the Langevin equations in terms of a constrained path integral that is averaged over the noise variables. The definition of the delta functional is then used to convert the constraints into a functional form.

4.2 Martin-Siggia-Rose generating functional

In order to implement the MSR scheme, the differential equations are expressed as constraints in the path integral

$$\mathcal{Z} = \left\langle \int \prod_{j=1}^{N}[dr_j(t)]\mathcal{J}[r_j(t)]\prod_{\tau=1}^{N}[d\bar{r}_\tau(t)]\bar{\mathcal{J}}[\bar{r}_\tau(t)]\prod_{j=1}^{N}\delta[\mathcal{L}_j(t)]\prod_{\tau=1}^{N}\delta[\bar{\mathcal{L}}_\tau(t)]\right\rangle_{\{f_i,\bar{f}_\tau\}}. \tag{4.4}$$

The delta function constraints can also be viewed as a way of imposing a coordinate transformation from microscopic variables f_i to r_i. In this way, we deal away with random

Stellenbosch University http://scholar.sun.ac.za

forces in favour of conformational variables. For more details about the transformation see appendix B.1. Here $\langle \cdots \rangle_{\{f_j, \bar{f}_\tau\}}$ denotes a path integral over stochastic forces, while $\int [dr_i(t)]$ type path integrals are carried over the particles position variables with a discretisation in time implied. The quantities $\mathcal{J}[r_j]$ and $\mathcal{J}[\bar{r}_\tau]$ are the Jacobians of the transformations. Upon using the exponential definition of a functional delta function we introduce auxilliary fields $\hat{r}_j(t)$ and $\hat{\bar{r}}_\tau(t)$, also known as response fields, since they are useful in the derivation of response functions. The resulting functional integral becomes

$$\mathcal{Z} = \left\langle \int \prod_{j=1}^{N} [dr_j(t)][d\hat{r}_j(t)] \mathcal{J}[r_j] \int \prod_{\tau=1}^{N} [d\bar{r}_\tau(t)][d\hat{\bar{r}}_\tau(t)] \bar{\mathcal{J}}[\bar{r}_\tau] \right. \\ \left. \exp\left[i \sum_{j=1}^{N} \int_t \hat{r}_j(t) \mathcal{L}_j(t) + i \sum_{\tau=1}^{N} \int_t \hat{\bar{r}}_\tau(t) \bar{\mathcal{L}}_\tau(t) \right] \right\rangle_{\{f_i(t), \bar{f}_\tau(t)\}} . \tag{4.5}$$

The Jacobians $\mathcal{J}[r_j(t)]$ and $\bar{\mathcal{J}}[\bar{r}_\tau(t)]$ are dealt with using the causal discretisation scheme employed by Jensen [Jensen, 1981]. The scheme demands that the functional integral be correctly normalised such that $\mathcal{Z} = 1$. The functional normalisation to unity in the Jensen scheme is achieved based on the following set or rules: Firstly, the averages of products containing functions of hatted fields such as $\hat{r}(t_1)$ must vanish, if the argument (t_1) is the latest time appearing within the product. Secondly, in a product having a physical field and a response field at equal times such as $r(t_1)\hat{r}(t_1)$, the argument of the hatted field is displaced infinitesimally to a later time leading to a vanishing average. This is consistent with causality as the response field should be within the time cone of an effect producing it.

The noise averaged functional in equation (4.5) contains all the information about the time evolution of the system and is therefore useful in calculating any particle position dependent observable. For example, an average over the observable $\Xi(r_j, \bar{r}_\tau)$, dependent on the particle position variables $r_j(t)$ and $\bar{r}_\tau(t)$, can be obtained from the constrained path integral

$$\langle \Xi(r_j, \bar{r}_\tau) \rangle = \int \prod_{j=1}^{N} [dr_j(t), d\bar{r}_j(t)] \int \prod_{\tau=1}^{N} [d\bar{r}_\tau(t), \bar{r}_\tau(t) \exp\{-L\} \Xi(r_j, \bar{r}_\tau), \tag{4.6}$$

Stellenbosch University http://scholar.sun.ac.za

with $L = L_0(r,\bar{r}) + L_{int}(r,\bar{r})$ where

$$L_0(r,\bar{r}) = \frac{1}{2\alpha}\sum_{j=1}^{N}\int_t \hat{r}_j^2(t) + \frac{1}{2\alpha}\sum_{\tau=1}^{N}\int_t \hat{\bar{r}}_\tau^2(t) + i\sum_{j=1}^{N}\int_t \hat{r}_j(t)\zeta\partial_t r_j(t) + i\sum_{\tau=1}^{N}\int_t \hat{\bar{r}}_\tau(t)\zeta\partial_t\bar{r}_\tau(t)$$

is the contribution from non-interacting particles and

$$L_{int}(r,\bar{r}) = -\sum_{\tau=1}^{N}\hat{\bar{r}}_\tau\frac{\partial}{\partial r_j}V(r_j(t)-\bar{r}_\tau(t)) + \sum_{j=1}^{N}\hat{r}_j\frac{\partial}{\partial\bar{r}_\tau}V(r_j(t)-\bar{r}_\tau(t))$$

being a contribution to the dynamic functional due to the inter-file interactions.

We can also obtain 2-point correlations and cross correlations of any group or pair of observables $\Xi(r_j)$ and $\Xi(\bar{r}_\tau)$ from a generating functional $\mathcal{Z}[\lambda_j,\lambda_\tau]$ defined as

$$\begin{aligned}\mathcal{Z}[\lambda_j,\bar{\lambda}_\tau] \quad &= \int\prod_{j=1}^{N}[dr_j(t)][d\hat{r}_j(t)]\int\prod_{\tau=1}^{N}[d\bar{r}_\tau(t)][d\hat{\bar{r}}_\tau(t)] \\ &\exp\left\{-L + \sum_{j=1}^{N}\int_t\lambda_j(t)\Xi(r_j) + \sum_{\tau=1}^{N}\int_t\bar{\lambda}_\tau(t)\bar{\Xi}(\hat{r}_\tau)\right\}. \qquad (4.7)\end{aligned}$$

This is achieved by taking appropriate functional derivatives of the generating functional with respect to $\lambda_j(t)$ or $\lambda_\tau(t)$. In particular, we can obtain

$$\langle\Xi(r_j)\Xi(r_\tau)\rangle = \left.\frac{\delta^2\mathcal{Z}[\lambda_j,\lambda_\tau]}{\delta(\lambda_j(t))\delta(\lambda_\tau(t'))}\right|_{\{\lambda_j(t)=0,\lambda_\tau(t')=0\}}. \qquad (4.8)$$

The generating functional in equation (4.7) can be suitably generalised to include conjugate fields to any needed variables. Response functions and correlation functions of interest can then be obtained by taking functional derivatives as demonstrated in the expression (4.8).

The particle interaction potential, expressed in terms of particle position variables $r_j(t)$ and $\bar{r}_\tau(t)$, is highly non-linear but it can be transformed to a quadratic form in the collective density variables $n(r,t)$. This is a more natural representation as experiments can easily measure density fields such as number density $n(r,t) = \sum_{j=1}^{N}\delta[r-r_j(t)]$ and current probability density $c(r,t) = \sum_{j=1}^{N}\partial_t r_j(t)\delta[r-r_j(t)]$ rather than particle conformational variables or particle velocities. The transformation of the functional from the conformational degrees of freedom for the particles to a collective particle density description tremendously reduces the complexity of the problem. However, this happens at the cost of loss of information

Stellenbosch University http://scholar.sun.ac.za

as the conformations of the particles cannot be recovered from the knowledge of particle density distribution in the system. For notational simplicity, it is of interest to present the collective density fields in k-space

$$f(x) = \int_k \exp(-ikx)\tilde{f}(k), \tag{4.9}$$

where we denote $\int_k \equiv \int \frac{dk}{2\pi}$ in one dimensional space. The microscopic definitions of the collective fields are

$$\tilde{n}_k(t) = \sum_{j=1}^{N} \exp\left(-ikr_j(t)\right), \tag{4.10a}$$

$$\tilde{\bar{n}}_k(t) = \sum_{j=1}^{N} \exp\left(-ik\bar{r}_j(t)\right), \tag{4.10b}$$

$$\tilde{\nu}_k(t) = \sum_{j=1}^{N} ik\hat{r}_j(t) \exp\left(-ikr_j(t)\right), \tag{4.10c}$$

$$\tilde{\bar{\nu}}_k(t) = \sum_{j=1}^{N} ik\hat{\bar{r}}_j(t) \exp\left(-ik\bar{r}_j(t)\right), \tag{4.10d}$$

$$\tilde{c}_k(t) = \sum_{j=1}^{N} \partial_t r_j(t) \exp\left(-ikr_j(t)\right) \tag{4.10e}$$

$$\text{and} \quad \tilde{\bar{c}}_k(t) = \sum_{\tau=1}^{N} \partial_t \bar{r}_\tau(t) \exp\left(-ik\bar{r}_\tau(t)\right). \tag{4.10f}$$

For the rest of the discussion we shall omit the tilde sign on Fourier variables to simplify the notation. Expressions (4.10a) and (4.10b) are density collective variables written in Fourier space for particles in the first and second file respectively, (4.10c) and (4.10d) are the corresponding dynamical conjugate variables of the collective density fields, (4.10e) and (4.10f) are the probability current density expressions in Fourier space for the respective files.

4.3 Random Phase Approximation

Since the particle distribution in our system is assumed to be uniform, small density fluctuations play an important role in the diffusive behaviour of the particles leading to

Stellenbosch University http://scholar.sun.ac.za

non-trivial density correlations which can be accessed by experiments or which can even be probed with simulations. We therefore express the collective densities in terms of small fluctuations about the average mean field densities, $n_0 = \langle n_k(t)\rangle_0$ and $\bar{n}_0 = \langle \bar{n}_k(t)\rangle_0$ as:

$$\rho_k(t) = n_k(t) - n_0, \quad \bar{\rho}_k(t) = \bar{n}_k(t) - \bar{n}_0, \tag{4.11a}$$

$$\varrho_k(t) = \nu_k(t), \quad \bar{\varrho}_k(t) = \bar{\nu}_k(t) \quad \text{and} \tag{4.11b}$$

$$\vartheta_k(t) = c_k(t) - c_0, \quad \bar{\vartheta}_k(t) = \bar{c}_k(t) - \bar{c}_0. \tag{4.11c}$$

RPA allows us to express the exponential term involving density fields as cumulant expansions of the integrals. To achieve this, we first use the condition that the fluctuation must equal the physical density fields minus a constant number density to define the following unity

$$\begin{aligned}
1 = & \int [d\rho_k(t), d\bar{\rho}_k(t), d\vartheta_k(t), d\bar{\vartheta}_k(t), d\varrho_k(t), d\bar{\varrho}_k(t)] \\
& \int [d\hat{\rho}_k(t), d\hat{\bar{\rho}}_k(t), d\hat{\vartheta}_k(t), d\hat{\bar{\vartheta}}_k(t), d\hat{\varrho}_k(t), d\hat{\bar{\varrho}}_k(t)] \\
& + \exp\left\{ i \int_{k,t} \hat{\rho}_k(t) \left(\rho_k(t) - n_k(t) + n_0\right) \right. \\
& + i \int_{k,t} \hat{\bar{\rho}}_k(t) \left(\bar{\rho}_k(t) - \bar{n}_k(t) + \bar{n}_0\right) \\
& + i \int_{k,t} \hat{\vartheta}_k(t) \left(\vartheta_k(t) - c_k(t)\right) \\
& + i \int_{k,t} \hat{\bar{\vartheta}}_k(t) \left(\bar{\vartheta}_k(t) - \bar{c}_k(t)\right) \\
& + i \int_{k,t} \hat{\varrho}_k(t) \left(\varrho_k(t) - \nu_k(t)\right) \\
& \left. + i \int_{k,t} \hat{\bar{\varrho}}_k(t) \left(\bar{\varrho}_k(t) - \bar{\nu}_k(t)\right) \right\}
\end{aligned} \tag{4.12}$$

.

In the previous equation, expressions (4.11a)-(4.11c) are used as functional delta function constraints. As we have seen in equation (4.5), raising the arguments of the delta functionals into the exponent introduces fluctuation response fields. In this case the response fields are $\hat{\rho}_k(t), \hat{\varrho}_k(t), \hat{\bar{\rho}}_k(t), \hat{\bar{\varrho}}_k(t), \hat{\vartheta}_k(t)$ and $\hat{\bar{\vartheta}}_k(t)$. The notation $\int [d\rho, d\varrho \cdots] \int [d\hat{\rho}] \int [d\hat{\varrho}] \cdots$ simply implies a product of functional integral measures. When substituted in the functional in equation (4.5), this unity implements a coordinate transformation from microscopic density fields to microscopic density fluctuations fields. The Jacobian of the transformation

Stellenbosch University http://scholar.sun.ac.za

is unity. The resulting functional, on putting together equation (4.12) and equation (4.5), can be written as follows

$$\begin{aligned}\mathcal{Z} &= \int [d\rho_k(t), d\bar{\rho}_k(t), d\vartheta_k(t), d\bar{\vartheta}_k(t), d\varrho_k(t), d\bar{\varrho}_k(t)] \\ &\quad \int [d\hat{\rho}_k(t), d\hat{\bar{\rho}}_k(t), d\hat{\vartheta}_k(t), d\hat{\bar{\vartheta}}_k(t), d\hat{\varrho}_k(t), d\hat{\bar{\varrho}}_k(t)] \\ &\quad \exp(-L_1 - L_2) \left\langle \exp(-L_3) \right\rangle_0 , \end{aligned} \tag{4.13}$$

where the interaction term, which is quadratic in the fluctuating fields, is given by

$$L_1 = \int_{k,t} \left(\rho_k(t) \widetilde{V}_{-k}(t) \bar{\varrho}_{-k}(t) + \bar{\rho}_k(t) \widetilde{V}_{-k}(t) \varrho_{-k}(t) \right). \tag{4.14}$$

The term

$$\begin{aligned} L_2 = - & \; i \int_{k,t} \rho_k(t) \hat{\rho}_{-k}(t) - i \int_{k,t} \varrho_k(t) \hat{\varrho}_{-k}(t) \\ - & \; i \int_{k,t} \bar{\rho}_k(t) \hat{\bar{\rho}}_{-k}(t) - i \int_{k,t} \bar{\varrho}_k(t) \hat{\bar{\varrho}}_{-k}(t) \\ & -i \int_{k,t} \hat{\vartheta}_k(t) \vartheta_{-k}(t) - i \int_{k,t} \hat{\bar{\vartheta}}_k(t) \bar{\vartheta}_{-k}(t), \end{aligned} \tag{4.15}$$

is also quadratic in the density fields (see Appendix C.2 for details). The term $\langle L_3 \rangle_0$ is a contribution from non-interacting files system. Here L_3 is given by

$$\begin{aligned} L_3 = & \; i \sum_{j=1}^{N} \int_{k,t} \hat{\rho}_k(t) e^{-ikr_j(t)} - \sum_{j=1}^{N} \int_{k,t} k \hat{\varrho}_k(t) \hat{r}_j(t) e^{-ikr_j(t)} \\ + & \; i \sum_{\tau=1}^{N} \int_{k,t} \hat{\bar{\rho}}_k(t) e^{-ik\bar{r}_j(t)} - \sum_{\tau=1}^{N} \int_{k,t} k \hat{\bar{\varrho}}_k(t) \hat{\bar{r}}_\tau(t) e^{-ik\bar{r}_\tau(t)} \\ + & \; i \sum_{j=1}^{N} \int_{k,t} \hat{\vartheta}_k(t) \partial_t r_j(t) e^{-ikr_j(t)} + i \sum_{\tau=1}^{N} \int_{k,t} \hat{\bar{\vartheta}}_k(t) \partial_t \bar{r}_\tau(t) e^{-ikr_\tau(t)}. \end{aligned} \tag{4.16}$$

In equation (4.13), $\langle (\ldots) \rangle_0$ denotes an average with statistical weight

$$\int \prod_{j=1}^{N} [dr_j(t), d\hat{r}_j(t)] \int \prod_{\tau=1}^{N} [dr_\tau(t), d\hat{r}_\tau(t)] \exp(-L_0).$$

Stellenbosch University http://scholar.sun.ac.za

To make the cumulant average L_3 quadratic in the fluctuating fields, we can use the approximation $\left\langle e^{-L_3}\right\rangle_0 \simeq e^{-\frac{1}{2}\left\langle L_3^2\right\rangle_0}$, hence the contributions from interaction and density fluctuations become $L = L_1 + L_2 + \frac{1}{2}\left\langle L_3^2\right\rangle_0$. Using vector notation, the effective theory can be expressed in a more compact notation as follows

$$\begin{aligned} L &= -\frac{1}{2}\int_{k,\omega} \hat{\boldsymbol{\rho}}(k,\omega)\mathbf{V}(k,\omega)\boldsymbol{\rho}^T(-k,-\omega) \\ &+ \int_{k,\omega} \hat{\boldsymbol{\rho}}(k,\omega)\boldsymbol{M}(k,\omega)\boldsymbol{\rho}^T(-k,-\omega) \\ &- \frac{1}{2}\int_{k,\omega} \hat{\boldsymbol{\rho}}(k,\omega)\boldsymbol{S}(k,\omega)\hat{\boldsymbol{\rho}}^T(-k,-\omega). \end{aligned} \tag{4.17}$$

We have introduced the vectors

$$\boldsymbol{\rho}(k,\omega) = \left(\rho_k(\omega), \bar{\rho}_k(\omega), \bar{\vartheta}_k(\omega), \vartheta_k(\omega), \varrho_k(\omega), \bar{\varrho}_k(\omega)\right), \tag{4.18a}$$

$$\hat{\boldsymbol{\rho}}(k,w) = \left(\hat{\rho}_k(\omega), \hat{\bar{\rho}}_k(\omega), \hat{\bar{\vartheta}}_k(\omega), \hat{\vartheta}_k(\omega), \hat{\varrho}_k(\omega), \hat{\bar{\varrho}}_k(\omega)\right), \tag{4.18b}$$

along with the dynamic interaction matrices

$$\boldsymbol{V}(k,\omega) = \begin{pmatrix} 0 & 0 & 0 & 0 & 0 & \widetilde{V}_{-k}(\omega) \\ 0 & 0 & 0 & 0 & \widetilde{V}_{-k}(\omega) & 0 \\ 0 & 0 & 0 & 0 & 0 & 0 \\ 0 & 0 & 0 & 0 & 0 & 0 \\ 0 & \widetilde{V}_k(\omega) & 0 & 0 & 0 & 0 \\ \widetilde{V}_k(\omega) & 0 & 0 & 0 & 0 & 0 \end{pmatrix} \tag{4.19}$$

and the non-interacting system correlation-response matrix

$$\boldsymbol{S}(k,\omega) = \begin{pmatrix} s_{11} & 0 & s_{13} & 0 & s_{15} & 0 \\ 0 & s_{22} & 0 & s_{24} & 0 & s_{26} \\ s_{31} & 0 & s_{33} & 0 & s_{35} & 0 \\ 0 & s_{42} & 0 & s_{44} & 0 & s_{46} \\ s_{51} & 0 & s_{53} & 0 & 0 & 0 \\ 0 & s_{62} & 0 & s_{64} & 0 & 0 \end{pmatrix}. \tag{4.20}$$

Stellenbosch University http://scholar.sun.ac.za

See Appendix C for details on how we obtain elements of the interaction matrix and the elements of the non-interacting system correlation matrix by simplifying the exponential term in equation (4.13). In the matrix $\boldsymbol{S}(k,\omega)$, the diagonal elements give the dynamic correlations for a non-interacting system while the off-diagonal entries are the response functions for the uncoupled system. A Fourier transform in time has been performed as it was done in equation (4.9), we use the shorthand notation $\int_w \equiv \frac{dw}{2\pi}$. The matrix $\boldsymbol{M}(k,\omega) = iI_6$, where I_6 is a 6×6 unit matrix. The matrices $\boldsymbol{S}(k,\omega)$ and $\boldsymbol{V}(k,\omega)$ are non-symmetric owing to our choice of the notation which include some complex pre-factors. Upon integrating out the correlation response field $\hat{\boldsymbol{\rho}}$, the resulting expression for the functional is

$$\mathcal{Z} \approx \int [d\boldsymbol{\rho}] \exp\left(-\frac{1}{2}\int_{k,\omega} \boldsymbol{\rho}(k,\omega)\left[\boldsymbol{V}(k,\omega)+\boldsymbol{S}^{-1}(k,\omega)\right]\boldsymbol{\rho}^{\top}(-k,-\omega)\right).$$

Finally we can now define the generating functional

$$\begin{aligned}\mathcal{Z}[\boldsymbol{h}(k,\omega)] &\approx \int [d\boldsymbol{\rho}] \exp\left(-\frac{1}{2}\int_{k,\omega} \boldsymbol{\rho}(k,\omega)\left[\boldsymbol{V}(k,\omega)+\boldsymbol{S}^{-1}(k,\omega)\right]\boldsymbol{\rho}^{\top}(-k,-\omega)\right.\\ &+ \left.\int_{k,\omega}\boldsymbol{\rho}(k,\omega)\boldsymbol{h}^{\top}(-k,-\omega)\right) \qquad (4.21)\\ &= \exp\left(-\frac{1}{2}\int_{k,\omega}\boldsymbol{h}(k,\omega)\left[\boldsymbol{V}(k,\omega)+\boldsymbol{S}^{-1}(k,\omega)\right]^{-1}\boldsymbol{h}^{\top}(-k,-\omega)\right).\end{aligned}$$

By taking a functional derivative with respect to $\boldsymbol{h}$, we then obtain the pair correlation function matrix of the collective fields

$$\begin{aligned}\langle\boldsymbol{\rho}(k,\omega)\boldsymbol{\rho}(k',\omega')\rangle &= \left[-\frac{\delta^2\mathcal{Z}}{\delta\boldsymbol{h}(k,\omega)\delta\boldsymbol{h}(k',\omega')}\right]_{\boldsymbol{h}=0}\\ &= \delta(k+k')\delta(w+\omega')\boldsymbol{C}(k,\omega),\end{aligned}$$

where

$$\boldsymbol{C}(k,\omega) = \left[\boldsymbol{V}(k)(k,\omega)+\boldsymbol{S}^{-1}(k,\omega)\right]^{-1}. \qquad (4.22)$$

4.4 RPA results

From the matrix $\boldsymbol{C}(k,\omega)$ we obtain the RPA-correlation and response functions. The diagonal elements $\boldsymbol{C}_{11}(k,\omega) = \boldsymbol{C}_{22}(k,\omega)$ are the intra-file density-density correlation function

Stellenbosch University http://scholar.sun.ac.za

in each of the the files while $\boldsymbol{C}_{12}(k,\omega) = \boldsymbol{C}_{21}(k,-\omega)$ is the inter-file density-density correlation function. The intra-file density-density correlation function, expressed in terms of a decoupled file correlation function s_{11} and response functions s_{15} and s_{51} that are coupled to the file interaction potential , is given by

$$\boldsymbol{C}_{11}(k,\omega) = \frac{s_{11}(k,\omega)\left(1-\widetilde{V}^2(k)s_{15}(k,\omega)s_{51}(k,\omega)\right)}{\left(1+\widetilde{V}^2(k)s_{15}^2(k,\omega)\right)\left(1+\widetilde{V}^2(k)s_{51}^2(k,\omega)\right)}. \tag{4.23}$$

while the inter-file density-density correlation function is expressed as,

$$\boldsymbol{C}_{12}(k,\omega) = \frac{is_{11}(k,\omega)\left(\widetilde{V}(s_{15}(k,\omega)+s_{51}(k,\omega))\right)}{\left(1+\widetilde{V}^2(k)s_{15}^2(k,\omega)\right)\left(1+\widetilde{V}^2(k)s_{51}^2(k,\omega)\right)}. \tag{4.24}$$

As we can see in expressions (4.23) and (4.24) the inter-file density-density correlation function is an even function of the interaction potential $\widetilde{V}$, while intra-file density-density correlation function is an odd function of $\widetilde{V}$. To explore the structure of these correlation functions we choose a short range interaction potential that is modelled by a Gaussian function expressed as

$$\widetilde{V}(k) = ACe^{-\frac{1}{2}C^2k^2}, \tag{4.25}$$

in Fourier transformed spatial variables. The constants A and C are the two arbitrary parameters of choice that we will be adjusting for the strength and range of the interaction. The two correlation functions expressed in terms of the Gaussian potential have a dominating maxima at finite length scales Fig. 4.2.

The position of the maxima shift towards higher values of k with increase in the strength of the interaction parameter A Fig. 4.3. For higher frequencies, the maxima position shift is very small, while for smaller frequencies the shift is significant. For frequencies smaller than $\omega = 0.01$ for $\boldsymbol{C}_{11}(k,\omega)$ and frequencies smaller than $\omega = 0.02$ for $\boldsymbol{C}_{12}(k,\omega)$, the correlation functions attain a local maxima. The values of the correlation functions around their second maxima is very small in comparison to their values around their respective global maxima. The maxima of the correlation functions tell us about the length scales of the particle distribution in the file. In section 4.7, on a discussion of the density-density correlation function for an elastically coupled multi-files system, we shall see that the value of an inter-file correlation function around the second maxima can get significantly large

Stellenbosch University http://scholar.sun.ac.za

as we increase the interaction parameter values. This points us to the possibility of an interesting dynamic phenomena that is associated with the particle distribution within a file.

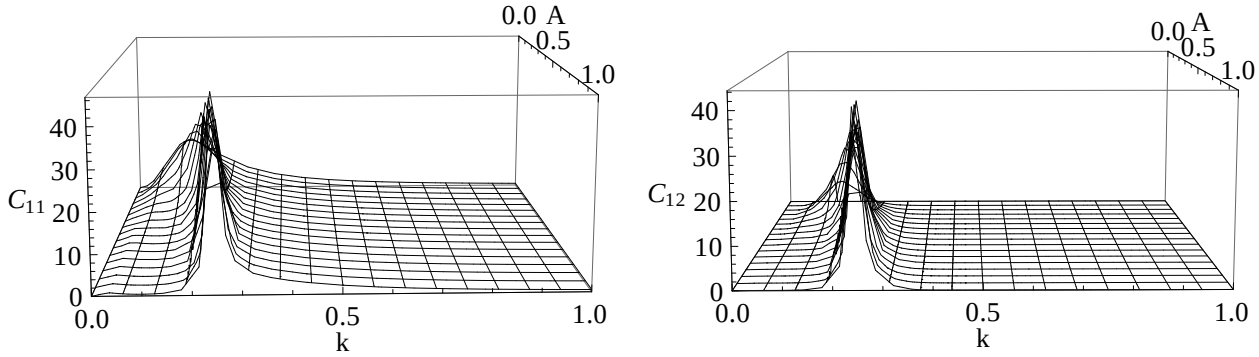

(a) $\boldsymbol{C}_{11}(k,\omega)$ (b) $\boldsymbol{C}_{12}(k,\omega)$

FIG. 4.2. (a) Graph of the intra-file density-density correlation function $\boldsymbol{C}_{11}(k,\omega)$ and (b) Graph of the intra-file correlation function $\boldsymbol{C}_{12}(k,\omega)$ for the two coupled file system at temperature $\beta = 1$ with each having file density $= \frac{3}{4}$ and friction coefficient $\zeta = 0.9$. The short range file interaction potential is modelled by a Gaussian function of amplitude A and with $C = 10$.

Upon comparing $\boldsymbol{C}_{11}(k,\omega)$ and $\boldsymbol{C}_{12}(k,\omega)$ we see that the dominating length scales is almost the same for a specific value of the interaction parameter. However, the frequency at which the second maxima starts to be seen is different. From this we can infer that the effect of deformation has a slight delay in manifesting at the local particle distribution in comparison to how it is communicated between files. This is manifestation of causality in connection with the self-exclusive behaviour of the particles across files.

The off-diagonal elements are the response functions. The density response functions are such that $\boldsymbol{C}_{51}(k,\omega) = \boldsymbol{C}_{62}(k,\omega) = \boldsymbol{C}_{15}(k,-\omega) = \boldsymbol{C}_{26}(k,-\omega)$ where

$$\boldsymbol{C}_{51}(k,\omega) = \frac{s_{51}(k,\omega)}{1+\widetilde{V}^2 s_{51}^2(k,\omega)}, \tag{4.26}$$

while current response functions are such that $\boldsymbol{C}_{53}(k,\omega) = \boldsymbol{C}_{64}(k,\omega) = \boldsymbol{C}_{35}(k,-\omega) =$

Stellenbosch University http://scholar.sun.ac.za

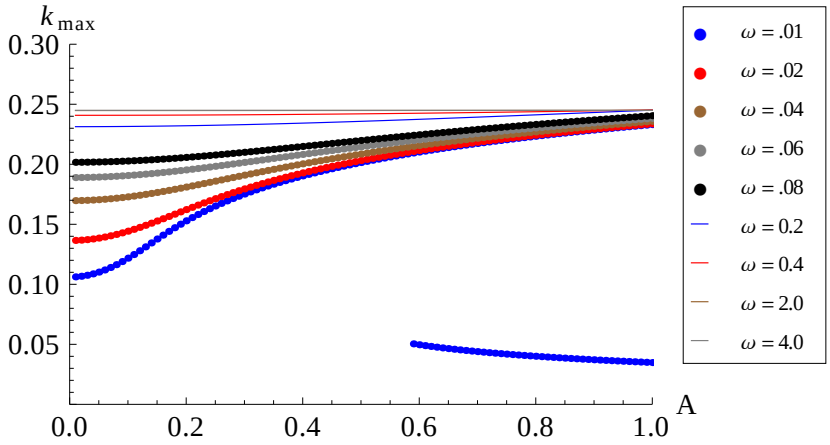

(a) $\boldsymbol{C}_{11}(k,\omega)$

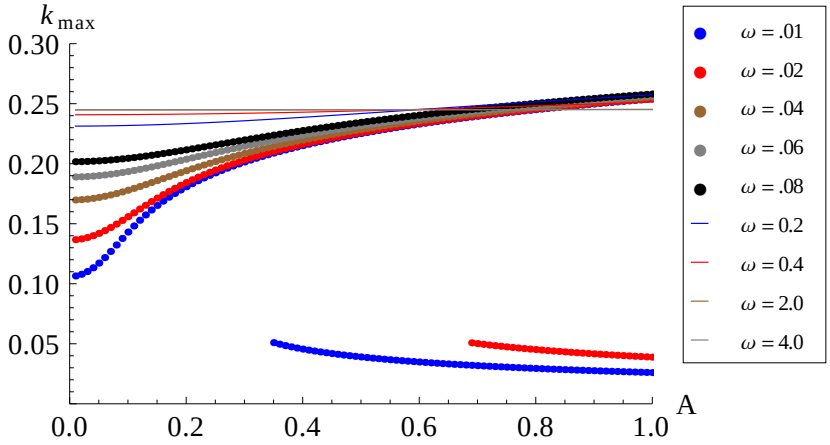

(b) $\boldsymbol{C}_{12}(k,\omega)$

FIG. 4.3. (a) Graph of the position $k_{\max}$ of the two coupled file intra-file density-density correlation function, $\boldsymbol{C}_{11}(k,\omega)$, and (b) intra-file correlation function, $\boldsymbol{C}_{12}(k,\omega)$, maxima for the two coupled file system at temperature $\beta = 1$ with each having file density $= \frac{3}{4}$ and friction coefficient $\zeta = 0.9$. The positions of the maxima are plotted for varied interaction strength A at different frequency ω. The short range file interaction potential is modelled by a Gaussian function of amplitude A and with $C = 10$.

Stellenbosch University http://scholar.sun.ac.za

$\boldsymbol{C}_{46}(k,-\omega)$ having

$$\boldsymbol{C}_{53}(k,\omega) = \frac{s_{53}(k,\omega)}{1+\widetilde{V}^2(k)s_{51}^2(k,\omega)}. \tag{4.27}$$

The relationship between the density-density correlation functions and the density response function per file is given by the fluctuation-dissipation theorem (FDT)

$$\beta w\boldsymbol{C}_{11}(k,\omega) = \boldsymbol{C}_{15}(k,\omega) - \boldsymbol{C}_{15}(k,-\omega), \tag{4.28}$$

where $\boldsymbol{C}_{33}(k,\omega) = \boldsymbol{C}_{44}(k,\omega)$ is the current-current correlation function. It can be expressed up to second order in $\widetilde{V}(k)$ leading to

$$\begin{aligned}\boldsymbol{C}_{33}(k,\omega) &= s_{33}(k,\omega) - \widetilde{V}^2(k)\left(s_{13}^2(k,\omega)s_{15}(k,\omega)\right.\\ &+ s_{11}(k,\omega)s_{13}(k,\omega)s_{31}(k,\omega)\\ &+ \left.s_{31}^2(k,\omega)s_{51}(k,\omega)\right).\end{aligned} \tag{4.29}$$

The current-current correlation and the current response function per file are related by the FDT

$$\beta^2 w\frac{\zeta}{k}\boldsymbol{C}_{33}(k,\omega) = \boldsymbol{C}_{35}(k,\omega) - \boldsymbol{C}_{35}(k,-\omega). \tag{4.30}$$

The rest of the non zero terms are various cross correlations of density or current density fields within the two coupled files. We would like to highlight, at this point, that the first order correction of the FDT within the RPA leads to the FDT for an uncoupled system that could also be constructed from the appropriate elements of the $\boldsymbol{S}(k,\omega)$ matrix. The fact that FDT is valid for current in the system re-affirms that current density contains similar information as density per given position in the system.

4.5 Mean field description of particle dynamics in a multi-coupled file system

We are now in a position to generalise the two coupled file system into a multiple-coupled file systems. In this section we show how the time evolution of a particle in some reference file within the system is influenced by the effective interaction attributed to the rest of the coupled files.

Stellenbosch University http://scholar.sun.ac.za

4.5.1 The generating functional of a multi-coupled file in collective variables

We think of the generalised multiple file system as consisting of $N+1$ files that are elastically coupled together with the inter-file interaction similar to that of the two file system. The dynamics of the jth particle inside a reference file at any time t is parametrised by a position variable $r_j(t)$. In a similar manner, the dynamics of the τth particle in any pth file other than the reference file, is parametrised by the position variable $r_\tau^{(p)}(t)$. The equal time dynamical evolution of particles in the reference file and any of its neighbouring files is described by the respective Langevin equations:

$$\mathcal{L}_j^{(ref)} = -\zeta\partial_t r_j(t) + \sum_{p=1}^{N'}\sum_{\tau=1}^{N} F(r_j(t) - r_\tau^{(p)}) + f_j(t) = 0 \tag{4.31}$$

and

$$\begin{aligned}\mathcal{L}_\tau^{(p)} &= -\zeta\partial_t r_\tau^{(p)}(t) - \sum_{\eta=1}^{N'}\sum_{j=1}^{N} F(r_\tau^{(p)}(t) - r_j^{\eta}(t)) \\ &- \sum_{j=1}^{N} F(r_\tau^{(p)}(t) - r_j(t)) + f_\tau^{(p)}(t) = 0.\end{aligned} \tag{4.32}$$

The mean field assumption is that each file has an equal number of interacting neighbouring files and that each file interacts with every other file in the system. We also assume that all the files have a uniform particle density. The term $F(r_\tau^{(p)}(t) - r_j^{(\eta)}(t))$ denotes the force the pth file experiences due to the deformation mediated by the particle at position $r_j^{(\eta)}(t)$ at time t. The random forces within the files retain similar properties as those in a two coupled file system and have similar correlators as given in equations (4.2a) and (4.2b) (with $f_\tau^p(t)$ in the place of $\bar{f}_\tau(t)$).

Following the standard MSR-functional integral representation of the system as described

Stellenbosch University http://scholar.sun.ac.za

by equations (4.31-4.32), the functional integral for the multi coupled file system becomes

$$\begin{aligned}\mathcal{Z}\left(\{h_j^{(p)}(t),\hat{h}_\tau^{(p)}(t)\}\right) = & \int\prod_{j=1}^{N}[dr_j(t)][d\hat{r}_j(t)]\int\prod_{p=1}^{N'}\prod_{\tau=1}^{N}[d\hat{\bar{r}}_\tau^{(p)}(t)][d\bar{r}_\tau^{(p)}(t)] \\ & \exp\left\{L_0^{ref}\{r_j(t),\hat{r}_\tau(t)\}+\sum_{p=1}^{N'}L_0^{(p)}\{r_j(t),\hat{r}_\tau^{(p)}(t)\}\right. \\ & +i\int_{t,k}\sum_{p=1}^{N'}\sum_{j=1,\tau=1}^{N,N}ik\hat{r}_\tau^{(p)}(t)\exp\{ik(r_j^{(p)}-r_\tau)\}\widetilde{V}(k) \\ & -i\int_{t,k}\sum_{p=1}^{N'}\sum_{j=1,\tau=1}^{N,N}ik\hat{r}_j(t)\exp\{ik(r_j-r_\tau^{(p)})\}\widetilde{V}(k) \\ & -i\int_{t,k}\sum_{p=1}^{N'}\sum_{\eta\neq p=1}^{N'}\sum_{j=1}^{N}\sum_{\tau=1}^{N}ik\hat{r}_j(t)\exp\{ik(r_j^{(p)}(t)-r_\tau^{(\eta)}(t))\} \\ & \left.\widetilde{V}(k)+\sum_{j=1}^{N}\int_t h_j^{(p)}(t)r_j^{(p)}(t))+\sum_{\tau=1}^{N}\int_t\hat{h}_\tau^{(p)}(t)r_\tau^{(p)}(t)\right\}, \quad (4.33)\end{aligned}$$

where $L_0^{(ref)}\{r_j(t),\hat{r}_\tau(t)\}$ and $L_0^{(p)}\{r_j(t),\hat{r}_\tau^{(p)}(t)\}$ are the MSR-actions for a noninteracting system given by:

$$L_0^{(ref)}(r_j(t),\hat{r}_\tau(t)) = \frac{1}{2\alpha}\sum_{j=1}^{N}\int_t\hat{r}_j^2(t)+i\sum_{j=1}^{N}\int_t\hat{r}_j(t)\zeta\partial_t r_j(t) \quad \text{and} \quad (4.34)$$

$$L_0^{(p)}(r_j^{(p)}(t),\hat{r}_\tau^{(p)}(t)) = \frac{1}{2\alpha}\sum_{\tau=1}^{N}\int_t(\hat{r}_\tau^{(p)}(t))^2+i\sum_{\tau=1}^{N}\int_t\hat{r}_\tau^{(p)}(t)\zeta\partial_t r_\tau^{(p)}(t). \quad (4.35)$$

The variables $\hat{h}_j^{(p)}(t)$ and $\hat{h}_\tau^{(p)}(t)$ are external fields conjugate to $r_j^{(p)}(t)$ and $r_\tau^{(p)}(t)$. In the same spirit as for the two file system, collective variables can now be introduced to the generating functional. We need to represent the functional in terms of the density fluctuation fields about the mean global density of the files $n_0 = \left\langle n_k^{(p)}(t)\right\rangle_0$. The density fields and density response fields are defined in Fourier space as in equations (4.10a) and equation (4.10c), but with the index p to enumerate the files other than the reference files. In terms of the collective variable the generating functional becomes

Stellenbosch University http://scholar.sun.ac.za

$$\mathcal{Z}(\cdots) \quad = \tag{4.36}$$

$$\int [d\rho_k(t)][d\varrho_k(t)] \int \prod_{p=1}^{N'} [d\rho_k^{(p)}(t)][d\varrho_k^{(p)}(t)] \exp\left\{ i \sum_{p=1}^{N'} \int_{k,t} \right.$$

$$\left(\rho_k(t)\widetilde{V}_{-k}(t)\varrho_{-k}^{(p)}(t) + \rho_k(t)^{(p)}\ \widetilde{V}_{-k}(t)\varrho_{-k}(t) + \sum_{\eta\neq p=1}^{N'} \rho_k^{(p)}(t)\widetilde{V}_{-k}(t)\varrho_{-k}^{(\eta)}(t) \right)$$

$$\left. + i\int_{k,t} (\hat{\rho}_k(t)\rho_k(t) + \hat{\varrho}_k(t)\varrho_k(t)) + i\int_{k,t} \left(\sum_{p=1}^{N'} \hat{\rho}_k^{(p)}(t)\rho_k^{(p)}(t) + \sum_{p=1}^{N'} \hat{\varrho}_k^{(p)}(t)\varrho_k^{(p)}(t) \right) \right\}$$

$$\left\langle \exp\left\{ -i\int_{k,t} (\hat{\rho}_k(t)n_k(t) + \hat{\varrho}_k(t)\nu_k(t))\ - i\int_{k,t} \left(\sum_{p=1}^{N'} \hat{\rho}_k^{(p)}(t)n_k^{(p)}(t) + \sum_{p=1}^{N'} \hat{\varrho}_k^{(p)}(t) \right.\right.\right.$$

$$\left.\left.\left. \times\nu_k^{(p)}(t) \right) \right\} \right\rangle_0 . \tag{4.37}$$

The notation $(\cdots)$ is used to remind us that arguments of the functional are left out just for notational convenience. Equation (4.37) is similar in structure to equation (4.6) and the RPA is handled in a similar way (See Appendix C for details). The argument of the first exponential contains contributions from inter-file interactions and it is quadratic in the fluctuation fields. The cumulant average of the second exponential term is taken with respect to the action of the noninteracting file system. Upon substituting the exponential definition of the density fields $\{n_k(t), n_k^{(p)}(t)\}$ and the density response fields $\{\nu_k(t), \nu_k^{(p)}(t)\}$, this term can be identified with the average $\langle \exp(-L_3) \rangle$ and merits similar approximations (as done in expression (C.19) in appendix C. This permits us to express the average up to quadratic order in the fluctuation fields, having the free system correlations $\{s_{11}(k,t), s_{11}^{(p)}(k,t)\}$ and response functions $\{s_{12}(k,t), s_{12}^{(p)}(k,t)\}$ as coefficients.

In the approximated form of the functional, we consider the fact that the files are indistinguishable and are presumed to have a uniform density. We therefore drop the index p on the fields and replace the sum by the number of summed over files. In order to express the resulting functional in a more compact form, it is convenient to introduce the notation

Stellenbosch University http://scholar.sun.ac.za

$$\begin{aligned}
\boldsymbol{\rho}_r(k,t) &= (\rho_k(t), \varrho_k(t))\,, \\
\hat{\boldsymbol{\rho}}_r(k,t) &= (\hat{\rho}_k(t), \hat{\varrho}_k(t))\,, \\
\boldsymbol{\rho}_m(k,t) &= \left(\rho_k^{(m)}(t), \varrho_k^{(m)}(t)\right) \quad \text{and} \\
\hat{\boldsymbol{\rho}}_m(k,t) &= \left(\hat{\rho}_k^{(m)}(t), \hat{\varrho}_k^{(m)}(t)\right). \qquad (4.38)
\end{aligned}$$

Here we use the subscript r and m to distinguish fluctuation fields from reference files and fields from other coupled files. Expressed in frequency space, the generating functional then becomes

$$\begin{aligned}
\mathcal{Z}(\cdots) &= \int [d\boldsymbol{\rho}_r(k,\omega), d\hat{\boldsymbol{\rho}}_r(k,\omega), d\boldsymbol{\rho}_m(k,\omega), d\hat{\boldsymbol{\rho}}_m(k,\omega)] \\
&\exp\left\{ \int_{k,\omega} \hat{\boldsymbol{\rho}}_r(k,\omega)\boldsymbol{M}(k,\omega)\boldsymbol{\rho}_r^{\top}(-k,-\omega) \right. \\
&-\frac{1}{2}\int_{k,\omega} \hat{\boldsymbol{\rho}}_r(k,\omega)\boldsymbol{S}(k,\omega)\hat{\boldsymbol{\rho}}_r^{\top}(-k,-\omega) \\
&-\frac{N'}{2}\int_{k,\omega} \boldsymbol{\rho}_r(k,\omega)\mathbf{V}(k,\omega)\boldsymbol{\rho}_m^{\top}(-k,-\omega) + \\
&N'\int_{k,\omega} \hat{\boldsymbol{\rho}}_m(k,\omega)\boldsymbol{M}(k,\omega)\boldsymbol{\rho}_{(m)}^{\top}(-k,-\omega) \\
&-\frac{N'}{2}\int_{k,\omega} \hat{\boldsymbol{\rho}}_m(k,\omega)\boldsymbol{S}(k,\omega)\hat{\boldsymbol{\rho}}_m^{\top}(-k,-\omega) \\
&\left. -\frac{1}{2}N'(N'-1)\int_{k,\omega} \boldsymbol{\rho}_m(k,\omega)\mathbf{V}(k)\boldsymbol{\rho}_m^{\top}(-k,-\omega) \right\}, \qquad (4.39)
\end{aligned}$$

where the matrix $\boldsymbol{M} = iI_2$, with I_2 being a 2×2 unit matrix,

$$\boldsymbol{V}(k) = i\begin{pmatrix} 0 & \widetilde{V}(k) \\ \widetilde{V}(k) & 0 \end{pmatrix},$$

and

$$\boldsymbol{S}(k,\omega) = \begin{pmatrix} s_{11}(k,\omega) & s_{12}(k,\omega) \\ s_{21}(k,\omega) & 0 \end{pmatrix}. \qquad (4.40)$$

Stellenbosch University http://scholar.sun.ac.za

Integrating out all the hatted fields and density fields, other than that of the reference file, the generating functional becomes

$$\begin{aligned}\mathcal{Z}\left(\boldsymbol{h}(k,\omega)\right) &= \int [d\boldsymbol{\rho}_k(k,\omega)] \exp\left\{-\frac{1}{2}\int_{k,\omega} \boldsymbol{\rho}_r(k,\omega)\right. \\ &\quad \left[(\boldsymbol{S}(k,\omega))^{-1} + \mathbb{A}(k,\omega)\right] \boldsymbol{\rho}_r^{\top}(-k,-\omega) \\ &\quad \left. + \int_{k,\omega} \boldsymbol{h}(k,\omega)\boldsymbol{\rho}_r^{\top}(-k,-\omega)\right\}. \end{aligned} \tag{4.41}$$

4.6 Dynamic correlation-response functions

Having integrated out the $\rho_r(k,\omega)$ in equation (4.41), we see that the multi-file system correlation or response function can finally be extracted from the 2×2 matrix $\mathbb{G}_{ab}$ whose inverse is given by

$$[\mathbb{G}^{-1}(k,\omega)]_{ab} = [s^{-1}(k,\omega)]_{ab} - \mathbb{A}_{ab}(k,\omega), \quad \text{with} \quad a,b \in \{1,2\} \tag{4.42}$$

where the matrix $\mathbb{A}(k,\omega)$ has a triangular block structure

$$\mathbb{A}(k,\omega) = \begin{pmatrix} 0 & \mathbb{A}_{12}(k,\omega) \\ \mathbb{A}_{21}(k,\omega) & \mathbb{A}_{11}(k,\omega) \end{pmatrix} \tag{4.43}$$

and can be expressed as

$$\mathbb{A}(k,\omega) = (N')^2 \boldsymbol{V}(k,\omega)\left(N'\boldsymbol{S}^{-1}(k,\omega) + N'(N'-1)\boldsymbol{V}(k,\omega)\right)^{-1}\boldsymbol{V}^{\top}(-k,-\omega).$$

The diagonal element

$$\mathbb{G}_{11}(k,\omega) = \frac{s_{11}(k,\omega)s_{12}^{-1}(k,\omega)s_{21}^{-1}(k,\omega)}{[s_{12}^{-1}(k,\omega) - \mathbb{A}_{12}(k,\omega)][s_{21}^{-1}(k,\omega) - \mathbb{A}_{21}(k,\omega)]} \tag{4.44}$$

gives dynamic correlation function while the off diagonal elements

$$\mathbb{G}_{12}(k,\omega) = \frac{1}{s_{12}^{-1}(k,\omega) - \mathbb{A}_{12}(k,\omega)}, \tag{4.45}$$

$$\mathbb{G}_{21}(k,\omega) = \frac{1}{s_{21}^{-1}(k,\omega) - \mathbb{A}_{21}(k,\omega)} \tag{4.46}$$

Stellenbosch University http://scholar.sun.ac.za

are the response functions for the elastically coupled multi file system. As we can see each of the matrix elements $\mathbb{G}_{ab}(k,\omega)$ is expressible as a function of the non-interacting file system density correlation functions $s_{11}(k,\omega)$ or response functions $s_{12}(k,\omega)$ and $s_{21}(k,\omega)$ that are coupled to the interaction potential $\widetilde{V}(k)$. The interacting system correlation function and response functions are also related by the FDT

$$\beta\omega\mathbb{G}_{11}(k,\omega) = \mathbb{G}_{12}(k,\omega) - \mathbb{G}_{21}(k,\omega). \tag{4.47}$$

The short range interaction potential is $V(k)$ is modelled by Gaussian function expressed as

$$\widetilde{V}(k) = ACe^{-\frac{1}{2}C^2k^2}, \tag{4.48}$$

in Fourier transformed spatial variables. The constants A and C are the two arbitrary parameters of choice that we will be adjusting for the strength and range of the interaction.

4.7 Density-density correlations

Upon substituting the explicit expressions for $s_{11}(k,\omega)$, $s_{12}(k,\omega)$ and $s_{21}(k,\omega)$ we can now discuss what the dynamic density correlation function tells us about the diffusive behaviour of particles in each of the files within the elastically coupled multi file system. In the context of the RPA approximation used, we will only consider terms up to second order in the interaction potential $\widetilde{V}(k)$ and we study the structure of intra-file density correlation for different values of the parameters of the system. Expressed up to second order in the inter-file interaction potential, the correlation function $\mathbb{G}_{11}(k,\omega)$ is given by

$$\begin{aligned}&\mathbb{G}_{11}(k,\omega)\\ &= \frac{2\beta\zeta k^2\rho}{(\beta^2\zeta^2\omega^2+k^4)}\left(1-\frac{\beta^2k^4\rho^2N'\widetilde{V}^2(k)\left(3k^4-\beta^2\zeta^2\omega^2\right)}{\left(\beta^2\zeta^2\omega^2+k^4\right)^2}\right).\end{aligned} \tag{4.49}$$

Upon exploring the dependence of the correlation function on the interaction strength, we identify three main finite frequency regimes in which the correlation function manifests different underlying dynamical structures. We refer to these regimes as high frequency, intermediate frequency and low frequency regime. In the high frequency regime $\omega > 1$

Stellenbosch University http://scholar.sun.ac.za

the correlation function has a single maximum for a specific interaction potential strength. Upon varying the strength of the interaction potential amplitude A, the position of the maxima changes minimally and the dominating length scale is comparable to that of a non-interacting particle distribution for the same frequency Fig. 4.4. This behaviour is indicative of the fact that a measurement of the system taken very early cannot capture the effect of the interaction as it takes time to communicate the interaction throughout the system.

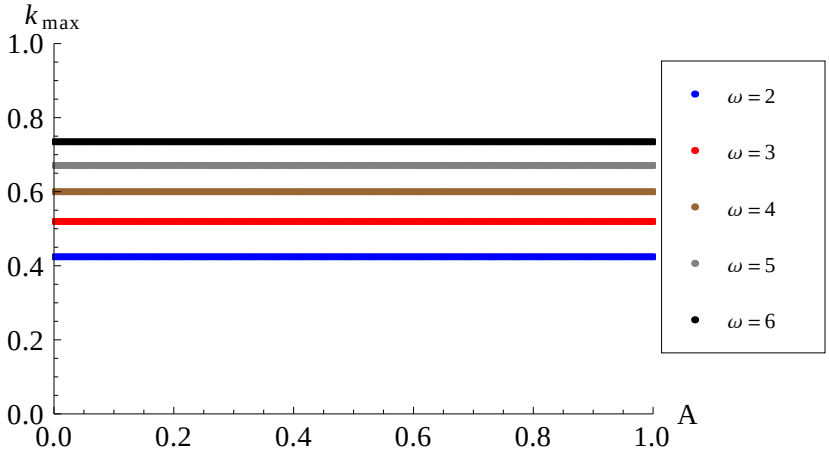

FIG. 4.4. Plot of the density correlation function maxima position $k_{\max}$ for varying interaction strength A within the high frequency ω regime. $N' = 4$, $\beta = 1$, $\frac{n}{L} = \frac{3}{5}$, $\zeta = 0.09$ and $C = 10$.

In the intermediate frequency regime, the correlation function is characterised by the emergence of two peaks that co-exist for a specific interaction strength Fig. 4.5. The dominating peak is usually positioned at small lengths upon increasing the interaction strength and its height varies strongly with increasing interaction strength. The two peaks are separated by a global minima Fig. 4.6. This peak structure implies that interactions make the system condense into particle clusters at length scales smaller than that of a non-interacting system correlation length that is probed at the same frequency. We dedicate the section 4.7.1 to showing that, for a narrow potential, when the system segregates into clusters of competing length scales that coincides with the break down of the random phase approximation.

In the low frequency regime, there is a single maximum for each interaction strength as it was the case in high frequency regime. Looking at the position of the maxima for

Stellenbosch University http://scholar.sun.ac.za

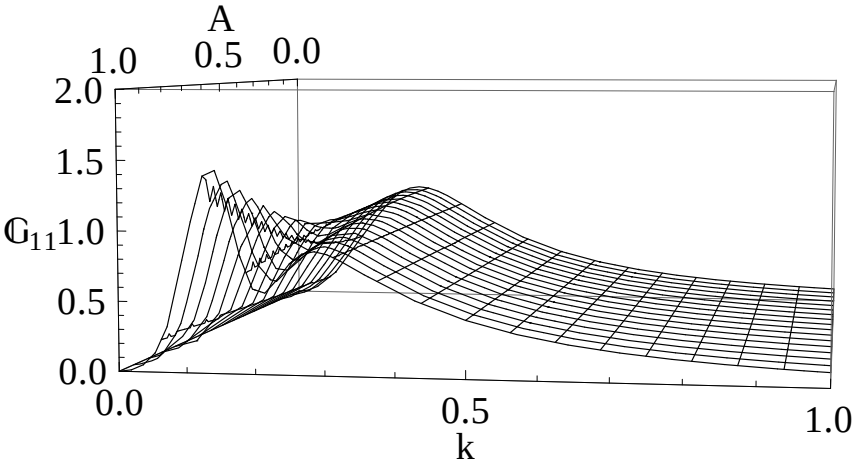

FIG. 4.5. density correlation function for system consisting of four coupled files at temperature $\beta = 1$ with each having file density $\rho = \frac{3}{5}$ and friction coefficient $\zeta = 0.09$. The system is probed at frequency $\omega = 0.6$. The short range file interaction potential is modelled by a Gaussian function of amplitude A and with $C = 10$.

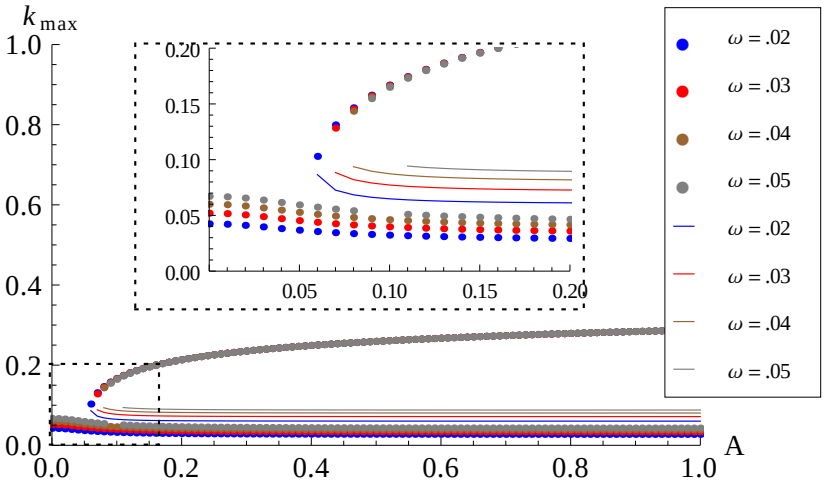

FIG. 4.6. Plot of the position $k_{\max}$ of the density correlation function maxima (dots) and minima (lines) for varying interaction strength A within the intermediate frequency ω regime for $N^{'} = 4$, $\beta = 1$, $\rho = \frac{3}{5}$, $\zeta = 0.09$ and $C = 10$.

Stellenbosch University http://scholar.sun.ac.za

each frequency, an interesting point to note is that at very weak interaction $A \to 0$, the correlation function becomes constant with variation in the interaction strengths Fig. 4.7. This is a signature of a system which has a tendency to equilibrate, which is typical of weakly interacting systems obeying some form of fluctuation dissipation law. On the other hand, stronger values of interaction, in this frequency regime, lead to a modified dominating length scale at least in comparison to a non-interacting system probed at the same frequency.

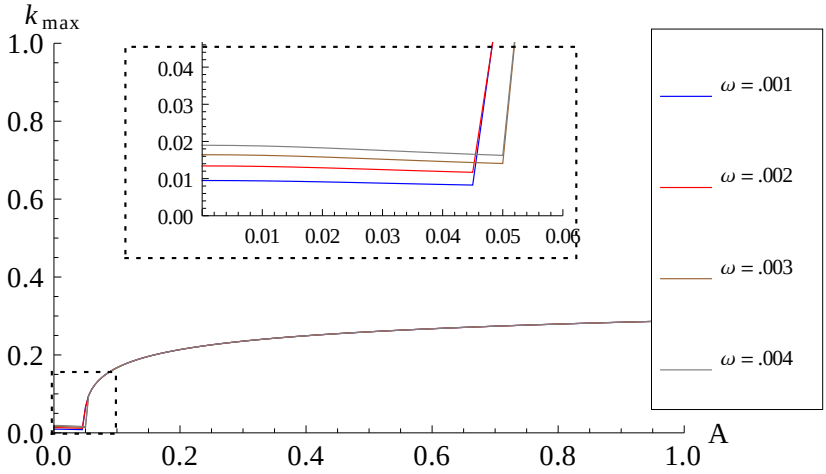

FIG. 4.7. Plot of the position $k_{\max}$ of the density correlation function maxima for varying interaction strength A within the low frequency ω regime. $N^{'} = 4$, $\beta = 1$, $\rho = \frac{3}{5}$, $\zeta = 0.09$ and $C = 10$.

4.7.1 Density correlation in the case of narrow interaction potential

We have noted that an increase in the interaction strength could lead to an emergence of a depletion zone (minima) separating two competing particle clusters of different length scales. In the limit when the interaction potential in equation (4.48) is so narrow that it can be reliably approximated by a delta function type potential $\widetilde{V}(k) = V_0$, we can define the critical density $\rho_c = \frac{1}{\sqrt{3N'\beta^2 V_0^2}}$. This turns out to be the density above which the random phase approximation breaks down. At densities above ρ_c, the dynamic fluctuations become as large as the system size and the background density is no longer homogeneous. Expressed in terms of the critical density the correlation function becomes

Stellenbosch University http://scholar.sun.ac.za

$$\begin{aligned}&\mathbb{G}_{11}(k,\omega)\\&=\frac{2\beta\zeta k^2\rho}{\left(\beta^2\zeta^2\omega^2+k^4\right)}\left[1-\frac{k^4\rho^2\left(3k^4-\beta^2\zeta^2\omega^2\right)}{3\rho_c^2\left(\beta^2\zeta^2\omega^2+k^4\right)^2}\right]\end{aligned}\tag{4.50}$$

It suffices to minimise the term in square brackets to determine the length k_m at which the correlation function changes from being positive to becoming negative. For the case when $\frac{\rho}{3\rho_c}\ll 1$, this happens at

$$k_m=\left(\frac{-\beta^2\zeta^2\left(1+\frac{\rho^2}{6\rho_c^2}\right)\omega^2}{\left(1-\frac{\rho^2}{\rho_c^2}\right)}\right)^{1/4}.\tag{4.51}$$

This is a physical quantity only at densities above which the random phase breaks. Thus in the case of a narrow potential the depletion occurs at lengths beyond the validity region of the random phase approximation. In Fig. 4.8, the contour plot of the correlation function in equation (4.50) depicts both the region of validity and region where the random phase approximation breaks down.

4.8 Effective Tagged particle Dynamics

From the correlation and response functions obtained using the collective description of the particle dynamics, we learn that the evolution of particles within a given reference file in the system induces some non trivial external responses on the rest of the system, which in turn feed back to the reference file. The free diffusive behaviour of a non-interacting particle system is modified upon switching on a small inter-file interaction force. This can be witnessed from the dependence of the multiple file correlation function in equation (4.49) on the interaction potential $\widetilde{V}(k)$. Essentially, a particle at position $r_i(t)$ within the reference file interacts indirectly with its neighbouring particles in the same file through an effective interaction mediated by the system response fields. The physical properties of the file experienced by the tagged particle, change due to inter-file interaction. For instance, the tagged particle experiences a friction whose coefficient $\zeta'(t)$ depends on the interaction potential as well as on other parameters of the system . The strength of the thermal random forces $\alpha(t)$ is also appropriately renormalised in response to the modified friction coefficient.

Stellenbosch University http://scholar.sun.ac.za

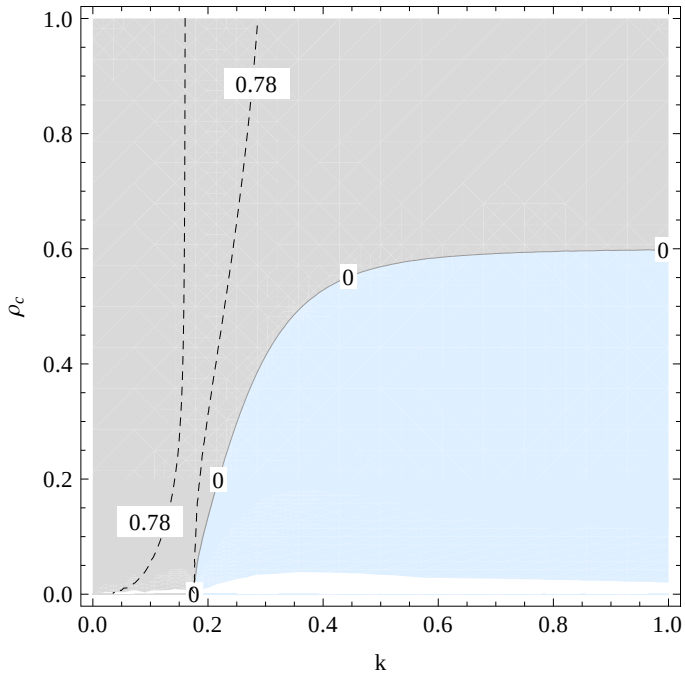

FIG. 4.8. A contour plot for the density correlation function (4.50) at different positions k for $N^{'} = 4$, $\beta = 1$, $\rho = \frac{3}{5}$, $\zeta = 0.09$ and $\omega = 0.6$. The grey coloured region marks the region of validity of the random phase approximation. The function attains its maxima in the area between the dashed contour lines. The zeroth contour demarcates the region where random phase approximation breaks down (coloured in blue). The critical density ρ_c must not be zero for the function to remain physical.

Stellenbosch University http://scholar.sun.ac.za

The tagged particle effective dynamics can be described by an equation of motion of the form

$$\zeta'(t)\frac{\partial}{\partial t}r_j(t) = \Gamma_j(t) + \sum_{j\neq\tau=1}^{n}\frac{\partial}{\partial r_\tau}W(r_i(t) - r_\tau(t)), \tag{4.52}$$

where the effective random forces Γ_j on the tagged particle are correlated as follows

$$\langle\Gamma_j(t)\Gamma_{j'}(t)\rangle = \alpha(t)\delta_{jj'}\delta(t-t'). \tag{4.53}$$

The sense of correlation in the movement of neighbouring particles at arbitrary positions $r_j(t)$ and $r_\tau(t)$ within the reference file is described by the effective potential $W(r_j(t) - r_\tau(t))$.

It is not immediately obvious how one can read off the explicit expressions for the effective physical parameters characterizing the dynamics of a tagged particle from correlation and response functions derived so far. In order to be able to do so, at least for a small interaction force, we will develop a generating functional describing the dynamics of particles inside a reference file using equation (4.52) as a delta functional constraint. We follow the standard MSR formalism using similar basic ideas as was done for a multiple file systems. The only difference here is that we are dealing with particle coordinates, and therefore particle densities, within a single file. The contribution of the other coupled files feature only through the effective friction coefficients, the modified random force strength and the effective interaction force.

4.8.1 Reference file effective dynamic generating functional in collective variables

After implementing the standard MSR-functional integral representation, introduced in the preceding sections, for the system equations (4.52-4.53), the generating functional obtained is of the form

Stellenbosch University http://scholar.sun.ac.za

$$
\begin{aligned}
Z\left(\left\{h_j(t),\hat{h}_j(t)\right\}\right) &= \int\prod_{i=1}^{N}[dr_i(t)][d\hat{r}_i(t)] \\
&\quad \exp\left\{-\int_t\frac{1}{2\lambda}\sum_{j=1}^{N}\hat{r}_j^2(t)+i\sum_{j=1}^{N}\int_t\hat{r}_j(t)\zeta'(t)\partial_t r_j(t)\right. \\
&\quad -\sum_{\tau\neq j=1}^{N}\sum_{j=1}^{N}\int_{t,k}ik\hat{r}_\tau(t)\exp\left\{ik(r_j(t)-r_\tau(t))\widetilde{W}(k)\right\} \\
&\quad \left.-\sum_{j=1}^{N}\int_t h_j(t)r_j(t)+\sum_{j=1}^{N}\hat{h}_j(t)\hat{r}_j(t)\right\}. \qquad (4.54)
\end{aligned}
$$

The external fields $h_j(t)$ and $\hat{h}_j(t)$ are conjugate to $r_j(t)$ and $\hat{r}_j(t)$ respectively, $\widetilde{W}(k)$ is the Fourier transform of $W(r_\tau(t)-r_j(t))$. As was done for the multi coupled file case, the collective fields can be introduced. We need to consider only the particle density field in equation (4.10a) and the density response field in equation (4.10c). The generating functional (4.54) then becomes

$$
\begin{aligned}
Z(\cdots) &= \int[d\rho_k(t)]\,[d\hat{\rho}_k(t)]\int[d\varrho_k(t)]\,[d\hat{\varrho}_k(t)] \\
&\quad \exp\left\{i\int_{k,t}\rho_{-k}(t)\widetilde{W}_{-k}(t)\varrho_k(t)+i\int_{k,t}\rho_{-k}(t)\hat{\rho}_k(t)\right. \\
&\quad \left.+i\int_{k,t}\varrho_{-k}(t)\hat{\varrho}_k(t)\right\} \\
&\quad \left\langle\exp\left\{-i\int_{k,t}\hat{\rho}_{-k}(t)n_k(t)-i\int_{k,t}\hat{\varrho}_{-k}(t)\nu_k(t)\right\}\right\rangle_0. \qquad (4.55)
\end{aligned}
$$

After performing the averaging as demonstrated in Appendix C, the last line in equation (4.55) simplifies to

$$
\begin{aligned}
&\left\langle\exp\left\{-i\int_{k,t}\hat{\rho}_{-k}(t)n_k(t)-i\int_{k,t}\hat{\varrho}_{-k}(t)\nu_k(t)\right\}\right\rangle_0 \\
&\approx\exp\left\{-\frac{1}{2}\int_{k,t,t}(\hat{\rho}_{-k}(t)s'_{11}(-k,t)\hat{\rho}_k(t)\right. \\
&\left.+\,2\hat{\rho}_{-k}(t)s'_{12}(-k,t)\hat{\varrho}_k(t))\right\}. \qquad (4.56)
\end{aligned}
$$

Stellenbosch University http://scholar.sun.ac.za

Upon making use of the two dimensional notation introduced in (4.38) and integrating out the hatted fields in $\hat{\boldsymbol{\rho}}(k,t)$, we obtain the generating functional

$$\begin{aligned} Z\left(\cdots\right) \quad &= \int \left[d\boldsymbol{\rho}(k,\omega)\right] \\ &\exp\left\{-\frac{1}{2}\boldsymbol{\rho}(k,\omega)\mathbb{K}^{-1}(k,\omega)\boldsymbol{\rho}^{\top}(-k,-\omega)\right\}. \end{aligned} \tag{4.57}$$

Note that a transformation from time t to frequency variables ω has been performed. The matrix $\mathbb{K}^{-1}(k,\omega)]_{ab}$ has the form

$$[\mathbb{K}^{-1}(k,\omega)]_{ab} = [\boldsymbol{s'}^{-1}(k,\omega)]_{ab} + i\boldsymbol{W}_{ab}(k,\omega). \tag{4.58}$$

with

$$\mathbb{K}(k,\omega)]_{11} = s'_{11}(k,\omega) = \frac{k^2\alpha(\omega)\rho}{\zeta'^2(\omega)\left(\omega^2 + \frac{\alpha(\omega)^2k^4}{4\zeta'^4(\omega)}\right)} \tag{4.59}$$

and

$$\begin{aligned} \mathbb{K}(k,\omega)]_{12} \quad &= s'_{12}(k.\omega) + i\boldsymbol{W}_{12}(k,\omega) \\ &= \frac{k^2\rho}{\zeta'(\omega)\left(\omega + \frac{ik^2\alpha(\omega)}{2\zeta'^2(\omega)}\right)} + i\boldsymbol{W}_{12}. \end{aligned} \tag{4.60}$$

Finally, by comparing these entries of the correlation-response matrices $\mathbb{K}_{ab}$ and the entries of the multiple file system correlation response matrix $\mathbb{G}_{ab}$, we are able to obtain the explicit expression for the effective friction coefficient $\zeta'(\omega)$, the strength of the random force $\alpha(\omega)$ and the correction to the response function $\boldsymbol{W}_{1,2}(k,\omega) = \boldsymbol{W}_{2,1}(k,-\omega)$.

Upon solving for $\zeta'(\omega)$ in the fluctuation dissipation relation

$$\beta\omega\mathbb{K}_{11}(k,\omega) = \mathbb{K}_{12}(k,\omega) - \mathbb{K}_{21}(k,\omega), \tag{4.61}$$

we obtain the usual relation between friction coefficient and strength of noise in an over-dumped system

$$\alpha(\omega) = 2k_BT\zeta'(\omega). \tag{4.62}$$

An explicit expression for the strength of the thermal forces can be obtained by solving for $\zeta'(w)$ in the equation

$$\mathbb{G}_{11}(k,\omega) = \mathbb{K}_{11}(k,\omega). \tag{4.63}$$

Stellenbosch University http://scholar.sun.ac.za

In the weak interaction limit we obtain the relation

$$\zeta'(\omega) = \zeta\left(1 - \frac{k^4\rho^2 N'\widetilde{V}^2\beta^2\left(3k^4 - \beta^2\zeta^2\omega^2\right)}{\left(k^8 - \beta^4\zeta^4\omega^4\right)}\right). \tag{4.64}$$

It is instructive to interpret the effective friction coefficient expression in the small frequency limit when the effect of interaction has averaged out through out the system. In this limit

$$\zeta' = \zeta\left(1 - 3\rho^2 N'\widetilde{V}^2\beta^2\right). \tag{4.65}$$

This suggests that inter-file interaction reduces the friction coefficient experienced by individual particles, hence the particles diffuse faster in a coupled file system in comparison to a single file. For a narrow interaction potential, parameterised by just V_0, we define a critical density $\rho_c = \frac{1}{\sqrt{3N'V_0^2\beta^2}}$, in terms of which the friction coefficient can be approximated to

$$\zeta' = \zeta\left(1 - \left(\frac{\rho}{\rho_c}\right)^2\right). \tag{4.66}$$

Notably, at densities above ρ_c the random phase approximation breaks down and the effective friction coefficient expression becomes unphysical. The effects of the reduced friction coefficient may possibly be countered by some other factors such as the effective interaction which can be expressed as

$$\boldsymbol{W}_{1,2}(k,\omega) = \rho^3 N'\beta^3\widetilde{V}^2 \tag{4.67}$$

in a small frequency limit.

4.9 Extending the random phase approximation

The random phase approximation as utilised here treats collective terms up to quadratic order, and it means that interaction terms are represented accurately whereas the remaining terms (not related to the forces) face a strong approximation. For practical reasons we used a gas of non-interacting particles as the basis of the approximation.

In principle, though, it is possible to include here effects of the single-file nature of the particles in extremely narrow pores. For many years the dynamics of single file systems

Stellenbosch University http://scholar.sun.ac.za

have been investigated. It is well-known [Levitt, 1973; Taloni and Lomholt, 2008] that the single-file nature of gas dynamics is not revealed through the measure of a single density, but becomes evident through correlation functions [Patzlaff et al., 1994]. A host of methods exist to derive the differential equations from which expressions for various correlations can be derived. Therefore, an appropriate density-density correlation function for a single-file, but otherwise non-interacting system, is available in the literature, and could be brought into the form of the expression for the RPA, where only the matrix $\mathbf{S}$ needs to be replaced by the single file expression. All other aspects of the derivation hold.

The quantities required are, of course, the two-time, two-point correlation function as well as the appropriate two-time and two-point response function. Expressions for these can be derived in a variety of ways, including the operator formalism based on the seminal work of Doi [Doi, 1976].

The literature mostly provides a single time correlation function, so that one might need to introduce an additional parameter for the decay of the correlations that come from the single-file nature, leaving only the dynamics, at long time scales, of a gas of normal Brownian particles—in as far as applicable to the correlation function utilised as a basis for the RPA.

4.10 Summary of the RPA dynamics calculation

In this chapter we presented a collective dynamical formalism of the coupled channel system. We started with a particle-based description of the particle dynamics in which effects such as channel deformation was modelled through a pair decomposable potential function. The particles time evolution equations were solved in the context of functional integral formalism which was used to convert the description into a field theory. The functional was simplified through a particle-to-field transformation which allowed us to describe the system in terms of fluctuating particle number density within a weak inhomogeneity expansion. This happened at a cost of introducing complex auxilliary field, conjugate to the density fluctuations field, to an otherwise real statistical field theory. However, the non locality of the auxilliary fields provided a much richer structure to the theory. Not only did the auxilliary fields allow us to decouple long range mechanical deformations and interfer-

Stellenbosch University http://scholar.sun.ac.za

ences, allowing interactions to factor through a local elastic coupling, but they also made it possible to compute response functions. The formalism made it possible the calculation of the density-density correlation functions, the effective friction coefficient and the effective interaction potential experienced by individual particles.

We calculated the density-density correlations functions. Upon plotting the correlation functions we saw peaks associated with particle distribution length scales. By varying the parameter values for the amplitude of the interaction potential between channels for the intra-channel density-density fluctuation correlation function, we learned that the system has a tendency to form competing dynamic particle clusters of different sizes. The break down of the RPA approximation indicated a transition to a behaviour that is no longer characterised by homogeneous density. We calculated how the effective friction coefficient varies to lower order. We hope that the equilibrium density-density correlation results contribute valuable insights for the calculation of the out-of-equilibrium density-density correlation function, which can potentially be adapted even for finite systems.

Stellenbosch University http://scholar.sun.ac.za

Chapter 5

Conclusion and outlook

The central theme of this study was to model particle diffusion in one dimensional elastically coupled molecular voids arranged in files. Two small scale numerical simulation algorithms have been constructed and used to characterise the system steady state behaviour. A simple analytical mean field theory, ignoring density fluctuations correlation, has also been developed and used to make predictions about the steady state particle flux as well as the steady state channel occupancy. The role played by dynamic density fluctuation correlations in the diffusive behaviour of particles has been described, using the MSR formalism in the context of the functional integral formalism.

The study benefited from the simulation in a two fold manner: The simulation was used as a computer experiment to calculate macroscopic properties of the system for an assumed particle evolution mechanism. It was also been used to test the mean field theory approximations in the limit of small channel coupling parameter. The open two coupled channel system has been studied first using a Monte Carlo simulation called random sequential updating (RSU) and secondly using a cellular automaton simulation. The two simulation algorithms allowed us to investigate the steady state kinetic properties of the system such as the channel mean global density, mean channel occupancy and the particle flux.

We found that in every Monte Carlo sweep, the steady state global channel density for the open system randomly fluctuates about a unique mean value for a given left and right reservoir densities settings. The mean global density values and the steady state particle flux for a single channel have been found to be directly determined by the reservoir density

Stellenbosch University http://scholar.sun.ac.za

n_L and n_R values. Looking at the different reservoir densities and measuring the resulting steady state flux, it was found that the open elastically coupled single file system, has three qualitative continuous current-density regimes. The regimes are analogous to the current-density phases observed in typical asymmetric simple exclusion process (ASEP) models observed in non-equilibrium statistical mechanics. These regimes are referred to as the HD, LD and MC regimes.

The sensitivity of the elastically coupled system to the strength of the coupling parameter in these current-density regimes has been characterised. Interestingly, the mean global density manifests dynamic temporal phases. When the system is close to equilibrium, for instance, we found that see-saw phases are predominant, otherwise the mean global density manifest mixed phases: A clear indication that the behaviour of the system is influenced by some dynamic correlations. The RSU algorithm is found to be unable to capture the steady state dynamic particle correlations. This limitation has been circumvented by introducing a cellular automaton algorithm which has been developed and used for calculating the steady state particle correlations. The cellular automaton simulation was useful in further investigating the sensitivity of the system to adjustments in the channel coupling parameter ϵ values.

From the cellular automaton simulation, we uncovered that for small ϵ (i.e $\epsilon \leq 0.5$) the contribution from the particle correlation is very small hence, the channel density profile appears very much like a simple linear density interpolation between reservoir density values. For the LD and the MC, for $\epsilon > 0.5$, the occupancy profile along the channels has been found to be non-linear with the particle occupancy getting higher in the less dense parts of the channel. For the HD regime, on the denser regions of the channel, a slight decrease in the density occupancy profile relative to the density profile of the regime observed for small values of the interactions $\epsilon \leq 0.5$ has bee noted.

The cellular automaton ideas, implemented in the stochastic simulation, were also employed in deriving analytic results for the system steady state occupancy and particle flux at a mean field level of approximation. In the limit when particle correlations could be ignored, the steady state particle occupancy profile for the multi-coupled channels consisting of z channels has been found to be describable by the expression

Stellenbosch University http://scholar.sun.ac.za

$$n^0_{ss}(x) = \frac{1}{(z-1)\epsilon} - \frac{1}{(z-1)\epsilon}\left\{1+\left(\frac{z-1}{L}\right)\epsilon\left(2\left[(z-1)\epsilon n_g - 1\right]\epsilon n_r - L\left[2n_L - (z-1)\epsilon n_L^2\right]\right)\right\}^{\frac{1}{2}},$$

where Δn_r is the difference between reservoir density and n_g is the sum of the reservoir densities. It has also been found that the steady state current $J^0_{ss} = \bar{J}^0_{ss}$ is given by

$$J^0_{ss} = \frac{1}{2L}\left[\Delta n_r - (z-1)\Delta n_r n_g\right]. \tag{5.1}$$

In this mean field description all the channels were assumed to be of the same length L. This theory works for small values of the coupling parameter with contributions from the density fluctuation correlations ignored. The simulation results for the particle flux and particle occupancy profile have been found to be in a reasonable agreement. On comparing the mean field theory results and simulation results it was realised that a successful general theory of the dynamics in narrow channels, must have as a basis, a good account of the density-density fluctuation correlations.

For an infinite version of the system at equilibrium, analytic mean field expressions for the correlations-response functions, has been derived using functional integral formalism within the RPA approximation. It has also been shown that the system density-density correlation and the response functions are related by some form of fluctuation dissipation relation. The density-density correlation results indicated that, for a short range inter-file interaction potential, there is a dominating length scale signalling that there is a bunching up of particles into clusters of specific size within the system. From the equilibrium mean field study we have postulated that there is a possibility of an emergence of competing length scales with increase in the interaction strength. We have also demonstrated that there exist a critical density below which the random phase approximation fails to describe the system. In order to achieve this, the channel interaction has been modelled through a narrow interaction potential.

For a multi-file system, it has been established that particles within each file experience an effective interaction and that individual particles experience a reduced friction coefficient. The analysis of the correlation functions alone has been found to be generally informative but inconclusive about the diffusion time scales. The reduced friction coefficient, for

Stellenbosch University http://scholar.sun.ac.za

instance, implies an enhanced particle diffusion speed in a multi-coupled channel system owever, there is a possibility that a feedback of the dynamic response fields may counter the effects of the reduced friction coefficient on the particles diffusivity.

An extension of the work presented in this dissertation will focus on incorporating the particle density fluctuation correlation terms. Clearly, the correlation terms presented in the last chapter, are amenable to improvement. Such an improvement will capture the single-file effects and the out-of-equilibrium nature of the open system with unequal left and right reservoir densities. The calculation of analytic expressions for correlations in single-file systems is currently a subject of intense study. For the finite elastically coupled single file system studied here, analytic correlation calculations are extremely complex. We hope to make progress in understanding the out-of-equilibrium dynamic correlations by introducing periodic particle sources and sinks at finite intervals on an otherwise infinite elastically coupled file system. This can potentially be done without violating the particle conservation within the file. In this way, the ideas employed in attaining the density-density correlations of the system under equilibrium considerations can be extended directly to obtain the contributions from particle correlation far from equilibrium.

As for the simulation study, the present model can be investigate further to incorporate more details pertaining to the host-host elastic deformation, for instance, this study could benefit from a broader investigation that incorporates the interactions from the next neighbour sites. This might not only yield better insights about the short range particle interaction but long range interaction behaviour of the system as well. It would be interesting to investigate the system more broadly by introducing second class particles and observe the nature of emerging dynamic structures and the effective system diffusive behaviour under the uniform particle evolution rules. It would also be fruitful to incorporate a possibility of particle channel switching while maintaining an elastic coupling between voids. This might be relevant for understanding particle diffusion in some types of molecular lattices in which particles do not necessarily diffuse in one dimension.

As inter-disciplinary research continues to be synonymous to current research, it is undeniable that the methods developed for traditional physics research have a strong potential for shedding light in our understanding of complex transport systems in chemistry and biology. Similarly dynamical systems in chemistry and biology fuel our understanding

Stellenbosch University http://scholar.sun.ac.za

of out-of-equilibrium statistical physics. No doubt, the corner stone of progress in these multi-disciplinary areas of research lies in sustained cross-fertilisation of ideas between the inter-disciplines.

Stellenbosch University http://scholar.sun.ac.za

Appendix A

A.1 RSU simulations details

Here we explain how the initial conditions are selected and how individual particles can be traced in order to compute some characteristics of distinguishable particles in single file diffusion.

Since we are dealing with an open system that exchanges particles with reservoirs at constant density, the initial conditions of the files could be set in various ways. The bottom line is that the steady state has unique constant mean particle flux and a mean density profile, that is independent of the initial site occupancy, for a given choice of the respective reservoirs densities. One system initialisation option is to start with the elastically coupled files empty and fill them to the steady state occupancy using the RSU dynamic hopping rules. Alternatively, we can start with particles occupying randomly chosen sites and allow the system to approach steady state occupancy through the application of the hopping equation over a large number of Monte Carlo steps. These initialisation techniques expend a great deal of computer time in reaching the steady state average occupancy.

We chose the initialisation as follows: First we set the boundary densities ρ_L and ρ_R then we assign the particle occupancy with a probability that depends on a linear interpolation of the density between the respective boundaries. In so doing, the simulation run starts with a global occupancy which is very close to the steady state average global occupancy for a non-interacting system thus saving a substantial amount for the system to approach steady state. Each run starts with a different sequence of initial occupancy.

Stellenbosch University http://scholar.sun.ac.za

Since the particles within a single file cannot pass through each other and particles cannot overtake, it is possible to follow individual particles simply by tracing a reference particle position and examining the site occupancy around the reference particle. If we denote a reference particle $\gamma = 1$ then we define an array $A(\gamma) = \tau_\gamma$ where τ_γ is the site at which the γth particle is located. Once the system has reached steady state, in order to investigate the diffusive behaviour of individual particles, the tracked particles are placed at the first site of the files and the simulation is allowed to run. If suffices to update the location of particle number 1 after every nth Monte Carlo cycle. If $A(1) = \tau^{'}$ after time $t_{MC} - 1$ then at time t_{MC} it is given by

$$A(1) = \begin{cases} \tau^{'} & \text{if} \quad JL(1) = JR(1) = 0 \\ \tau^{'} + 1 & \text{if} \quad JR(1) = 1 \\ \tau' - 1 & \text{if} \quad JL(1) = 1 \end{cases}$$

.

Where $JL(1)$ and $JR(1)$ denote the reference particle current to the left and to the right respectively. If $A(1) = i_1$, then $A(2) = i_1 + b_1 = i_2$ and $A(3) = i_2 + b_2 = i_3$ etc. The lattice variable b_γ denote the number of unoccupied sites, to the right, before the next occupied site is found in front of a given reference particle.

A.2 Cellular automaton simulations details

In this subsection we explain how the cellular automata simulation is initialised and how the collision and propagation steps are implemented using a multi-dimensional array of particle occupancies for the respective files in a two coupled file system.

For the cellular automaton lattice, the state of a node is sufficiently described by the boolean fields $\tau_i(t_{CA}, x)$, where the index i runs from 1 to 3 designating the three cell directions within a node. τ_i is an occupancy number which assumes values 0 or 1. At time $t_{CA} = 0$, before the evaluation of the cellular automaton algorithm, an array A of size $n \times N$ is initialised. Where n corresponds to the number of interacting channels while N is the number of nodes. The bits for the occupancy of each note are set by a random process with probabilities such that the occupancy of each cell approximates an occupancy determined through a linear interpolation of the density between the respective reservoirs as it was

Stellenbosch University http://scholar.sun.ac.za

done for RSU method. $A[y][x]$ for instance, would contain state information for the node at lattice site x within yth channel at $t_{CA} = 0$. For a two file system $y \in [0, 1]$, where $0, 1$ denote the first channel and the second channel respectively. The cellular Automaton algorithm for a two file system is carried out as follows:

- For any node at a lattice position x, the occupancy of the neighbouring nodes $\bar{x}$ is examined in order to evaluate the inter-file interaction as induced by particle occupancies in cells $\bar{\tau}_1, \bar{\tau}_2$ and $\bar{\tau}_3$ of the node. The interaction penalties are for deciding the probabilities for possible after collision states.
- For each and every node, the probabilistic collision rules are applied and the results are stored in an auxiliary array B of size $n \times N$. The auxiliary array is then used as a reference array for the propagation step.
- During the propagation step a node at position x of the auxiliary array B, a particle on the left cell is shifted to the left cell of the node at position $x - 1$, while a particle on the right cell is translated to the right cell of the node at position $x + 1$. The middle particle stays stationary. This allows of a synchronous updating of all nodes.
- At the boundary the translation step ejects the particles occupying cells on the extreme ends of the channels.
- In order to implement a symmetric exchange of particles between the extreme lattice sites and the respective boundary reservoirs lattice sites, the translation of particles into the end lattice must be handled separately. In this case the particle uptake step is implemented before the collision step of every iteration.
- The occupancy information in the auxiliary array B is then copied into the array A for the next collision step.

At each and every time step the above steps are repeated. In order to calculate the average global density we keep record of the total count of particles in each channel after every time step. The average system steady state occupancy profile and average steady state current are calculated at equally spaced bins on each of the files.

Stellenbosch University http://scholar.sun.ac.za

Appendix B

B.1 Martin-Siggia-Rose Formalism

We dedicate this section in giving a brief illustration of how the Martic-Siggia-Rose formalism works. We base our discussion on some of the ideas that have been presented by [Arenas and Barci, 2010] in a discussion about an extension of functional integral for correlation functions of a multiplicative stochastic process. Lets consider the equations of motion (4.1a) and (4.1b) for individual particles in each of the files expressed as

$$0 = \mathcal{L}_i(t) = -\zeta\frac{\partial}{\partial t}r_j(t) - \sum_{\tau=1}^{N}\frac{\partial}{\partial r_j}V(r_j(t)-\bar{r}_\tau(t)) + f_j(t), \tag{B.1a}$$

$$0 = \bar{\mathcal{L}}_\tau(t) = -\zeta\frac{\partial}{\partial t}\bar{r}_\tau(t) + \sum_{j=1}^{N}\frac{\partial}{\partial \bar{r}_\tau}V(r_j(t)-\bar{r}_\tau(t)) + \bar{f}_\tau(t). \tag{B.1b}$$

Our primary objective is to find multi-particle correlation functions of the form

$$\left\langle r_1(t^{(1)}),\cdots,r_N(t^{(n)})\right\rangle \tag{B.2}$$

$$\left\langle \bar{r}_1(t^{(1)}),\cdots,\bar{r}_N(t^{(n)})\right\rangle \quad \text{or} \tag{B.3}$$

$$\left\langle r_1(t^{(1)}),\cdots,r_N(t^{(n)}),\bar{r}_1(t^{(n+1)}),\cdots,\bar{r}_N(t^{(n)})\right\rangle. \tag{B.4}$$

The averaging is done with respect to the distribution of non interacting particles within the channels. The superscript on the time variable reminds us that we are not necessarily looking for equal time particle correlations. A precaution must be taken to ensure that the

Stellenbosch University http://scholar.sun.ac.za

causality condition holds thus ensuring that the generating functional is normalised such that $\mathcal{Z} = 1$. The multi-particle correlation function for the system can be calculated by solving the coupled equations of motion (B.1a) and (B.1b) and then averaging the product of the solution set $\{r_i([f_i]; t^n)\}$ over the distribution of the stochastic force. This leads to the correlation results that we are looking for since

$$\left\langle r_1(t^{(1)}), \cdots, r_N(t^{(n)}) \right\rangle = \left\langle r_1([f_1]; t^{(')}), \cdots, r_N([f_N]; t^{(n)}) \right\rangle_{\{f\}}. \tag{B.5}$$

A similar relation holds for inter-channel and intra-channel particle position correlations. We can get the right-hand side of the above equation by using a generating functional

$$\mathcal{Z}\left[\{\lambda_j(t), \bar{\lambda}_\tau(t)\}\right] = \left\langle \exp\left\{ \sum_{j=1}^{N} \int_t \lambda_j(t) r_j([f_j]; t) + \sum_{\tau=1}^{N} \int_t \bar{\lambda}_\tau(t) \bar{r}_\tau([\bar{f}_\tau]; t) \right\} \right\rangle_{\{f,\bar{f}\}}, \tag{B.6}$$

by taking the N-th order functional derivative of the type

$$\begin{aligned} & \frac{\delta^{(N)} \mathcal{Z}\left[\{\lambda_j(t), \bar{\lambda}_\tau(t)\}\right]}{\delta\lambda_1(t^{(1)}) \cdots \delta\lambda_N(t^{(N)})} \\ = \; & \left\langle r_1([f_1]; t^{(')}), \cdots, r_N([f_N]; t^{(n)}) \right. \\ \times \; & \left. \exp\left\{ \sum_{j=1}^{N} \int_t \lambda_j r_j([f_j]; t) + \sum_{\tau=1}^{N} \int_t \bar{\lambda}_\tau \bar{r}_\tau([\bar{f}_\tau]; t) \right\} \right\rangle_{\{f,\bar{f}\}} \Bigg|_{\{\lambda_j=1, \bar{\lambda}_\tau=1\}} \\ = \; & \left\langle r_1([f_1]; t^{(')}), \cdots, r_N([f_N]; t^{(n)}) \right\rangle, \end{aligned} \tag{B.7}$$

where the source terms $\lambda_j(0) = 1$ and $\bar{\lambda}_\tau(0) = 1$ by definition. The MSR formalism allows us to find the correlation functions without having to solve for the particular solution $r_i([f_i]; t)$ for each i-th particle. The basic idea in this formalism is to use the delta functional constraint $\delta\left[r_i(t) - r_i([f_i]; t)\right]$ to express the generating functional

Stellenbosch University http://scholar.sun.ac.za

$$\mathcal{Z}\left[\{\lambda_j(t),\bar{\lambda}_\tau(t)\}\right] = \left\langle \int \prod_{j=1}^{N}[dr_j(t)] \prod_{\tau=1}^{N}(t)[d\bar{r}_\tau] \prod_{j=1}^{N}\delta\left[r_j(t)-r_j([f_j];t)\right] \prod_{\tau=1}^{N}\delta\left[r_\tau(t)-r_\tau([f_\tau];t)\right] \exp\left\{\sum_{j=1}^{N}\int_t \lambda_j r_j([f_j];t)+\sum_{\tau=1}^{N}\int_t \bar{\lambda}_\tau\bar{r}_\tau([\bar{f}_\tau];t)\right\}\right\rangle_{\{f,\bar{f}\}} \tag{B.8}$$

and then transform the functional from the stochastic variables $\{r_i([f_i];t)\}$ to the equation of motion (B.1a) and (B.1b). The resulting generating functional becomes

$$\begin{aligned}\mathcal{Z}\left[\{\lambda_j(t),\bar{\lambda}_\tau(t)\}\right] &= \int \prod_{j=1}^{N}[dr_j(t)]\mathcal{J}(r_j) \int \prod_{\tau=1}^{N}[d\bar{r}_\tau(t)]\bar{\mathcal{J}}(\bar{r}_\tau) \\ &\times \left\langle \prod_{j=1}^{N}\delta\mathcal{L}(r_j)(t)\right\rangle_f \left\langle \prod_{\tau=1}^{N}\delta\bar{\mathcal{L}}(\bar{r}_\tau)(t)\right\rangle_{\bar{f}} \\ &\times \exp\left\{\sum_{j=1}^{N}\int_t \lambda_j(t)r_j([f_j];t)+\sum_{\tau=1}^{N}\int_t \bar{\lambda}_\tau(t)\bar{r}_\tau([\bar{f}_\tau];t)\right\},\end{aligned} \tag{B.9}$$

where we define the Jacobians of the transformation

$$\mathcal{J}(r_j(t)) = \det\left(\frac{\delta\mathcal{L}(r_j(t))}{\delta r_j(t)}\right) \quad \text{and} \quad \bar{\mathcal{J}}(r_\tau(t)) = \det\left(\frac{\delta\bar{\mathcal{L}}(\bar{r}_\tau(t))}{\delta\bar{r}_\tau(t)}\right) \tag{B.10}$$

respectively. The Jacobian terms are always positive and the differential operator is given by

$$\frac{\delta\mathcal{L}(r_i(t))}{\delta r_i(t)} = \left[\frac{d}{dt}-\frac{df(x_i)}{dx_i(t)}\right]\delta(t-t'). \tag{B.11}$$

To move from (B.8) to (B.9), we have used the relation

$$\delta\left[r_i(t)-r_i([f_i];t)\right] = \delta\mathcal{L}(r_i)\det\left(\frac{\delta\mathcal{L}(r_i(t))}{\delta r_i(t)}\right). \tag{B.12}$$

For a reader who is interested in further mathematical details about how the expression (B.12) is derived see [Moller, 2011] and references therein. The remaining step is to deal

Stellenbosch University http://scholar.sun.ac.za

with the Jacobian explicitly. We follow a technique that is presented by [Jouvet and Phythian, 1979] where a trivial expression for the Jacobian is established using a limiting process. The time interval $(0, T)$ is split into N equal subintervals of length $l = \frac{T}{N}$ and the equations of motion are discretised. The functional is then defined as a limit of multiple integrals of order N with $N \to \infty$. On discretising the equations of motion, each of the delta functionals in (B.9) can be re-expressed as

$$\begin{aligned}\delta\left[-\frac{dr(t)}{dt} + F(r(t)) + f(t)\right] &= \delta\left(-\frac{r_n - r_{n-1}}{l} + F(r_{n-1}) + f_{n-1}\right) \\ &\times \delta\left(-\frac{r_{n-1} - r_{n-2}}{l} + F(r_{n-2}) + f_{n-2}\right) \\ &\vdots \\ &\times \delta\left(-\frac{r_1 - r_0}{l} + F(r_0) + f_0\right), \end{aligned} \tag{B.13}$$

where $F(r_n)$ represents the discretised channel interaction force. To simplify the notation the particle index on the left hand side of the above equation is omitted. The identity $\int_{-\infty}^{\infty} f(r)\delta(ar) = \frac{1}{|a|}f(0)$ can be used to integrate over the index N in the order $N, N-1, \cdots 0$. The Jacobian is obtained as the limit of an ordinary Jacobian as $N \to \infty$. For the case when the discretised equations of motion are such that $f_n = f(nl)$, with each $r(t=0)$ being given by the initial conditions, the Jacobian relating the variables $\{r_1 \cdots r_N\}$ and $\{f_1 \cdots f_N\}$ is given by

$$\det\left(\frac{\delta\mathcal{L}(r_j(t))}{\delta r_j(t)}\right) = \det\left(\frac{\delta\bar{\mathcal{L}}(\bar{r}_\tau(t))}{\delta\bar{r}_\tau(t)}\right) = \frac{1}{l^N}. \tag{B.14}$$

Different discretisation processes may lead to a different expressions for the Jacobian however, in the continuum limit all discretisation processes are found lead to a trivial result which can be set to unity without loss of generality.

Stellenbosch University http://scholar.sun.ac.za

Appendix C

C.1 Making the interaction term quadratic in collective variables

In this section we will show details about how the interaction terms can be made quadratic in the fluctuating fields in Fourier space in the context of random phase approximation. The term $\sum_{j=1,\tau=1}^{N,N} \partial_{r_j} V(r_j(t) - \bar{r}_\tau(t))\hat{r}_j(t)$ can be re-expressed as follows

$$\begin{aligned}
& \sum_{j=1,\tau=1}^{N,N} \partial_{r_j} V(r_j(t) - \bar{r}_\tau(t))\hat{r}_j(t) \\
= & \sum_{\tau=1}^{N} \int_{r,\bar{r}} \delta[\bar{r} - \bar{r}_\tau(t)] \sum_{j=1}^{N} \hat{r}_j(t) \partial_{r_j} \delta[r - r_j(t)] V(r - \bar{r}) \\
= & \sum_{j=1}^{N} \int_{r,\bar{r}} \int_k ik\hat{r}_j(t) \exp\{ik(r - r_j(t))\} \sum_{\tau=1}^{N} \int_{k'} \exp\{ik'(\bar{r} - \bar{r}_\tau(t))\} V(r - \bar{r}) \\
= & \int_{k,k'} \int_{r,\bar{r}} \exp\{ikr + ik'\bar{r}\} \left(ik \sum_{j=1}^{N} \hat{r}_j(t) \exp\{-ikr_j(t)\} \right) \left(\sum_{\tau=1}^{N} \exp\{-ik'\bar{r}_\tau(t)\} \right) \\
& V(r - \bar{r}). \qquad \text{(C.1)}
\end{aligned}$$

In expression (C.1) we denote the collective density fields in Fourier space as:

$$\tilde{\nu}_k(t) = ik \sum_{\tau=1}^{N} \hat{r}_\tau(t) \exp\{-ikr_\tau(t)\}, \qquad \text{(C.2)}$$

$$n_k(t) = \sum_{j=1}^{N} \exp\{-ikr_j(t)\}. \qquad \text{(C.3)}$$

Stellenbosch University http://scholar.sun.ac.za

This allows us to express the interaction in terms of the collective fields in Fourier space as

$$\sum_{j=1,\tau=1}^{N,N}\int_t \partial_{r_j} V(r_j(t)-\bar{r}_\tau(t))\hat{r}_j = \int_{k,k'}\int_{r,\bar{r}} e^{(ikr+ik'\bar{r})}\bar{n}_{k'}(t)V(r-\bar{r})\tilde{\nu}_k(t).$$

Upon introducing the transformation to the centre of mass coordinates $R=\frac{1}{2}(r(t)+\bar{r}(t))$ and difference of the particle positions $R'=r(t)-\bar{r}(t)$ we get

$$\begin{aligned}\int_{k,k'}\int_{r,\bar{r}} e^{i(kr+k'\bar{r})}\tilde{\bar{n}}_k(t)\tilde{\nu}_{k'}V(r-\bar{r}) &= \int_{k,k'}\int_{R,R'}\bar{n}_{k'}e^{iR\left(k+\frac{k'}{2}\right)}V(R')e^{i\frac{R'}{2}(k-k')}\tilde{\nu}_k(t)\\ &= \int_{k,k'}\int_{R'}\bar{n}_{k'}(t)\delta(k+k')V(R')e^{i\frac{R'}{2}(k-k')}\tilde{\nu}_k(t)\\ &= \int_k\int_{R'}\bar{n}_{-k}(t)V(R')e^{-ikR'}\tilde{\nu}_k(t)\\ &= \int_k \bar{n}_{-k}(t)\widetilde{V}_k(t)\tilde{\nu}_k(t). \qquad \text{(C.4)}\end{aligned}$$

thus

$$\sum_{j=1,\tau=1}^{N,N}\partial_{r_j}V(r_j(t)-\bar{r}_\tau(t))\hat{r}_j = \int_k \bar{n}_{-k}(t)\tilde{\nu}_k(t)\widetilde{V}_k(t). \qquad \text{(C.5)}$$

Following a similar calculational strategy, one can show that

$$\sum_{j=1,\tau=1}^{N,N}\partial_{\bar{r}_\tau}V(r_j(t)-\bar{r}_\tau(t))\hat{\bar{r}}_\tau = -\int_k \tilde{n}_k(t)\tilde{\bar{\nu}}_{-k}(t)\widetilde{V}_{-k}(t).$$

Finally, we can express the contribution from the file interaction as

$$\begin{aligned}L_{int}(t) &= \sum_{j,\tau=1}^{N}\partial_{r_j}V(r_j(t)-\bar{r}_\tau(t))\hat{r}_j - \sum_{j,\tau=1}^{N}\partial_{\bar{r}_\tau}V(r_j(t)-\bar{r}_\tau(t))\hat{\bar{r}}_\tau\\ &= \frac{1}{2}\left(\int_k \tilde{\bar{n}}_k(t)\tilde{\nu}_{-k}(t)\widetilde{V}_{-k}(t)+\int_k \tilde{n}_k(t)\tilde{\bar{\nu}}_{-k}(t)\widetilde{V}_{-k}(t)\right.\\ &\left.+\int_k \tilde{\nu}_k(t)\tilde{\bar{n}}_{-k}(t)\widetilde{V}_k(t)+\int_k \tilde{\bar{\nu}}_k(t)\tilde{n}_{-k}(t)\widetilde{V}_k(t)\right). \qquad \text{(C.6)}\end{aligned}$$

Stellenbosch University http://scholar.sun.ac.za

Note that, because of our choice of notation, the interaction term contains some complex contribution. We can make it real by including the complex conjugate through the substitution $n_k\nu_{-k} \to \frac{1}{2}(n_k\nu_{-k} + \nu_k n_{-k})$. In this way, the interaction is well defined as it includes the possibility that interaction may be due to a response field. It is therefore relevant to introduce the fluctuation fields about the mean densities n_0 and $\bar{n}_0$ as

$$\rho_k(t) = n_k(t) - n_0, \quad \hat{\rho}_k(t) = \nu_k(t) \quad \text{and} \tag{C.7}$$

$$\bar{\rho}_k(t) = \bar{n}_k(t) - \bar{n}_0, \quad \hat{\bar{\rho}}_k(t) = \bar{\nu}_k(t). \tag{C.8}$$

The interaction term, expressed in terms of the dynamic fluctuation fields, becomes

$$\begin{aligned}\int_t\int_k \bar{n}_k(t)\nu_{-k}(t)\widetilde{V}_{-k}(t) &= \int_t\int_k \bar{\rho}_k(t)\hat{\rho}_{-k}(t)\widetilde{V}_k(t) + n_0^2\int_t\int_k \widetilde{V}_{-k}(t) \\ &- n_0\int_t\int_k (\bar{\rho}_k(t) + \hat{\rho}_{-k}(t))\widetilde{V}_k(t),\end{aligned} \tag{C.9}$$

In a similar way

$$\begin{aligned}\int_t\int_k n_k(t)\bar{\nu}_{-k}(t)\widetilde{V}_{-k}(t) &= \int_t\int_k \rho_k(t)\hat{\bar{\rho}}_k(t)\widetilde{V}_{-k}(t) + n_0^2\int_t\int_k \widetilde{V}_{-k}(t) \\ &- n_0\int_t\int_k (\rho_k(t) + \hat{\bar{\rho}}_{-k}(t))\widetilde{V}_{-k}(t).\end{aligned} \tag{C.10}$$

On performing the average over the expression (C.9) and (C.10), we shall retain the first term on the right as the second term does not affect the dynamics and the third term averages to zero.

C.2 Averaging over terms inside the exponential

C.2.1 First order terms

In order to approximate the exponential term $\exp\langle -\mathcal{L}_3\rangle_0$, a series expansion of the exponential function truncated up to second order,

$$\exp\langle -\mathcal{L}_3\rangle_0 \approx 1 + \langle\mathcal{L}_3\rangle_0 + \frac{1}{2}\langle\mathcal{L}_3^2\rangle_0, \tag{C.11}$$

Stellenbosch University http://scholar.sun.ac.za

is done. The expression L_3 is given by

$$\begin{aligned} L_3 &= i\sum_{j=1}^{N}\int_{k,t}\hat{\rho}_k(t)e^{-ikr_j(t)} - \sum_{j=1}^{N}\int_{k,t}k\hat{\varrho}_k(t)\hat{r}_j(t)e^{-ikr_j(t)} \\ &+ i\sum_{\tau=1}^{N}\int_{k,t}\hat{\bar{\rho}}_k(t)e^{-ik\bar{r}_j(t)} - \sum_{\tau=1}^{N}\int_{k,t}k\hat{\bar{\varrho}}_k(t)\hat{\bar{r}}_\tau(t)e^{-ik\bar{r}_\tau(t)} \\ &+ i\sum_{j=1}^{N}\int_{k,t}\hat{\vartheta}_k(t)\partial_t r_j(t)e^{-ikr_j(t)} + i\sum_{\tau=1}^{N}\int_{k,t}\hat{\bar{\vartheta}}_k(t)\partial_t\bar{r}_\tau(t)e^{-ikr_\tau(t)}. \end{aligned} \tag{C.12}$$

Because of the symmetry of the model about the two files, the average over the first and third terms in (C.11) are equal and lead to a constant. The average over the other remaining first order terms are found to vanish. Thus, we can write

$$\langle\mathcal{L}_3\rangle_0 = 2\sum_{J=1}^{N}\int_{k,t}\rho_k\left\langle\exp(-ikr(t))\right\rangle_0 = 2\int_{k,t}\rho_k s_1 \tag{C.13}$$

where

$$\begin{aligned} s_1(t) &= \frac{1}{\mathcal{N}}\sum_{p=1}^{N}\int\prod_{j=1}^{N}[dr_j(t)][d\hat{r}_j(t)]\exp\{-ikr_p(t)\} \\ &\quad \exp\left\{\sum_{j=1}^{N}\int_t\left(i\hat{r}_j(t)(-\zeta\partial_t r_j(t)) - \frac{\alpha}{2}\hat{r}_j^2(t)\right)\right\}. \end{aligned}$$

All particles in the system are similar, therefore, without loss of generality, the summation can be replaced by the number of summed over terms N and the index P can also be dropped. Having performed the $\hat{r}$ path integral, we obtain

$$s_1(t) = \frac{N}{\mathcal{N}}\int\prod_{j=1}^{N}[dr_j]\exp\{-ikr(t)\}\exp\left\{-\frac{1}{2\alpha}\sum_{j=1}^{n}\int_t(\zeta\partial_t r_j)^2)\right\}. \tag{C.14}$$

In the above expression the path integrals in which $r_j(t) \neq r(t)$ cancel with their corresponding integrals in the denominator leading to

$$s_1(t) = \frac{N}{\mathcal{N}'}\int[dr(t)]\exp\left\{-\frac{1}{2\alpha}\int_t(\zeta\partial_t r(t))^2 - ikr(t))\right\}, \tag{C.15}$$

Stellenbosch University http://scholar.sun.ac.za

which upon discretising in time yields,

$$\begin{aligned} s_1(t) &= \frac{N}{\mathcal{N}'}\int\prod_{\eta=0}^{n} dr_\eta \exp\left\{-\frac{1}{2\alpha}\sum_{\eta=1}^{n}\epsilon\left(\zeta\left(\frac{r_\eta - r_{\eta-1}}{\epsilon}\right)\right)^2\right. \\ &- \left. ikr_0 - i\sum_{\eta=1}^{n} k(r_\eta - r_{\eta-1})\right\} \\ &= \frac{\delta(k)N}{\mathcal{N}'L}\int\prod_{\eta=1}^{n} b_\eta \exp\left\{-\frac{1}{2\alpha\epsilon}\sum_{\eta=1}^{n}\left((\zeta b_\eta)^2 - ikb_\eta\right)\right\}. \end{aligned} \tag{C.16}$$

Here $r(t) = r_0 + \sum_{\eta=1}^{n} b_\eta$, where $b_\eta = r_j - r_{j-1}$. On performing the b_η integral, the resulting expression becomes

$$\begin{aligned} s_1(t) &= \frac{N}{L}\delta(k)\left(\exp\left\{\frac{\alpha\epsilon}{2\zeta^2}(ik)^2\right\}\right)^n \\ &= \frac{N}{L}\delta(k)\exp\left\{-\left(\frac{k^2\alpha}{2\zeta^2}\right)|t-t'|\right\}, \end{aligned} \tag{C.17}$$

where the index n is given by $n = \frac{|t-t'|}{\epsilon}$. Putting equation (C.17) in equation (C.13) and performing the k integral, we get

$$\int_{k,t} s_1 = \frac{Nn_0}{L} = n_0^2. \tag{C.18}$$

C.2.2 Second order terms

The first order terms of the expansion (C.11) do not contribute to the dynamics as they are constant. Moreover, they cancel out with the constant terms obtained on averaging over the interaction term in (C.9) and (C.10). The remaining terms of the expansion can safely be re-exponentiated to obtain

Stellenbosch University http://scholar.sun.ac.za

$$
\begin{aligned}
&\left\langle \exp -\mathcal{L}_3^2 \right\rangle_0 \approx \exp\left(-\frac{1}{2}\left\langle \mathcal{L}_3^2 \right\rangle_0\right) \\
= \;& \exp\left\{-\frac{1}{2}\left(\int_{k,t}\int_{k',t'} \rho_k(t)\rho_{k'}(t')s_{11} + 2\int_{k,t}\int_{k',t'} \rho_k(t)\bar{\rho}_{k'}t')s_{15} + 2\int_{k,t}\int_{k',t'} \rho_k(t)\hat{\vartheta}_{k'}(t')s_{13}\right.\right. \\
+ \;& 2\int_{k,t}\int_{k',t'} \rho_k(t)\hat{\bar{\vartheta}}_{k'}(t')s_{14} + 2\int_{k,t}\int_{k',t'} \rho_k(t)\hat{\varrho}_{k'}(t')s_{15} + 2\int_{k,t}\int_{k',t'} \rho_k(t)\hat{\bar{\varrho}}_{k'}(t')s_{16} \\
+ \;& \int_{k,t}\int_{k',t'} \hat{\bar{\rho}}_k(t)\hat{\bar{\rho}}_{k'}(t')s_{22} + 2\int_{k,t}\int_{k',t'} \hat{\bar{\rho}}_{k'}(t)\hat{\vartheta}_{k'}(t')s_{35} + 2\int_{k,t}\int_{k',t'} \hat{\bar{\rho}}_k(t)\hat{\bar{\vartheta}}_{k'}(t')s_{24} \\
+ \;& 2\int_{k,t}\int_{k',t'} \hat{\bar{\rho}}_k(t)\hat{\varrho}_{k'}(t')s_{25} + 2\int_{k,t}\int_{k',t'} \hat{\bar{\rho}}_k(t)\hat{\bar{\varrho}}_{k'}(t')s_{26}\int_{k,t}\int_{k',t'} \hat{\vartheta}_k(t)\hat{\vartheta}_{k'}(t')s_{33} \\
+ \;& 2\int_{k,t}\int_{k',t'} \hat{\vartheta}_k(t)\hat{\bar{\vartheta}}_{k'}(t')s_{34} + 2\int_{k,t}\int_{k',t'} \hat{\vartheta}_k(t)\hat{\varrho}_{k'}(t')s_{35} + 2\int_{k,t}\int_{k',t'} \hat{\vartheta}_k(t)\hat{\bar{\varrho}}_{k'}(t')s_{36} \\
+ \;& \int_{k,t}\int_{k',t'} \hat{\bar{\vartheta}}_k(t)\hat{\bar{\vartheta}}_{k'}(t')s_{44} + 2\int_{k,t}\int_{k',t'} \hat{\bar{\vartheta}}_k(t)\hat{\varrho}_{k'}(t')s_{45} + 2\int_{k,t}\int_{k',t'} \hat{\bar{\vartheta}}_k(t)\hat{\bar{\varrho}}_{k'}(t')s_{46} \\
+ \;& \left.\left.\int_{k,t}\int_{k',t'} \hat{\varrho}_k(t)\hat{\varrho}_{k'}(t')s_{55} + 2\int_{k,t}\int_{k',t'} \hat{\varrho}_k(t)\hat{\bar{\rho}}_{k'}(t')s_{56} + \int_{k,t}\int_{k',t'} \hat{\bar{\varrho}}_k(t)\hat{\bar{\varrho}}_{k'}(t')s_{66},\right.\right.
\end{aligned}
\tag{C.19}
$$

where we denote the statistical averages over the second order terms by s_{ij} for $i, j \in \{1, \ldots 6\}$. As we mentioned earlier our choice of the notation is such that the density conjugate field involve a complex prefactor, the exponential term can be made real by introducing complex conjugate through

$$
\phi_k(t)\rho_k(t')s_{ij}(k,t) \quad = \frac{1}{2}\left(\phi_k(t)\rho_{k'}(t')s_{ij}(k,t) + \rho_k(t)\phi_{k'}(t')s_{ji}(k',t')\right).
$$

We must ensure that the averages are correctly time ordered. The model is also symmetric about exchange of interacting density fields because the particles are assumed to be indistinguishable. Since the calculations for the averages in $\langle \mathcal{L}_3^2 \rangle$ are performed with respect to the distribution of particles in a decoupled file, some of the terms are a decoupled system correlation functions while others are the associated response functions. These terms constitute the elements of the correlation-response matrix $\boldsymbol{S}(k, w)$. In the next section we take the reader through a step by step derivation of each of the terms.

Stellenbosch University http://scholar.sun.ac.za

C.3 non-coupled system correlation-response Matrix elements

The calculation of the decoupled system correlation-response matrix elements involve similar calculational strategies and assumptions. In this appendix section we take the reader through the calculations steps for completeness sake. An expert reader can go directly to the list of the matrix elements found in expressions (C.62a)-(C.62e).

For the correlation-response matrix, the important contribution comes from terms in which $J = P$. Terms in which $J \neq P$ are uncorrelated and can easily be dealt away with in the exponential term of the functional (C.19). As stated earlier the average $\langle \cdots \rangle_0$ is done with respect the distribution of non-interacting particle. Since all particles are identical without loss of generality, the summation over particle number index p can be replaced by the number of summed over terms N and the index P could also be dropped.

C.3.1 Matrix element S_{11} calculation

$$s_{11} = \sum_{J=1,P=1}^{N,N} \left\langle e^{-(ikr_J(t)+ik'r_p(t'))} \right\rangle_0 = \sum_{J=P=1}^{N} \left\langle e^{-(ikr_p(t)+ik'r_p(t'))} \right\rangle_0 . \tag{C.20}$$

This could be expressed as

$$\begin{aligned} s_{11}(t) &= \frac{1}{\mathcal{N}} \sum_{p=1}^{N} \int \prod_{j=1}^{N} [dr_j(t)][d\hat{r}_j(t)] \exp\left\{ i \sum_{j=1}^{N} \int_t \hat{r}_j(t) \left(-\zeta \partial_t r_j(t)\right) - \frac{\alpha}{2} \hat{r}_j^2(t) \right\} \\ &\times \; e^{-(ikr_p(t)+ik'r_p(t'))}. \end{aligned} \tag{C.21}$$

Having performed the $\hat{r}$ path integral, we obtain

$$s_{11}(t) = \frac{N}{\mathcal{N}} \int \prod_{j=1}^{N} [dr_j(t)] \exp\left\{ -\frac{\zeta^2}{2\alpha} \sum_{j=1}^{n} \int_t \left(\partial_t r_j(t))^2 - ikr(t) - ik'r(t') \right) \right\}. \tag{C.22}$$

In equation (C.22) path integrals in which $r_j(t) \neq r(t)$ cancel with their corresponding integrals in the denominator leading to

$$s_{11}(t) = \frac{N}{\mathcal{N}'} \int [dr(t)] \exp\left\{ -\frac{\zeta^2}{2\alpha} \int_t (\partial_t r(t))^2 - i \left(kr(t) + k'r(t') \right) \right\}.$$

Stellenbosch University http://scholar.sun.ac.za

Time discretisation of equation (C.23) yields

$$\begin{aligned} s_{11}(t) &= \frac{N}{\mathcal{N}'}\int\prod_{\eta=0}^{n}dr_\eta\exp\left\{-\frac{\zeta^2}{2\alpha\epsilon}\sum_{\eta=1}^{n}(r_\eta-r_{\eta-1})^2-i(k+k')r_0\right. \\ &- \left. i\sum_{\eta=1}^{n}(kr_\eta+k'r_{\eta-1})\right\} \\ &= \frac{N}{\mathcal{N}'L}\delta(k+k')\int\prod_{\eta=1}^{n}dr_\eta\exp\left\{-\frac{\zeta^2}{2\alpha\epsilon}\sum_{\eta=1}^{n}(r_\eta-r_{\eta-1})^2\right. \\ &- \left. i\sum_{\eta=1}^{n}(kr_\eta+k'r_{\eta-1})\right\}. \end{aligned} \tag{C.23}$$

Introducing the bond vector definitions $b_\eta = r_\eta - r_{\eta-1}$ and considering only the case $k = -k'$, equation (C.23) reduces to

$$s_{11}(t) = \frac{N}{\mathcal{N}'L}\delta(k+k')\int\prod_{\eta=1}^{n}b_\eta\exp\left\{-\frac{1}{2\alpha}\sum_{\eta=1}^{n}\left(\frac{\zeta^2}{\epsilon}b_\eta^2\right)-ik\sum_{\eta=1}^{n}b_\eta\right\}. \tag{C.24}$$

Having performed the b_η integrals, the resulting expression becomes

$$\begin{aligned} s_{11} &= \frac{N}{L}\delta(k+k')\left(\exp\left\{-\frac{\alpha\epsilon k^2}{2\zeta^2}\right\}\right)^n \\ &= \frac{N}{L}\delta(k+k')\exp\left\{-\frac{\alpha k^2}{2\zeta^2}|t-t'|\right\}, \quad \text{where } n=\frac{|t-t'|}{\epsilon} \\ &= \frac{N}{L}\delta(k+k')\exp\left\{-\frac{\alpha k^2}{2\zeta^2}|t|\right\}, \quad \text{having chosen } t'=0. \end{aligned} \tag{C.25}$$

Upon taking the Fourier transform on the s_{11} in time, we obtain

$$s_{11}(w) = \frac{N}{(2\pi)^{\frac{1}{2}}\zeta^2}\frac{\delta(k+k')\alpha k^2}{L\left(w^2+\frac{\alpha^2k^4}{4\zeta^4}\right)}. \tag{C.26}$$

Stellenbosch University http://scholar.sun.ac.za

C.3.2 Matrix element S_{13} calculation

$$\begin{aligned} s_{13} &= \left\langle \sum_{J=1}^{N} \partial_t r_J \exp\left\{-ikr_J(t) - ik^{'} r_J(t)\right\} \theta(t) \right\rangle_0 \\ &= \frac{1}{\mathcal{N}} \sum_{J=1}^{N} \int \prod_{j=1}^{N} [dr_j(t)] \prod_{j}^{N} [d\hat{r}_j(t)] \exp\left\{ \int_j i\hat{r}_j(t) \left(-\zeta \partial_t r_j(t)\right)^2 - \frac{\alpha}{2} \hat{r}_j^2(t) \right\} \\ &\quad \partial_t r_J \exp\left\{-ikr_J(t) - ik^{'} r_J(t')\right\} \theta(t). \end{aligned} \tag{C.27}$$

The heavy-side unit step function $\theta(t)$ imposes the condition that the average should be correctly time ordered. On replacing the sum by the number of particles and dropping the index J, having integrated out all the hatted fields, we get

$$S_{13} = \frac{N}{\mathcal{N}} \int \prod_{j=1}^{N} [dr_j(t)] \exp\left\{ -\frac{\zeta^2}{2\alpha} \sum_{j=1}^{N} \int_t (\partial_t r_j(t))^2 - ikr(t) - ik^{'} r(t^{'}) \right\} \partial_t r(t) \theta(t). \tag{C.28}$$

The result of the integrals where $r_j(t) \neq r(t)$ in the denominator and numerator cancel out, therefore

$$S_{13} = \frac{N}{\mathcal{N}} \int [dr(t)] \exp\left\{ -\frac{\zeta^2}{2\alpha} \int_t (\partial_t r(t))^2 - ikr(t) - ik^{'} r(t^{'}) \right\} \partial_t r(t) \theta(t). \tag{C.29}$$

The spatial variables $r(t)$ can be discretised into $r(t) = r_0 + \sum_{\eta=1}^{N} b_\eta$, where $b_\eta = r_\eta - r_{\eta-1}$. In terms of the b_η (C.29) can be written as

$$s_{13} = \frac{N}{\mathcal{N}'} \delta(k + k^{'}) \int \prod_{\eta=1}^{N} db_\eta \exp\left\{ -\frac{\zeta^2}{2\alpha\epsilon} \sum_{\eta=1}^{n} b_\eta^2 - ik \sum_{\eta=1}^{n} b_\eta \right\} \left(\frac{b_\eta}{\epsilon}\right) \theta(t). \tag{C.30}$$

Upon introducing the generating function $\exp\left\{\sum_{\eta=1}^{n} h_\eta b_\eta\right\}$ in equation (C.30), the resulting expression becomes

$$\begin{aligned} s_{13} &= \frac{N}{\mathcal{N}'} \delta(k + k^{'}) \\ &\times \int \prod_{\eta=1}^{N} db_\eta \frac{\partial}{\partial h_{\eta'}} \exp\left\{ -\frac{\zeta^2}{2\alpha\epsilon} \sum_{\eta=1}^{n} b_\eta^2 + \sum_{\eta=1}^{n} b_\eta (-ik + h_\eta) \right\} \left(\frac{b_\eta}{\epsilon}\right) \theta(t) \Big|_{h_\eta(0)=0}. \end{aligned} \tag{C.31}$$

Stellenbosch University http://scholar.sun.ac.za

The order of the integral and the functional derivatives could be swapped. This allows us to perform the integral first getting

$$\begin{aligned} s_{13} &= \frac{N}{L\epsilon}\delta(k+k')\frac{\partial}{\partial h_{\eta'}}\exp\left\{\frac{\alpha\epsilon}{2\zeta^2}(-ik+h_{\eta'})^2\right\}\left(\exp\left\{\frac{\alpha\epsilon}{2\zeta^2}(-ik+h)^2\right\}\right)^{n-1}\theta(t)\Big|_{h_\eta(0)=0} \\ &= -\frac{iN\alpha k}{L\zeta^2}\delta(k+k')\left(\exp\left\{-\frac{\alpha\epsilon k^2}{2\zeta^2}\right\}\right)^n\theta(t) \\ &= -\frac{iN\alpha k}{L\zeta^2}\delta(k+k')\exp\left\{-\frac{\alpha k^2}{2\zeta^2}|t-t'|\right\}\theta(t) \quad \text{where we let} \quad n=\frac{|t-t'|}{\epsilon}. \end{aligned} \tag{C.32}$$

Finally, we can take a Fourier transform of the resulting expression leading to

$$s_{13} = \frac{2kN\alpha}{L\zeta^2 2\pi}\left(\frac{\delta(k+k')}{w+\frac{ik^2\alpha}{2\zeta^2}}\right). \tag{C.33}$$

C.3.3 Matrix element S_{15} calculation

$$s_{15} = \sum_{J,P=1}^{N}\left\langle ik\hat{r}_J e^{-(ikr_J(t)+ik'r_p(t'))}\right\rangle_0$$

This could explicitly be expressed as

$$\begin{aligned} s_{15}(t) &= \frac{ik}{\mathcal{N}}\sum_{p=1}^{N}\int\prod_{j=1}^{N}[dr_j(t)][d\hat{r}_j(t)]\exp\left\{\sum_{j=1}^{N}\int_t\left(-i\zeta\hat{r}_j(t)\partial_t r_j(t)-\frac{\alpha}{2}\hat{r}_j^2(t)\right)\right\} \\ &\times \hat{r}_p(t)\theta(t)e^{-(ikr_p(t)+ik'r_p(t'))}. \end{aligned} \tag{C.34}$$

The generating functional approach is then used to get the hatted conformation field $\hat{r}$ into the exponent. This leads to

$$\begin{aligned} s_{15}(t) &= \frac{ikN}{\mathcal{N}}\int\prod_{j=1}^{N}[dr_j(t)][d\hat{r}_j(t)]\frac{\delta}{\delta h(t)}\exp\left\{\sum_{j=1}^{N}\int_t(-i\zeta\hat{r}_j(t)\partial_t r_j(t)+\hat{r}_j(t)h_j(t)\right. \\ &+ \left.-\frac{\alpha}{2}\hat{r}_j^2(t)\right)\Big\}\theta(t)e^{-(ikr(t)+ik'r(t'))}\Big|_{h(0)=0}. \end{aligned} \tag{C.35}$$

By performing the $\hat{r}$ integral first, the equation (C.35) can then be simplified further to

$$\begin{aligned} s_{15}(t) &= \frac{ikN}{\mathcal{N}}\int\prod_{j=1}^{N}[dr_j(t)]\frac{\delta}{\delta h(t)}\exp\left\{\frac{1}{2\alpha}\sum_{j=1}^{N}\int_t(-i\zeta\partial_t r_j(t)+h_j(t))^2\right\} \\ &\times \theta(t)e^{-(ikr(t)+ik'r(t'))}\Big|_{h(0)=0}. \end{aligned} \tag{C.36}$$

Stellenbosch University http://scholar.sun.ac.za

Upon taking the functional derivative in $h(t)$, we are left with

$$\begin{aligned} s_{15}(t) &= \frac{kN\zeta}{\mathcal{N}\alpha}\int\prod_{j=1}^{N}[dr_j(t)]\exp\left\{-\frac{\zeta^2}{2\alpha}\sum_{j=1}^{N}\int_t(\partial_t r_j(t))^2\right\} \\ &\times \theta(t)\partial_t r(t)e^{-(ikr(t)+ik^{'}r(t^{'}))}. \end{aligned} \tag{C.37}$$

As noted earlier, integrals in which $r_j \neq r(t)$ cancel out with their corresponding integrals in the normalisation leaving us with

$$\begin{aligned} s_{15}(t) &= \frac{kN\zeta}{\mathcal{N}^{'}\alpha}\int[dr(t)]\exp\left\{-\frac{\zeta^2}{2\alpha}\int_t(\partial_t r(t))^2\right\} \\ &\times \theta(t)\partial_t r(t)e^{-(ikr(t)+ik^{'}r(t^{'}))}, \end{aligned} \tag{C.38}$$

which upon discretising leads to

$$\begin{aligned} s_{15}(t) &= \frac{kN\zeta}{\mathcal{N}^{'}\alpha}\int\prod_{\eta=0}^{n}dr_\eta\exp\left\{-\frac{\zeta^2}{2\alpha\epsilon}\sum_{\eta=1}^{n}(r_\eta - r_{\eta-1})^2\right. \\ &- \left. i(k+k^{'})r_0 - i\sum_{\eta=1}^{n}(kr_\eta + k^{'}r_{\eta-1})\right\}\theta(t)\left(\frac{r_\gamma - r_{\gamma-1}}{\epsilon}\right), \\ &= \frac{kN\zeta}{\mathcal{N}^{'}L\alpha}\delta(k+k^{'})\int\prod_{\eta=1}^{n}dr_\eta\exp\left\{-\frac{\zeta^2}{2\alpha\epsilon}\sum_{\eta=1}^{n}\left((r_\eta - r_{\eta-1})^2\right.\right. \\ &- \left.\left. i\sum_{\eta=1}^{n}(kr_\eta + k^{'}r_{\eta-1})\right\}\theta(t)\left(\frac{r_\gamma - r_{\gamma-1}}{\epsilon}\right). \end{aligned} \tag{C.39}$$

For the case $k = -k^{'}$, when introducing the definitions $b_\gamma = r_\gamma - r_{\gamma-1}$ and $b_\eta = r_\eta - r_{\eta-1}$, equation (C.39) becomes

$$\begin{aligned} s_{15}(t) &= \frac{kN\zeta}{\mathcal{N}^{'}L\alpha\epsilon}\delta(k+k^{'})\int\prod_{\eta=1}^{n}db_\eta\exp\left\{-\frac{\zeta^2}{2\alpha\epsilon}\sum_{\eta=1}^{n}b_\eta^2 - ik\sum_{\eta=1}^{n}b_\eta\right\} \\ &\theta(t)b_\gamma. \end{aligned} \tag{C.40}$$

The generating functional can be used again to get all the b's in to the exponent hence,

Stellenbosch University http://scholar.sun.ac.za

the above expression can be written as

$$\begin{aligned} s_{15} &= \frac{kN\zeta}{\mathcal{N}' L\alpha\epsilon}\delta(k+k') \\ &\times \int \prod_{\eta=1}^{n} db_\eta \frac{\partial}{\partial h_\gamma(t)} \exp\left\{-\frac{\zeta^2}{2\alpha\epsilon}\sum_{\eta=1}^{n}\left(b_\eta^2\right) - \sum_{\eta=1}^{n}(ikb_\eta - b_\eta h_\eta(t))\right\}\theta(t)\Big|_{h_\gamma(0)=0}. \end{aligned} \tag{C.41}$$

Upon taking the b_η integrals, the resulting expression becomes

$$\begin{aligned} s_{15} &= \frac{kN\zeta}{L\alpha\epsilon}\delta(k+k') \\ &\times \left(\exp\left\{\frac{\alpha\epsilon}{2\zeta^2}\left(-ik+h(t)\right)^2\right\}\right)^{n-1} \qquad \text{(C.42)} \\ &\times \frac{\partial}{\partial h_\gamma(t)} \exp\left\{\frac{\alpha\epsilon}{2\zeta^2}\left(-ik+h_\gamma(t)\right)^2\right\}\Big|_{h(0)=0}\theta(t). \qquad \text{(C.43)} \end{aligned}$$

The normalisation cancels out since $\mathcal{N}' = \sqrt{\frac{2\pi\alpha\epsilon}{\zeta^2}}^n$. Having taken the partial derivative, the equation (C.43) simplifies to

$$s_{15} = -\frac{iNk^2}{L\zeta}\delta(k+k')\exp\left\{-\left(\frac{k^2\alpha}{2\zeta^2}\right)|t|\right\}\theta(t). \tag{C.44}$$

In Fourier representation the expression becomes

$$S_{12}(w) = \frac{2Nk^2\delta(w+w')}{L\zeta\sqrt{2\pi}\left(w+i\frac{k^2\alpha}{2\zeta^2}\right)}. \tag{C.45}$$

C.3.4 Matrix element S_{35} calculation

$$\begin{aligned} s_{35} &= ik\sum_{J=1}^{N}\left\langle \hat{r}_J(t')\partial_t r_J(t)\exp\left\{-ikr_J(t)-ik'r_J(t')\right\}\right\rangle \\ &= \frac{ik}{\mathcal{N}}\sum_{J=1}^{N}\int\prod_{j=1}^{N}[dr_j(t)][d\hat{r}_j(t)]\exp\left\{\sum_{j=1}^{N}\int_t\left(i\hat{r}_j(t)(-\zeta(\partial_t r_j(t))-\frac{\alpha}{2}\hat{r}_j^2(t)\right)\right\} \\ &\times \partial_t r_J(t)\hat{r}_J(t'\exp\left\{-ikr_J(t)-ik'r_J(t')\right\}\theta(t) \\ &= \frac{ikN}{\mathcal{N}}\int\prod_{j=1}^{N}[dr_j(t)][d\hat{r}_j(t)]\exp\left\{\sum_{j=1}^{N}\int_t\left(i\hat{r}_j(t)(-\zeta(\partial_t r_j(t))-\frac{\alpha}{2}\hat{r}_j^2(t)\right)\right\} \\ &\times \partial_t r(t)\hat{r}(t')\exp\left\{-ikr(t)-ik'r(t')\right\}\theta(t), \end{aligned} \tag{C.46}$$

Stellenbosch University http://scholar.sun.ac.za

Terms in which $r(t) \neq r_j(t)$ cancel with corresponding terms in the denominator. This allows us to get the simplified expression

$$\begin{aligned} s_{35} &= \frac{ikN}{\mathcal{N}} \int [dr(t)][d\hat{r}(t)] \exp\left\{ \int_t \left(i\hat{r}(t)(-\zeta(\partial_t r(t)) - \frac{\alpha}{2}\hat{r}^2(t) \right) \right\} \\ &\quad \partial_t r(t) \hat{r}(t') \exp\left\{ -ikr(t) - ik' r(t') \right\} \theta(t). \end{aligned} \tag{C.47}$$

After introducing the generating functional $\exp\{h(t)\hat{r}(t)\}$ in equation (C.47), we can then rewrite the expression as

$$\begin{aligned} s_{35} &= \frac{ikN}{\mathcal{N}} \int [dr(t)][d\hat{r}(t)] \frac{\partial}{\partial h(t')} \exp\left\{ \int_t \left(\hat{r}(t)(-i\zeta(\partial_t r(t) + h(t)) - \frac{\alpha}{2}\hat{r}^2(t) \right) \right\} \\ &\quad \partial_t r(t) \exp\left\{ -ikr(t) - ik' r(t') \right\} \Big|_{h(0)=0} \theta(t). \end{aligned} \tag{C.48}$$

Performing the $\hat{r}(t)$ integral first we obtain

$$\begin{aligned} s_{35} &= \frac{ikN}{\mathcal{N}} \int [dr(t)] \frac{\partial}{\partial h(t')} \exp\left\{ \int_t \left(\frac{1}{2\alpha}(-i\zeta(\partial_t r(t) + h(t))^2 \right) \right\} \\ &\quad \partial_t r(t) \partial_{t'} r(t') \exp\left\{ -ikr(t) - ik' r(t') \right\} \Big|_{h(0)=0} \theta(t). \end{aligned} \tag{C.49}$$

Equation (C.49) can further be simplified by taking the derivative and then discretising the resulting expression in time leading to

$$\begin{aligned} s_{35}(t) &= \frac{kN\zeta}{\mathcal{N}'\alpha} \int \prod_{\eta=0}^{n} dr_\eta \exp\left\{ -\frac{\zeta^2}{2\alpha\epsilon} \sum_{\eta=1}^{n} (r_\eta - r_{\eta-1})^2 - i(k+k')r_0 - i\sum_{\eta=1}^{n}(kr_\eta + k' r_{\eta-1}) \right\} \\ &\quad \theta(t) \left(\frac{r_{\eta'} - r_{\eta'-1}}{\epsilon} \right) \left(\frac{r_{\eta''} - r_{\eta''-1}}{\epsilon} \right). \end{aligned} \tag{C.50}$$

If we let $b_\eta = r_\eta - r_{\eta-1}$ and $b_{\eta'} = r_{\eta'} - r_{\eta'-1}$ the above equation can be written as

$$\begin{aligned} s_{35} &= \frac{kN\zeta}{\mathcal{N}\alpha\epsilon^2} \delta(k+k') \int \prod_{\eta=1}^{N} db_\eta \exp\left\{ -\frac{1}{2\alpha\epsilon} \sum_{\eta=1}^{n} \zeta^2 b_\eta^2 + \sum_{\eta=1}^{n}(-ikb_\eta) \right\} \\ &\quad b_{\eta'} b_{\eta''}\ \theta(t)|_{h_\eta=0} \quad \text{for all} \quad \eta \in [1,n]. \end{aligned} \tag{C.51}$$

Upon introducing the generating functional $\exp\left\{\sum_\eta^n b_\eta h_\eta\right\}$, equation (C.51) can be further expressed as

$$\begin{aligned} s_{35} &= \frac{kN\zeta}{\mathcal{N}\alpha\epsilon^2} \delta(k+k') \int \prod_{\eta=1}^{N} db_\eta \frac{\delta}{\delta h_{\eta'} \delta h_{\eta''}} \exp\left\{ -\frac{1}{2\alpha\epsilon} \sum_{\eta=1}^{n} \zeta^2 b_\eta^2 + \sum_{\eta=1}^{n}(-ikb_\eta + h_\eta b_\eta) \right\} \\ &\quad \theta(t)|_{h_\eta=0} \quad \text{for all} \quad \eta \in [1,n]. \end{aligned} \tag{C.52}$$

Stellenbosch University http://scholar.sun.ac.za

Having performed the integration step first and then the derivative we obtain

$$\begin{aligned} s_{35} &= -\frac{k^3 N\alpha}{l\zeta^3}\delta(k+k^{'})\left(\exp\left\{-\frac{\alpha\epsilon k^2}{2\zeta^2}\right\}\theta(t)\right)^n\theta(t) \quad \text{let} \quad n=\frac{t-t^{'}}{\epsilon} \\ &= -\frac{k^3 N\alpha}{l\zeta^3}\delta(k+k^{'})\exp\left\{\frac{-\alpha k^2}{2\zeta^2}|t-t^{'}|\right\}\theta(t). \end{aligned} \tag{C.53}$$

If we assume that $t^{'}=0$ and take the Fourier transform in time on equation (C.53) we obtain

$$s_{35} = -\frac{2k^3 N\alpha}{L\zeta^3}\frac{\delta(k+k^{'})}{\left(\frac{k^2\alpha}{2\zeta^2}-iw\right)}. \tag{C.54}$$

C.3.5 Matrix element S_{33} calculation

$$s_{33} = \left\langle \sum_{J=1}^{N}\partial_t r(t)\partial_{t'} r_J(t^{'})\exp\{-ikr_J(t)-ikr_J(t^{'})\}\right\rangle_0 \tag{C.55}$$

The statistical average can be explicitly written as

$$\begin{aligned} s_{33} &= \frac{N}{\mathcal{N}}\int\prod_{j=1}^{N}[dr_j(t)][d\hat{r}_t(t)]\exp\left\{i\int_t\left(\hat{r}_j(t)\left(-\zeta\partial_t r_j(t)\right)-\frac{\alpha}{2}\sum_j^N\hat{r}_j^2\right)\right\} \\ &\quad (\partial_t r(t))(\partial_{t'} r(t^{'}))\exp\left\{-ikr-ik^{'}r(t^{'})\right\} \\ &= \frac{N}{\mathcal{N}}\int\prod_{j=1}^{N}[dr_j(t)]\exp\left\{-\frac{\zeta^2}{2\alpha}\sum_{j=1}^{N}\int_j\left(\partial_j r_j(t)\right)^2-ikr(t)-ik^{'}r(t^{'})\right\} \\ &\quad (\partial_t r(t))(\partial_{t'} r(t^{'})) \end{aligned} \tag{C.56}$$

As it was the case in other matrix elements calculations, the result of path integrals in which $r_j \neq r(t)$ in the numerator and denominator trivially cancel out and we are left with

$$\begin{aligned} s_{33} &= \frac{N}{\mathcal{N}}\int[dr(t)]\exp\left\{-\frac{\zeta^2}{2\alpha}\int_j\left(\partial_j r(t)\right)^2-ikr(t)-ik^{'}r(t^{'})\right\} \\ &\quad (\partial_t r(t))(\partial_{t'} r(t^{'})). \end{aligned} \tag{C.57}$$

Stellenbosch University http://scholar.sun.ac.za

After discretising the position variables in time, we get

$$s_{33} = \frac{N}{\mathcal{N}} \int \prod_{n=0}^{n} dr_n \exp\left\{ -\frac{\zeta^2}{2\alpha} \sum_{n=1}^{n} \epsilon \left(\frac{r_\eta - r_{\eta-1}}{\epsilon} \right)^2 - i(k+k^{'})r_0 - i(kr_\eta + k^{'} r_{\eta-1}) \right\} \left(\frac{r_{\gamma^{'}} - r_{\gamma^{'}-1}}{\epsilon} \right) \left(\frac{r_{\gamma^{''}} - r_{\gamma^{''}-1}}{\epsilon} \right). \tag{C.58}$$

The discretised position variable can be expressed as $r(t) = r_0 + \sum_{\eta=1}^{N} b_\eta$, where we denote $b_\eta = r_\eta - r_{\eta-1}$ and $b_\eta = r_\gamma - r_{\gamma-1}$. Taking only the case when $k = -k^{'}$, equation (C.58) becomes

$$s_{33} = \frac{N}{\mathcal{N} L \epsilon^2} \delta(k+k^{'}) \int \prod_{n=1}^{n} db_\eta \exp\left\{ -\frac{\zeta^2}{2\alpha\epsilon} \sum_{\eta=1}^{n} b_\eta^2 - ik \sum_{\eta=1}^{n} b_\eta \right\} b_{\gamma^{'}} b_{\gamma^{''}}. \tag{C.59}$$

Upon introducing the generating function $\exp\left\{\sum_{\eta=1}^{n} b_\eta h_\eta(t)\right\}$ in equation (C.59), we are able to write s_{33} as

$$s_{33} = \frac{n}{\mathcal{N}^{'} L \epsilon^2} \delta(k+k^{'}) \int \prod_{\eta=1}^{n} db_\eta \frac{\partial^2}{\partial h_{\gamma^{'}} \partial h_{\gamma^{''}}} \exp\left\{ -\frac{\zeta^2}{2\alpha} \sum_{\eta=1}^{n} b_\eta^2 + \sum_{\eta=1}^{n} (-ik + h_\eta) b_\eta \right\} \Bigg|_{h_\eta(0)=0 \quad \text{for all} \quad \eta \in \{1,\cdots n\}}.$$

Having performed the integral first, we obtain the expression

$$\begin{aligned} s_{33} &= \frac{N}{L\mathcal{N}^{'}\epsilon^2} \left(\exp\left\{ \frac{\alpha\epsilon}{2\zeta^2}(-ik+h)^2 \right\} \right)^{n-1} \frac{\partial}{\partial h_{\gamma^{'}}} \exp\left\{ \frac{\alpha\epsilon}{2\zeta^2}(-ik+h_{\gamma^{'}})^2 \right\} \\ &\quad \frac{\partial}{\partial h_{\gamma^{''}}} \exp\left\{ \frac{\alpha\epsilon}{2\zeta^2}(-ik+h_{\gamma^{''}})^2 \right\} \Bigg|_{h_\eta(0)=0} \\ &= -\frac{N\alpha^2}{L\zeta^4} \delta(k+k^{'}) k^2 \exp\left\{ -\frac{\alpha k^2}{2\zeta^2} |t-t^{'}| \right\} \end{aligned} \tag{C.60}$$

We assume $t^{'} = 0$ then we express the s_{33} in Fourier transform in time as

$$s_{33} = -\frac{N\alpha^3 k^4}{2L\zeta^6} \frac{\delta(k+k^{'})}{\left(\omega^2 + (\frac{\alpha^2 k^4}{4\zeta^4})\right)}. \tag{C.61}$$

Stellenbosch University http://scholar.sun.ac.za

After performing the $k^{'}$ integral, we finally obtained the following non-coupled channel correlation terms:

$$s_{11}(k,\omega) = s_{22}(k,\omega) = \frac{2\beta\zeta k^2 N}{L\left(k^4+\beta^2\zeta^2\omega^2\right)}, \tag{C.62a}$$

$$s_{13}(k,\omega) = s_{24}(k,\omega) = \frac{2kN}{L\left(ik^2+\ \beta\zeta\omega\right)}, \tag{C.62b}$$

$$s_{15}(k,\omega) = s_{26}(k,\omega) = \frac{k^2 N\beta}{L\left(ik^2+\beta\zeta\omega\right)}, \tag{C.62c}$$

$$s_{35}(k,\omega) = s_{46}(k,\omega) = -\frac{4k^3 N}{L\left(k^2\zeta-i\beta\zeta^2\omega\right)}, \tag{C.62d}$$

$$s_{33}(k,\omega) = s_{44}(k,\omega) = -\frac{4k^4 N}{L\left(\beta\zeta k^4+\beta^3\zeta^3\omega^2\right)}. \tag{C.62e}$$

where we have used the fact that $\alpha = \frac{2}{\beta}\zeta$. In each of these terms a constant factor of $\sqrt{2\pi}$ is left out as it does not contribute in the dynamics. Because of the causality condition,

$$s_{44}(k,\omega) = s_{55}(k,\omega) = 0. \tag{C.63}$$

Each of diagonal entry $s_{ij}(k,w) = s_{ji}(k^{'},w^{'})$ for $i,j \in \{1,\cdots 6\}$. Furthermore, the entries $s_{44} = s_{55} = 0$ due to the causality condition. The rest of the statistical averages that vanish are because they involve a product of uncorrelated terms whose average decouple leading to a product of two independent statistical averages with one of them averaging trivially to zero, such as

$$\begin{aligned} s_{ij} &= \left\langle \sum_{J=1,\tau=1}^{N} \int_{k,t} ik\bar{r}_\tau(t)\hat{r}_j(t)\exp(-ikr_j)(t) - ik\bar{r}_j(\tau) \right\rangle_0 \\ &= \left\langle \sum_{J=1}^{N} \int_{k,t} ik\hat{r}_j \exp(-ikr_j)(t) \right\rangle_0 \left\langle \sum_{J=1}^{N} \int_{k,t} \exp(-ik\bar{r}(t)) \right\rangle_0 . \end{aligned} \tag{C.64}$$

C.3.6 The probability current

The probability current at a specific node x on the file can be obtained by performing a statistical average over the product of particle density and velocity at a given position x, which is simply defined by

$$J(x,t) := \left\langle \sum_{p=1}^{N} \partial_t r_p(t)\delta(x-r_p(t)) \right\rangle . \tag{C.65}$$

Stellenbosch University http://scholar.sun.ac.za

Where the sum runs over the number of particles on the node. The average $\langle\cdots\rangle_0$, is taken with respect to the non interacting particle distribution. Fourier spatial variables the probability current can be expressed as

$$\begin{aligned}\tilde{j}_k(t) &= \left\langle \int_k \partial_t r_p(t) e^{-ikr_p(t)} \right\rangle \\ &= \frac{1}{\mathcal{N}} \sum_{p=1}^{N} \int_k \int \prod_{j=1}^{N} [dr_j(t)] \exp\left\{ -\frac{1}{2\alpha} \sum_{j=1}^{N} \int_t \left(\zeta \partial_j r_j(t)\right)^2 - ikr_p(t) \right\} \\ &\quad \partial_t r_p(t). \end{aligned} \tag{C.66}$$

Since all the particles are identical, the subscript p in the position variables $r_p(t)$ can be dropped and the summation over the variables can be replaced by the number of summed over variables N. The fact that the integrals over variables $r_j \neq r(t)$ cancel with integrals of corresponding subscript in the normalisation leads to the following simplified expression for the current density

$$\tilde{j}_k(t) = \frac{N}{\mathcal{N}} \int_k \int [dr(t)] \exp\left\{ -\frac{1}{2\alpha} \int_t \left(\zeta \partial_t r(t)\right)^2 - ikr_p(t) \right\} . \partial_t r(t).$$

To deal with the path integral, it is best to discretise it in time. Then equation (C.67) reads

$$\begin{aligned}\tilde{j}_k(t) &= \int_k \int \prod_{\eta=0}^{n} dr_\eta \exp\left\{ -\frac{\zeta^2}{2\alpha\epsilon} \sum_{\eta=1}^{n} \left(r_\eta(t) - r_{\eta-1}(t)\right)^2 \right. \\ &\quad \left. ikr_0 + ik \sum_{\eta=1}^{n} (r_\eta - r_{\eta-1}) \right\} \left(\frac{r_\gamma - r_{\gamma-1}}{\epsilon} \right). \end{aligned} \tag{C.67}$$

Following the change of variables $b_\eta(t) = r_\eta(t) - r_{\eta-1}(t)$ and as introduction of a generating functional $\exp\left\{\sum_{\eta=1}^{N} b_\eta(t) h_\eta(t)\right\}$, the current density can be re-expressed as

$$\begin{aligned}\tilde{j}_k(t) &= \frac{N\epsilon}{L\mathcal{N}'} \int_k \delta(k) \int \prod_{\eta=1}^{n} db_\eta(t) \frac{\partial}{\partial h_\gamma} \exp\left\{ -\frac{\zeta^2}{2\alpha\epsilon} \sum_{\eta=1}^{n} b_\eta^2 \right. \\ &\quad \left. + \sum_{\eta=1}^{n} b_\eta(t) \left(h_\eta(t) - ik\right) \right\} \Bigg|_{h_\gamma(0)=0 \quad \text{for all } \gamma} . \end{aligned} \tag{C.68}$$

Taking the b_j integrals first followed by the derivative, we are left with

$$\tilde{j}_k(t) = \int_k \delta(k) \left(-ik\right) \left(\exp\left\{ -\frac{k^2 \alpha\epsilon}{2\zeta^2} \right\} \right)^n . \tag{C.69}$$

Stellenbosch University http://scholar.sun.ac.za

Upon performing the final k integral we obtain the current density as

$$\tilde{j}_k(t) = 0. \tag{C.70}$$

Stellenbosch University http://scholar.sun.ac.za

Bibliography

E. Akkermans, T. Bodineau, B. Derrida, and O. Shpielberg. Universal current fluctuations in the symmetric exclusion process and other diffusive systems. *EPL (Europhysics Letters)*, 103(2):20001, 2013. URL http://stacks.iop.org/0295-5075/103/i=2/a=20001.

B. V. Alexeev. *Generalized Boltzmann Physical Kinetics*. ELSEVIER, 2004.

Z. G. Arenas and D. G. Barci. Functional integral approach for multiplicative stochastic processes. *Phys. Rev. E*, 81:051113, May 2010. doi: 10.1103/PhysRevE.81.051113. URL http://link.aps.org/doi/10.1103/PhysRevE.81.051113.

D. S. Banks and C. Fradin. Anomalous diffusion of proteins due to molecular crowding. *Biophysical Journal*, 89(5):2960 – 2971, 2005. ISSN 0006-3495. doi: http://dx.doi.org/10.1529/biophysj.104.051078. URL http://www.sciencedirect.com/science/article/pii/S0006349505729404.

L. J. Barbour. Crystal porosity and the burden of proof. *Chem. Commun.*, pages 1163–1168, 2006. doi: 10.1039/B515612M. URL http://dx.doi.org/10.1039/B515612M.

C. Bastien and D. Michel. *Cellular automata modeling of physical systems*. Cambridge University, 1998.

A. Berezhkovskii and G. Hummer. Single-file transport of water molecules through a carbon nanotube. *Phys. Rev. Lett.*, 89:064503, Jul 2002. doi: 10.1103/PhysRevLett.89.064503. URL http://link.aps.org/doi/10.1103/PhysRevLett.89.064503.

R. K. Bowles, K. K. Mon, and J. K. Percus. Calculating the hopping times of confined fluids: Two hard disks in a box. *The Journal of Chemical Physics*,

Stellenbosch University http://scholar.sun.ac.za

121(21):10668–10673, 2004. doi: http://dx.doi.org/10.1063/1.1811075. URL http://scitation.aip.org/content/aip/journal/jcp/121/21/10.1063/1.1811075.

A. Brzank and G. M. Schütz. Phase transition in the two-component symmetric exclusion process with open boundaries. *Journal of Statistical Mechanics: Theory and Experiment*, 08(2007):P08028, 2007. URL http://stacks.iop.org/1742-5468/2007/i=08/a=P08028.

S. Chatterjee and G. M. Schütz. The importance of boundary effects in diffusion of hydrocarbon molecules in a one-dimensional zeolite channel. *Journal of Statistical Mechanics: Theory and Experiment*, 2010(01):P01017, 2010. URL http://stacks.iop.org/1742-5468/2010/i=01/a=P01017.

T. Chou. How fast do fluids squeeze through microscopic single-file pores? *Phys. Rev. Lett.*, 80:85–88, Jan 1998. doi: 10.1103/PhysRevLett.80.85. URL http://link.aps.org/doi/10.1103/PhysRevLett.80.85.

T. Chou and D. Lohse. Entropy-driven pumping in zeolites and biological channels. *Phys. Rev. Lett.*, 82:3552–3555, Apr 1999. doi: 10.1103/PhysRevLett.82.3552. URL http://link.aps.org/doi/10.1103/PhysRevLett.82.3552.

C. De Dominicis and L. Peliti. Field-theory renormalization and critical dynamics above T_c: Helium, antiferromagnets, and liquid-gas systems. *Phys. Rev. B*, 18:353–376, Jul 1978. doi: 10.1103/PhysRevB.18.353. URL http://link.aps.org/doi/10.1103/PhysRevB.18.353.

P. Demontis and G. B. Suffritti. Structure and dynamics of zeolites investigated by molecular dynamics. *Chemical Reviews*, 97(8):2845–2878, 1997. doi: 10.1021/cr950253o. URL http://pubs.acs.org/doi/abs/10.1021/cr950253o.

B. Derrida and A. Gerschenfeld. Current fluctuations of the one dimensional symmetric simple exclusion process with step initial condition. *Journal of Statistical Physics*, 136(1):1–15, 2009. ISSN 0022-4715. doi: 10.1007/s10955-009-9772-7. URL http://dx.doi.org/10.1007/s10955-009-9772-7.

B. Derrida and M. Retaux. Finite size corrections to the large deviation function of the density in the one dimensional symmetric simple exclusion process. *Journal of Statistical*

Stellenbosch University http://scholar.sun.ac.za

Physics, 152(5):824–845, 2013. ISSN 0022-4715. doi: 10.1007/s10955-013-0797-6. URL http://dx.doi.org/10.1007/s10955-013-0797-6.

B. Derrida, J. Lebowitz, and E. Speer. Large deviation of the density profile in the steady state of the open symmetric simple exclusion process. *Journal of Statistical Physics*, 107(3-4):599–634, 2002. ISSN 0022-4715. doi: 10.1023/A:1014555927320. URL http://dx.doi.org/10.1023/A%3A1014555927320.

W. Dieterich and I. Peschel. Pair diffusion in an ideal lattice gas. *Journal of Physics C: Solid State Physics*, 16(20):3841, 1983. URL http://stacks.iop.org/0022-3719/16/i=20/a=009.

M. Doi. Second quantization representation for classical many-particle system. *J. Phys. A: Math. Gen*, 9(9):1465–1477, Jan. 1976.

R. Eisenberg. Computing the field in proteins and channels. *The Journal of Membrane Biology*, 150(1):1–25, 1996. ISSN 0022-2631. doi: 10.1007/s002329900026. URL http://dx.doi.org/10.1007/s002329900026.

R. Eisenberg. From structure to function in open ionic channels. *The Journal of Membrane Biology*, 171(1):1–24, 1999. ISSN 0022-2631. doi: 10.1007/s002329900554. URL http://dx.doi.org/10.1007/s002329900554.

G. H. Fredrickson and E. Helfand. Collective dynamics of polymer solutions. *The Journal of Chemical Physics*, 93(3):2048–2061, 1990. doi: 10.1063/1.459082. URL http://link.aip.org/link/?JCP/93/2048/1.

C. W. Gardiner. *Handbook of Stochastic Methods for Physics, Chemistry and the Natural Sciences*. Springer, 1985.

G. Guigas and M. Weiss. Sampling the cell with anomalous diffusionthe discovery of slowness. *Biophysical Journal*, 94(1):90 – 94, 2008. ISSN 0006-3495. doi: http://dx.doi.org/10.1529/biophysj.107.117044. URL http://www.sciencedirect.com/science/article/pii/S0006349508707677.

K. Hahn and J. Kärger. Propagator and mean-square displacement in single-file systems. *Journal of Physics A: Mathematical and General*, 28(11):3061, 1995. URL http://stacks.iop.org/0305-4470/28/i=11/a=010.

Stellenbosch University http://scholar.sun.ac.za

K. Hahn and J. Kärger. Molecular dynamics simulation of single-file systems. *The Journal of Physical Chemistry*, 100(1):316–326, 1996. doi: 10.1021/jp951807u. URL http://pubs.acs.org/doi/abs/10.1021/jp951807u.

B. Hille. *Ion Channels of Excitable Membranes*. Sinauer, Sunderland, Massachusetts, 2001.

T. Jacobs. *Self-assembly of new porous materials*. PhD thesis, Department of Chemistry and Polymer Science University of Stellenbosch, 2009. URL http://hdl.handle.net/10019.1/3970.

T. Jacobs, G. O. Lloyd, J.-A. Gertenbach, K. K. Müller-Nedebock, C. Esterhuysen, and L. J. Barbour. In situ x-ray structural studies of a flexible host responding to incremental gas loading. *Angewandte Chemie International Edition*, 51(20):4913–4916, 2012. ISSN 1521-3773. doi: 10.1002/anie.201201281. URL http://dx.doi.org/10.1002/anie.201201281.

R. V. Jensen. Functional integral approach to classical statistical dynamics. *Journal of Statistical Physics*, 25(2):183–210, 1981. ISSN 0022-4715. doi: 10.1007/BF01022182. URL http://dx.doi.org/10.1007/BF01022182.

B. Jouvet and R. Phythian. Quantum aspects of classical and statistical fields. *Phys. Rev. A*, 19:1350–1355, Mar 1979. doi: 10.1103/PhysRevA.19.1350. URL http://link.aps.org/doi/10.1103/PhysRevA.19.1350.

P. Kalinay and J. Percus. Exact dimensional reduction of linear dynamics: Application to confined diffusion. *Journal of Statistical Physics*, 123(5): 1059–1069, 2006. ISSN 0022-4715. doi: 10.1007/s10955-006-9081-3. URL http://dx.doi.org/10.1007/s10955-006-9081-3.

P. Kalinay and J. K. Percus. Projection of two-dimensional diffusion in a narrow channel onto the longitudinal dimension. *The Journal of Chemical Physics*, 122(20):204701, 2005. doi: http://dx.doi.org/10.1063/1.1899150. URL http://scitation.aip.org/content/aip/journal/jcp/122/20/10.1063/1.1899150.

S. Lawrence. *Physics and chance Philosophical issues in the foundations of statistical mechanics*. Cambridge University press, 1993.

Stellenbosch University http://scholar.sun.ac.za

V. Lecomte, J. P. Garrahan, and F. van Wijland. Inactive dynamical phase of a symmetric exclusion process on a ring. *Journal of Physics A: Mathematical and Theoretical*, 45(17): 175001, 2012. URL http://stacks.iop.org/1751-8121/45/i=17/a=175001.

D. G. Levitt. Dynamics of a single-file pore: Non-Fickian behavior. *Physical Review A*, 8: 3050–3054, 1973.

J.-R. Li, R. J. Kuppler, and H.-C. Zhou. Selective gas adsorption and separation in metal-organic frameworks. *Chem. Soc. Rev.*, 38:1477–1504, 2009. doi: 10.1039/B802426J. URL http://dx.doi.org/10.1039/B802426J.

T. Liggett. *Interacting Particle Systems*. New York: Springer, 1985.

S. Ma. Gas adsorption applications of porous metalorganic frameworks. *Pure Appl. Chem.*, 81:22352251, 2009.

P. C. Martin, E. D. Siggia, and H. A. Rose. Statistical dynamics of classical systems. *Phys. Rev. A*, 8:423–437, Jul 1973. doi: 10.1103/PhysRevA.8.423. URL http://link.aps.org/doi/10.1103/PhysRevA.8.423.

K. Moller. Dynamics of an active crosslinker on a chain and aspects of the dynamics of polymer networks. Master's thesis, Stellenbosch University, 2011. URL http://hdl.handle.net/10019.1/18001.

K. K. Müller-Nedebock and T. A. Vilgis. Collective dynamics of random polyampholytes. *The Journal of Chemical Physics*, 110(9): 4651–4657, 1999. doi: http://dx.doi.org/10.1063/1.478348. URL http://scitation.aip.org/content/aip/journal/jcp/110/9/10.1063/1.478348.

B. Nadler, Z. Schuss, A. Singer, and R. S. Eisenberg. Ionic diffusion through confined geometries: from langevin equations to partial differential equations. *Journal of Physics: Condensed Matter*, 16(22):S2153, 2004. URL http://stacks.iop.org/0953-8984/16/i=22/a=015.

K. Nelissen, V. R. Misko, and F. M. Peeters. Single-file diffusion of interacting particles in a one-dimensional channel. *EPL (Europhysics Letters)*, 80(5):56004, 2007. URL http://stacks.iop.org/0295-5075/80/i=5/a=56004.

Stellenbosch University http://scholar.sun.ac.za

H. Patzlaff, S. Sandow, and S. Trimper. Diffusion and correlation in a coherent representation. *Z. Phys. B*, 95(3):357–362, Sept. 1994.

J. K. Percus. Anomalous self-diffusion for one-dimensional hard cores. *Phys. Rev. A*, 9:557–559, Jan 1974. doi: 10.1103/PhysRevA.9.557. URL http://link.aps.org/doi/10.1103/PhysRevA.9.557.

V. Popkov and I. Peschel. Symmetry breaking and phase coexistence in a driven diffusive two-channel system. *Phys. Rev. E*, 64:026126, Jul 2001. doi: 10.1103/PhysRevE.64.026126. URL http://link.aps.org/doi/10.1103/PhysRevE.64.026126.

V. Popkov and M. Salerno. Hydrodynamic limit of multichain driven diffusive models. *Phys. Rev. E*, 69:046103, Apr 2004. doi: 10.1103/PhysRevE.69.046103. URL http://link.aps.org/doi/10.1103/PhysRevE.69.046103.

L. Radzihovsky and E. Frey. Kinetic theory of flux-line hydrodynamics: Liquid phase with disorder. *Phys. Rev. B*, 48:10357–10381, Oct 1993. doi: 10.1103/PhysRevB.48.10357. URL http://link.aps.org/doi/10.1103/PhysRevB.48.10357.

N. Rajewsky, L. Santen, A. Schadschneider, and M. Schreckenberg. The asymmetric exclusion process: Comparison of update procedures. *Journal of Statistical Physics*, 92(1-2):151–194, 1998. ISSN 0022-4715. doi: 10.1023/A:1023047703307. URL http://dx.doi.org/10.1023/A%3A1023047703307.

P. M. Richards. Theory of one-dimensional hopping conductivity and diffusion. *Phys. Rev. B*, 16:1393–1409, Aug 1977. doi: 10.1103/PhysRevB.16.1393. URL http://link.aps.org/doi/10.1103/PhysRevB.16.1393.

V. G. Rostiashvili, M. Rehkopf, and T. A. Vilgis. Langevin dynamics of the glass forming polymer melt: fluctuations around the random phase approximation. Technical report, July 1998.

J. E. Santos and G. M. Schütz. Exact time-dependent correlation functions for the symmetric exclusion process with open boundary. *Phys. Rev. E*, 64:036107, Aug 2001. doi: 10.1103/PhysRevE.64.036107. URL http://link.aps.org/doi/10.1103/PhysRevE.64.036107.

Stellenbosch University http://scholar.sun.ac.za

W. Stephan, B. Kleutsch, and E. Frehland. Rate theory models for ion transport through rigid pores. iii. continuum vs discrete models in single file diffusion. *Journal of theoretical biology*, 105(2):287–310, Nov. 1983. ISSN 0022-5193. URL http://view.ncbi.nlm.nih.gov/pubmed/6317988.

A. Taloni and M. Lomholt. Langevin formulation for single-file diffusion. *Physical Review E*, 78(5):51116, 2008.

V. N. Uversky, C. J. Oldfield, and A. K. Dunker. Intrinsically disordered proteins in human diseases: Introducing the d2 concept. *Annual Review of Biophysics*, 37(1):215–246, 2008. doi: 10.1146/annurev.biophys.37.032807.125924. URL http://www.annualreviews.org/doi/abs/10.1146/annurev.biophys.37.032807.125924. PMID: 18573080.

H. van Beijeren, K. W. Kehr, and R. Kutner. Diffusion in concentrated lattice gases. iii. tracer diffusion on a one-dimensional lattice. *Phys. Rev. B*, 28:5711–5723, Nov 1983. doi: 10.1103/PhysRevB.28.5711. URL http://link.aps.org/doi/10.1103/PhysRevB.28.5711.

Q.-H. Wei, C. Bechinger, and P. Leiderer. Single-file diffusion of colloids in one-dimensional channels. *Science*, 287(5453):625–627, 2000. doi: 10.1126/science.287.5453.625. URL http://www.sciencemag.org/content/287/5453/625.abstract.

M. Weiss, M. Elsner, F. Kartberg, and T. Nilsson. Anomalous subdiffusion is a measure for cytoplasmic crowding in living cells. *Biophysical Journal*, 87(5):3518 – 3524, 2004. ISSN 0006-3495. doi: http://dx.doi.org/10.1529/biophysj.104.044263. URL http://www.sciencedirect.com/science/article/pii/S0006349504738163.

R. Zwanzig. Diffusion past an entropy barrier. *The Journal of Physical Chemistry*, 96(10):3926–3930, 1992. doi: 10.1021/j100189a004. URL http://pubs.acs.org/doi/abs/10.1021/j100189a004.